UNIVERSIDADE DE ÉVORA

ESCOLA CIÊNCIAS E TECNOLOGIAS

DEPARTAMENTO DE FÍSICA

Instrumentation and signal processing applied to Atmospheric Electricity

Ricardo Filipe Carrão da Conceição

Orientação:

Orientador:

Professor Doutor Mouhaydine Tlemçani

Coorientador:

Doutor Hugo Manuel Gonçalves da Silva

Mestrado em Engenharia Mecatrónica

Dissertação

Évora, 2015

UNIVERSIDADE DE ÉVORA

ESCOLA CIÊNCIAS E TECNOLOGIAS

DEPARTAMENTO DE FÍSICA

Instrumentation and signal processing applied to Atmospheric Electricity

Ricardo Filipe Carrão da Conceição

Orientação:

Orientador:

Professor Doutor Mouhaydine Tlemçani

Coorientador:

Doutor Hugo Manuel Gonçalves da Silva

Mestrado em Engenharia Mecatrónica

Dissertação

Évora, 2015

Resumo

Intrumentação e processamento de sinal aplicado à Electricidade Atmosférica

O conhecimento atual diz-nos que a atmosfera da Terra em si aprensenta-se como um circuito elétrico global, que proporciona uma atmosfera continuamente eletrificada. O estudo deste circuito global, bem como os efeitos, globais e locais, sobre a componente vertical do campo eléctrico atmosférico, geralmente designada como gradiente de potencial, são de grande importância não só devido à resposta dinâmica do gradiente de potencial em relação a estes efeitos, mas também porque é possível recuperar informações a partir das suas medidas para inferir propriedades importantes de fatores externos. Desta forma, o impacto dos efeitos externos sobre o gradiente de potencial foram estudados para Lisboa desde 1955 a 1991. As medições foram feitas usando um electrómetro Benndorf na estação meteorológica de Portela (nos subúrbios de Lisboa e perto do Aeroporto de Lisboa). Como Lisboa é uma cidade histórica, muito povoada e perto do mar, que fornece um conjunto de efeitos externos, como a poluição, que podem e devem ser estudados com recurso a mediadas de gradiente de potencial. O estudo elaborado contempla o efeito da poluição antropogénica como um efeito local no gradiente de potencial e a confirmação de um ciclo semanal persistente, devido à poluição urbana. Este estudo foi complementado com uma análise da dependência da direção do vento. Um segundo estudo foi feito sobre o efeito da humidade relativa sobre o gradiente de potencial. Uma formulação foi desenvolvida para relacionar propriedades microfísicas dos aerossóis, principalmente o parâmetro de higroscospicidade, com a medida macrofísica que é o gradiente de potencial. Resultados razoáveis foram obtidos entre o modelo e os dados experimentais, indicando a presença de uma fracção de aerossóis higroscópicos. Um terceiro estudo foi baseado num evento particular, o incêndio do Chiado, que teve lugar no dia 25 de agosto de 1986 e é considerado o acidente mais trágico que ocorreu em Lisboa desde o terramoto de 1755. O efeito da pluma de fumo sobre o gradiente de potencial, assim como o transporte da pluma desde área do Chiado até à Portela foram estudados. Foi observado pela primeira vez que o fumo do incêndio foi responsável por um

aumento de gradiente de potencial significativo com uma baixa probabilidade de ocorrer por acaso. Este estudo pode incentivar o uso de medições gradiente de potencial em detectores de rede de incêndios. Finalmente, foram realizadas simulações sobre o Circuito Global Elétrico (circuito primário) e seu acoplamento para medições locais (circuito secundário). O objectivo foi o de separar os efeitos globais dos efeitos locais gerados pela poluição sobre a resistência colunar na superfície da Terra onde as medições são realizadas.

Abstract

Present knowledge tells us that Earth's atmosphere itself represents a global electrical circuit, which provides a continuous electrified atmosphere. The study of this global circuit as well as the effects, globally and locally wise, on the vertical component of the atmospheric electrical field, usually referred as Potential Gradient, are of great importance not only because of the dynamical response of the Potential Gradient to those effects, but also because it is possible to retrieve information from its measurements to infer the proprieties of important external factors. In this way, the impact of external effects on the Potential Gradient was studied for Lisbon from 1955 to 1991. The measurements were done using a Benndorf Electrograph at the Portela meteorological station (in the suburbs of Lisbon and near the Lisbon Airport). Since Lisbon is an historical city, very populated and near sea, it provides a set of external effects, like pollution, which can and should be studied through measurements of Potential Gradient. The core study done contemplates the effect of anthropogenic pollution as a local effect on the Potential Gradient and the confirmation of a persistent weekly cycle, due to urban pollution. This study was complemented with a wind direction dependence analysis. A second study was made regarding the effect of relative humidity on the Potential Gradient. A formulation was developed to relate microphysical proprieties of the aerosols, mainly the hygroscopicity parameter, with the macrophysical measure of Potential Gradient. Reasonable fits were obtained between the model and the experimental data indicating the presence of a small fraction of hygroscopic aerosols. A third study was based on a particularly event, the Chiado's fire that took place on 25th of August 1989 and is considered the most significant hazard which occurred in Lisbon since the 1755 earthquake. The effect of the smoke plume on the Potential Gradient, but also how the plume travelled from the Chiado area to Portela was studied. It was observed (for the first time) that the fire smoke was responsible for a significant Potential Gradient increase with a low probability to occur by chance. This study might encourage the use of Potential Gradient measurements in fire network detectors. Finally, simulations regarding the Global Electrical Circuit (primary circuit) and its coupling to local measurements (secondary circuit) were performed. The objective was to separate the global effects from the local effects generated by pollution on the columnar resistance at Earth surface where measurements are made.

"I have no special talents. I am only passionately curious"

Einstein, The Ultimate Quotable Einstein (Einstein Archives 39-013)

I dedicate this dissertation especially to my mother Maria, my sister Vera, my nephew Francisco, my niece Carminho, my grandmothers Angelica and Clotilde, my grandfather Narciso and my girlfriend Catarina.

Acknowledgments

Firstly, I would like to thank to my supervisor, Mouhaydine Tlemçani, for his effort in the development of this dissertation and for his humor and ideas given through the all process. Secondly I would like to mention the help of my co-supervisor, Hugo Gonçalves Silva, since he was the main pillar of this dissertation, not only because of his academic experience, namely from a scientific point of view, but also for his guidance, leading me always in the right path.

I am also grateful to Professor Giles Harrison and Keri Nicoll for their massive knowledge and help through the scientific articles, which compose this dissertation. Besides the fact that they are two of the major figures on atmospheric electrical field in the world for quite some time they were also very helpful. Having the chance to work with these figures was quite an honor for me and I feel privileged.

I want to express my thanks to Professor Heitor Reis for his support on article revision and for his thoughts, which contributed greatly for the evolution of this dissertation and my academic experience.

Marta Melgão and Samuel Bárias for their disposition of helping me understating how to assemble an electrical field measurement system, which we tested in Beja air force base and Évora.

I am grateful to James Matthews and Matthew Wright from University of Bristol and Sergio Pereira for his experience in the aerosols field and for their help in aerosol hygroscopic growth matter.

Paula Brás Mendes for her help in Lisbon's climatology, Claudia Serrano for data digitalization and Dr. Mário Figueira, from the former Institute of Meteorology, for installing the Potential Gradient sensor and make such measurements.

Bruno Besser from Graz University for his effort in providing information about Benndorf Electrometer.

My family and my girlfriend offered a support pillar through which I could maintain myself confident and keep up my moral through the adversities found along this dissertation. They kept my motivation always high and helped me to understand how obstacles can be overcome and how to learn from them.

Finally, I would like to acknowledge the support of the Portuguese Foundation for Science and Technology (Fundação para Ciência e Tecnologia, FCT) through the 1 year research grant from a FCT/COMPETE project EAC: FCOMP-01-0124-FEDER-029197 PTDC/GEO-FIQ/4178/2012; which Hugo G. Silva is responsible for and that allowed me to fulfill the objectives outlined for the present work.

Contents

List of Figures

List of Tables

Nomenclature

Symbol	Description	Units
a_w	*Water activity*	-
C_{IE}	*Ionosphere-Earth capacitor*	F
C_{BL}	*Boundary layer capacitor*	F
E_z	*Atmospheric Eletric Field*	Vm^{-1}
e	*Elementary charge*	C
f	*Frequency*	Hz
GF	*Growing factor*	-
$\bar{h}$	*Mean*	-
h	*Runge-Kutta step*	s
i_s	*Electrode current*	A
J_C	*Conduction current density*	pAm^{-2}
J_D	*Maxwell current density*	pAm^{-2}
k_B	*Boltzmann constant*	JK^{-1}
M	*Smoke concentration*	mgm^{-3}
N	*Larger ion number concentration*	cm^{-3}
N_f	*Number of independent frequencies*	-
n	*Total ion number concentration*	cm^{-3}
$\bar{n}$	*Total ion mean*	cm^{-3}
n_+	*Positive ion number concentration*	cm^{-3}

n_-	*Negative ion number concentration*	cm^{-3}
n-exponent	$S(T) \propto T^n$	-
PG	*Potential Gradient*	Vm^{-1}
Q_1	*Firt quartile*	-
Q_3	*Third quartile*	-
q	*Ion production rate*	$cm^{-3}s^{-1}$
q_s	*Electrode charge*	C
R^2	*Goodness of the fit*	-
R_a	*Particle radius*	μm
RH	*Relative humidity*	%
R_{BL}	*Boundary layer resistor*	$P\Omega$
R_C	*Atmospheric columnar resistor*	$P\Omega m^2$
R_{FT}	*Free Troposphere resistor*	$P\Omega$
R_{FW}	*Fair-weather resistor*	$P\Omega$
R_S	*Thunder storm region resistor*	$P\Omega$
S	*Power spectral density*	-
T	*Period*	*days*
T_e	*Ambient temperature*	K
t	*time*	s
V_I	*Ionospheric Potential*	kV
K	*Larger ion number*	cm^{-3}
Z_a	*Aerosol number concentration*	cm^{-3}

z	*Heigth*	m
μ_+	*Positive ion electric mobility*	$cm^2V^{-1}s^{-1}$
μ_-	*Negative ion electric mobility*	$cm^2V^{-1}s^{-1}$
σ^2	*Variance*	-
σ_+	*Positive electric conductivity*	Sm^{-1}
σ_-	*Negative electric condutivity*	Sm^{-1}
σ_T	*Total electric conductivity*	Sm^{-1}
ϵ	*Electric permittivity of air*	$C^2N^{-1}m^{-2}$
υ	*Number of elementary charges*	-
β_a	*Effective ion-aerosol attachment coefficient*	cm^3s^{-1}
α	*Ion-ion attachment coefficient*	cm^3s^{-1}
κ	*Higrocospicity parameter*	-
τ	*Lomb Scargle parameter*	-

Acronyms

ADC	Analog-to-Digital Converter
AEC	Atmospheric Electric Conductivity
AW	All Weather
CCN	Cloud Condensation Nuclei
FW	Fair-Weather
GCRs	Galatic Cosmis Rays
GEC	Global Electric Circuit
GPC	Gas to Particle Conversion
IQR	Interquartil Range
IpDFT	Interpolated Discrete Fourier Transform
LSP	Lomb Scargle Periodogram
MAD	Median Absolute Deviation
MCS	Mesospheric Convective System
MW	Manually observed Weather
ODE	Ordinary Differential Equation
SPEs	Solar Proton Events
TLEs	Transient Luminous Events
UB	Upper Boudary
LB	Lower Boundary
WD	Workday
WK	Weekend

1 Introduction

In the current chapter, an overview of the history of atmospheric electricity will be presented from the beginning until nowadays. The key concepts will be discussed, allowing the full understanding of the contents referred in this dissertation. In addition, the objectives will be explained and the motivation behind this work.

1.1 Historical Overview

Since ancient times, humanity has tried to understand the natural phenomena, which occur in the planet Earth and in the Universe. Therefore, many issues were related to the Gods and mythology, because what could not be understood by human mind was instead attributed to work of mysterious identities with supernatural powers. One of these cases happens to be thunderstorms and lightnings, which were associated with the anger of Gods upon humans. Obviously, this was a way to explain what was unexplainable by science in past times. Over the years, those superstitions were slowly changed and nowadays, at least for most people, they are explained by science with help of scientists.

One of the first documents, which shows the beginning of the understanding about atmospheric electricity, was written by Benjamin Franklin and published in 1751 as "*Experiments and Observations on Electricity, Made at Philadelphia in America".* This document is an assemble of a series of letters that Benjamin Franklin sent to Peter Collinson, member of Royal Society, about his experiments on the static electricity using a glass tube commonly used to excite electricity. In his second letter, written in July 11, 1747, he states something very interesting:

"The first is the wonderful effect of pointed bodies, both in drawing off and throwing off the electrical fire".

This refers to what we know today as electrical discharges. He tried different materials in his experiments and noticed that sharp configurations and metallic objects work better than dry wood and bluntly ones. Along his letters he started to use terms like "sparking", "positively

electrified", "negatively electrified", which demonstrates an understanding of how the charging and discharging process was occurring and how the electric current circulates.

Figure 1.1 *Benjamin's Franklin portrait by Joseph Siffred Duplessis (http://www.nPG.si.edu).*

Concerning the fact that clouds are electrified, Benjamin Franklin proposed the next experience:

"On the top of some high tower or steeple, place a kind of a centry-box (as in FIG. 9.) big enough to contain a man and an electrical stand. From the middle of the stand let an iron rod rise, and pass bending out of the door, and then upright 20 or 30 feet, pointed very sharp at the end. If the electrical stand were kept clean and dry, a man standing on it when such clouds are passing low, might be electrified, and afford sparks, the rod drawing fire to him from the cloud. If any danger to the man be apprehended (though I think there would be none) let him stand on the floor of his box, and now and then bring near to the rod the loop of a wire, that has one end fastened to the leads, he holding it by a wax-handle; so the sparks, if the rod is electrified, will strike from the rod to the wire and not affect him."

Figure 1.2 *Benjamin's experiment proposal to check cloud electrification, (Experiments and Observations on Electricity, Made at Philadelphia in America).*

It is thought that he never put this idea into practice. Although, it was Thomas-François Dalibard, a French scientist who translated "*Experiments and Observations on Electricity,*

Made at Philadelphia in America" into French, to be the first one, at least documented, that was able to draw sparks from the rod, in Marly-la-Ville, (France) in 1752 (Fleming, 1939).

The apparatus used by Dalibard is presented in **Figure 1.3**; marked with (a) it is the metallic rod, as (g) the silk ropes, as (h) the protection against rain for the silk ropes and as (e) the wine bottles to ensure insulation from the ground. With this setup, it was possible to draw sparks from the rod or charge a Leyden jar.

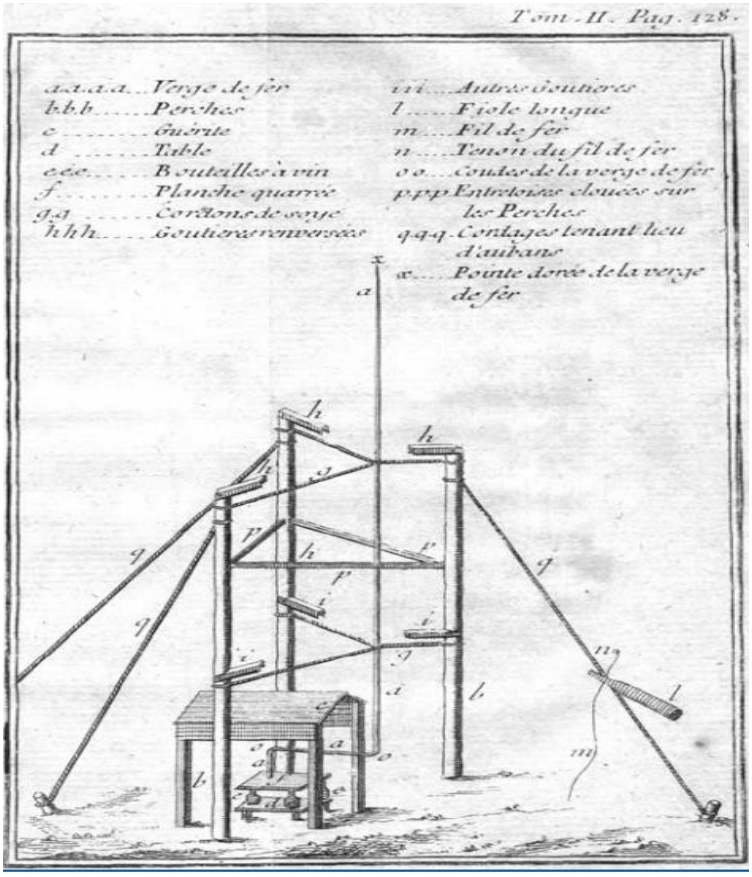

Figure 1.3 *Apparatus used by T.F.Dalibard for Benjamin's experience. (Franklin, Expériences et Observations sur Électricité…, 2nd ed., vol.2, pag. 128, an extended translation from English by T.F.Dalibard).*

After Dalibard successful experience, Benjamin Franklin in 1752 worked on the nature of the thunderclouds' charge using what we know today as "Franklin bells". Although, this instrument was an invention of Andrew Gordon, around 1740, a University teacher in Germany (Jefimenko, 1973).

Figure 1.4 *Pierre-Charles Le Monnier portrait by Nicolas-Bernard Lépicié (http://fr.wikipedia.org).*

Pierre-Charles Le Monnier, a French scientist, achieved the next breakthrough in this matter, reproducing Benjamin's Franklin experience with few modifications, (Chambers, 1967). He used dust as an indicator of the experience objective and observed that the dust particles were attracted to the wire when it was electrified. However, the true discover he made was the fact that even in fair-weather, that phenomenon could happen; meaning that there also was a clear sky electrification. In 1753 John Canton, a member of Royal Society, did several experiments and built a new version of the electrometer at the time, which is documented by him in "*Electrical Experiments, with an Attempt for account for their several Phenomena; together with some Observations on Thunder-Clouds "*, and with this invention he studied the electrification of thunderclouds. Also on that same year, he wrote a letter to the President of Royal society about his observations where he states two very interesting thing:

"The air without-doors I have sometimes known to be electrical in clear weather."

Which is the same effect detected by Pierre-Charles Le Monnier, but he made a deeper study during different seasons of the year and accounted several different meteorological phenomena, leading him to say:

"[…] for in the succeeding months of January, February and March, my apparatus was electrified no less than twenty-five times, both positively and negatively, by snow, as well as by hail and rain."

This statement shows that clouds were electrified both positively and negatively. At this point, the scientific community already knew that the clouds and the air itself are charged and that different meteorological phenomena can modify the charge state, in a positive or negative way. Later, several other scientist, worldwide, kept working on this thematic, like Francesco Ludovico Beccaria, who begun in 1775 to measure daily variations in the atmospheric electricity, (Harrison, 2005), where he noticed the effect of fog and the positive electrification in fair-weather. He kept this task for several years and in 1789, John Read, driven by Beccaria's work, made a two-year series of atmosphere electrification measurements (Harrison, 2005).

Figure 1.5 *Giovanni Battista Beccaria portrait by Franz Joseph Anton von Thun-Hohenstein (http://www.gettyimages.pt).*

Working on the line of Beccaria was Horace Bénédict de Saussure (Switzerland), who found diurnal variations in atmospheric electricity, between 1785 and 1788, (Chauveau, 1925), reporting:

"In winter, the season during which I have the best observations of serene1 electricity…the electricity undergoes an ebb and flow like the tides, which increases and decreases twice in the span of twenty-four hours. The times of greatest intensity are a few hours after sunrise and sunset, and the weakest before sunrise and sunset"

Figure 1.6 *Horace Bénédict de Saussure portrait by Jean Pierre Saint-Ours (http://www.summitpost.org).*

With only primitive instruments, considering the ones existing today, it already could be seen a very distinct cycle in atmospheric electricity, which was going to be well defined only in 1920s through the Carnegie cruises. Nevertheless, it is very important to state that it was Charles Augustin Coulomb, who through experiments, noticed that a charge of an isolated

object decays to the air with time, (Leblanc, 2008). He did not have enough theoretical basis to explain this phenomenon, the electron was not yet been discovered, but he is credited as the one who discovered the electrical conductivity of the air, reporting:

"L'électricité des deux balles diminue un peu pendant le temps que dure l'experience… si l'air est humide et que l'électricité se perd rapidement [. . .]" (Coulomb, Mémoires sur l'électricité et le magnétisme, 1785).

After almost 80 years, in 1859 Lord Kelvin developed a new electric field sensor, usually called "water dropper potential equaliser" (Aplin and Harrison, 2013). On one hand, with this instrument he was able to measure what is known today as potential gradient (*PG*[1]) related with the vertical component of the atmospheric electrical field. On the other hand, the method of photography recording was also discovered around that time and Lord Kelvin was able to build a system to obtain continuous measures of *PG*, known as Kelvin Electrograph. This system was used in several places like the Kew Observatory of London from 1861 to 1864 (Everett, 1868) and in the Eifel Tower (Harrison and Aplin, 2003).

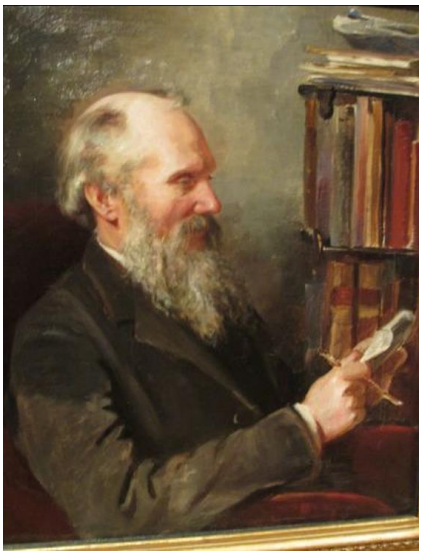

Figure 1.7 *Lord Kelvin portrait by Elizabeth King (http://www.docbrown.info).*

In **Figure 1.8** is presented probably one of the first automatic and continuous records ever made of *PG*, measured in the Kew Observatory and that marked a new advanced in the study of atmospheric electricity and automatic measurements:

[1] The convention is that $PG = dV_I/dz$, where V_I is the potential difference between the Ionosphere and Earth's surface and z the vertical coordinate. It is defined to be positive for fair-weather and is related with the vertical component of the atmospheric electric field by $E_z = -PG$.

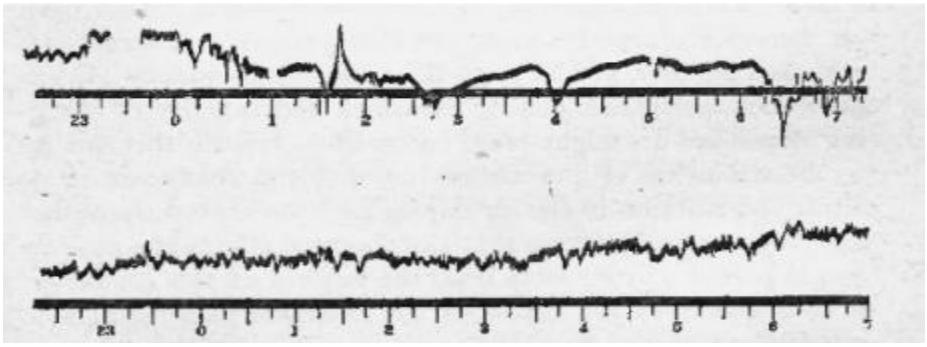

Figure 1.8 *Photographically recorded PG at Kew Observatory in 1861 (Aplin and Harrison, 2013).*

After Lord Kelvin, there were crucial discoveries, which allowed the progress in atmospheric electricity science, like the one made by Wilhelm Conrad Roentgen who discovered the ionizing radiation in 1895 and the one by Joseph John Thompson in 1897 where he found what was called the electron.

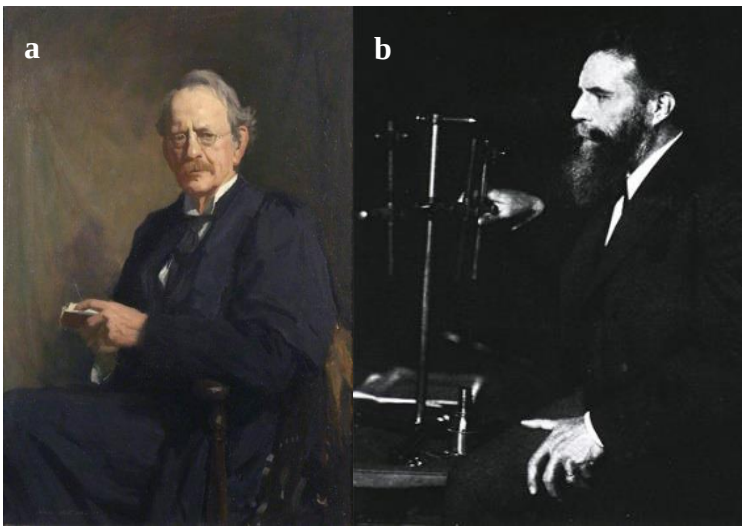

Figure 1.9 *a) J. J. Thompson portrait by George Fiddes Watt (http://www.bbc.co.uk); b) Wilhelm Conrad Roentgen (http://www.nobelprize.org).*

With various new instruments and through the development of science in all of its areas, Gerdien (1905a) was able to verify that air was slightly electrical conductive, just like Coulomb noticed. Gerdier also found that there was a current flowing from the upper atmosphere to the Earth's surface and Charles Thompson Rees Wilson (Wilson 1906, 1908) built an apparatus to measure what was called as "air-Earth" current.

Figure 1.10 *C.T.R Wilson portrait by James Gunn (http://www.sid.cam.ac.uk).*

During 1920s, the Carnegie vessel sailed all over the world in order to make magnetic and electric measurements, specifically to measure *PG*. The ocean is an excellent location to make those measurements since it is less polluted than the continents and they found what is known as the *Carnegie Curve*, which is a characteristically *PG* variation curve. It was noticed that it was almost independent from the location where it was measured.

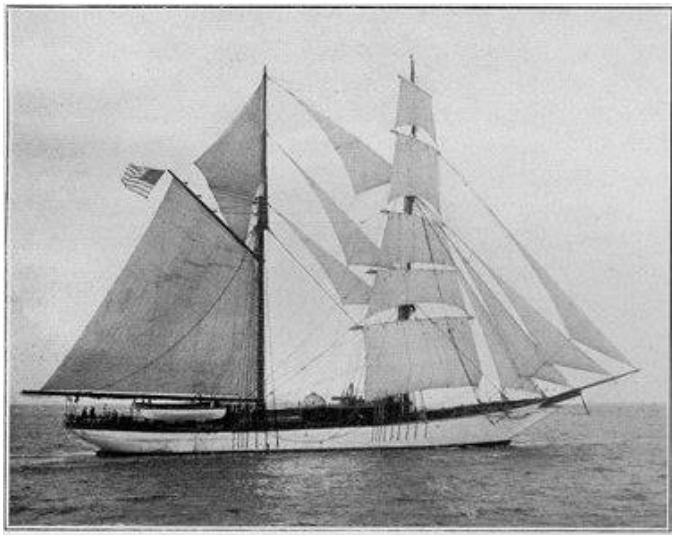

Figure 1.11 *Carnegie vessel photograph courtesy of Carnegie Institution of Washington.*

At this point, there was a lot of speculation about the source of this air current and the charging mechanism of earth's surface and ionosphere and it was C.T.R. Wilson (1921, 1929) who proposed that the sources were thunderstorms and rain clouds (bad-weather regions).

Since the beginning of the radio wave studies, it was known that the upper atmosphere was highly conductive so it was considered that the current was flowing from bad-weather to fair-weather regions, forming a global electric circuit, (Leblanc, 2008). Further proofs of this Global Electric Circuit (GEC) were found using measurements of the daily thunderstorm area, where it was found a strong positive correlation with the *Carnegie Curve* (Whipple and Scrase, 1936), see **Figure 1.12** and **Figure 1.13**. At this stage, the basis of the present knowledge was built. Such knowledge is still growing today, with the study of new models for the Global Electric Circuit as well as the study of external factors impact on local *PG*.

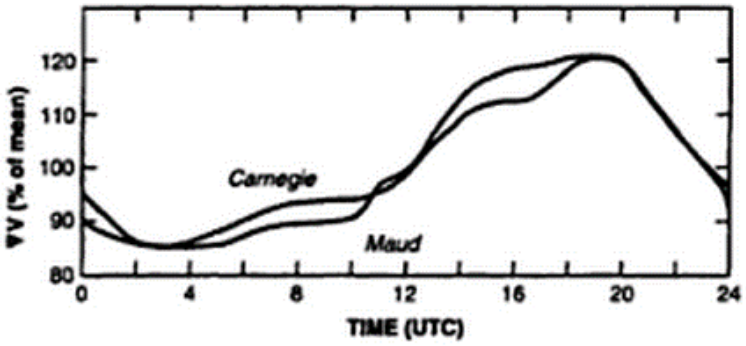

Figure 1.12 *Carnegie and Maud hourly averaged PG in % of mean (Whipple and Scrase, 1936).*

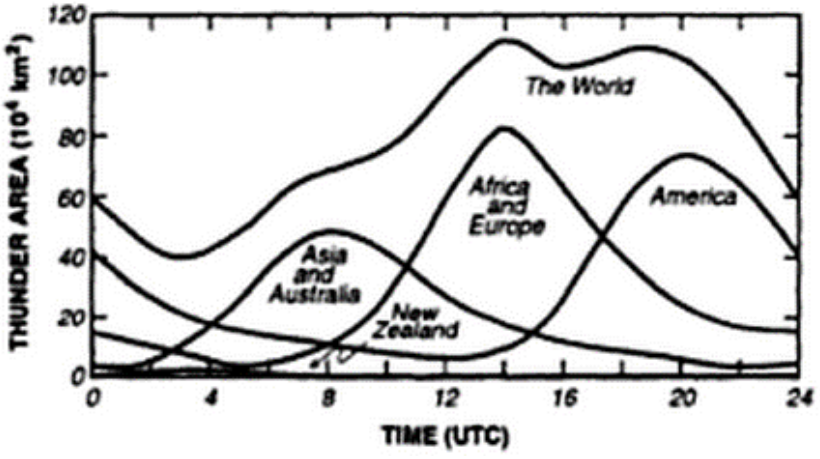

Figure 1.13 *Active Thunder area around the world (Whipple and Scrase, 1936).*

Linss (1887) concluded that the negative charge of the Earth would leak away in a period of approximately 10 minutes when it was not maintained by any charge generating process in

the atmosphere. Israel and Kasemir (1949) calculated how fast a charge, which is injected into the atmosphere at a point *P*, distributes itself over a spherical shell with a given air conductivity around the globe. Israel (1957, 1970) made other calculations and concluded that the atmospheric electric equilibrium, at ground level, is reached in about 30 min. It is also known that the electric charge generated by a thunderstorm takes about 10 to 15 min to spread along the ionosphere around the all globe. This fact is the reason why hourly mean values are most common for investigation of the Global Electric Circuit.

1.2 Motivation

The study of the atmosphere, more concretely the study of its electrical properties as well as their effects, are a point of deep interest since it can be used to analyze natural phenomena related to humankind. Not only weather conditions can be retrieved from *PG* analysis but also the consequences of *PG* variations can dictate the start of, for example fires or fog events. The importance of *PG* is so vast in many different areas of society and it can be very handy in several situations that the curiosity to study it is too tempting.

In this context, Lisbon has vast records of *PG* measurements, from 1955 to 1991, which is a rare case. This situation provides the ideal opportunity to study a long time series and characterize Lisbon's atmospheric electrical field. It is also of great importance since not much was done with this time series, which naturally improves its significance. Beside this, Lisbon also went through a long population and industrialization evolution, contributing to changes in the atmospheric electrical field among other things. Thus studding the *PG* records at Lisbon is a way of recovering its historical evolution, in particular in the 1980's (after the democratic revolution).

On a deeper level, the study of things which humankind cannot see, at least at naked eye, but can measure, was from a certain point of my life not only a cause of motivation but also a continuous source of learning. The case of *PG*, among all other things that we cannot see at naked eye, made me think of what knowledge is and realize an important self-true about what

is called Engineering and Physics. One conclusion that I arrived was that knowledge cannot come only from books or whatever you may read.

Experience is and always will be a principal component for humans to understand nature, not only as a consequence to test theory results but also a cause to build theories. I also concluded another thing, which also came with my experience during my studies in the University of Évora, that there is only one object that, for humankind, provides the mechanism to understand the Universe where we live. That object is called mathematics and it rules almost everything we see and touch, excluding the things that even today we cannot even understand, and made me realize that there is no such thing as Engineering or Physics or anything else. These are divisions made by humankind to make easier for it to store the Knowledge in our own small minds. It does not matter if you called it Mechanics, Chemistry, Electricity or whatever.

In the end equations rules them all, even if slightly simplified. But the most important conclusion that I discovered is that all these subjects have one little thing in common with each other that most people cannot see or do not want to see, which is that they are all based in particles motion and interaction between them. If almost everything is motion and Mathematics, why not study the motion we cannot see but might be very important to society or actually have some usefulness or just because is just a thing that you want to learn more about? These are the questions, which led me to write this dissertation as an attempt to answer it.

1.3 Formulation of the global electric circuit

Thunderstorms, shower clouds and precipitation, cause separation of electric charge between the ground and ionosphere (also known as the equalizing layer), an electrically conductive layer about 60 km above the surface. This charge separation causes the ionosphere to have a potential (V_I) between 200 and 300 kV with respect to the Earth's surface. Ionization from cosmic rays (mainly in the upper atmosphere) and terrestrial sources (chiefly radon decay

near Earth's surface), produces cluster ions (small ions) which make the atmosphere weakly electrical conductive. These ions flow vertically because of the vertical potential difference, V_I, causing the air-Earth conduction current density, J_C, of order ~2 pAm^{-2}. The total electrical resistance for a unit area of the atmospheric column from the surface to the ionosphere is called the columnar resistance, R_C and has value about ~ 300 PΩm^2. A schematic of the global circuit is given in **Figure 1.14**. Ohm's law relates Ionosphere-Earth potential difference (V_I), columnar resistance and air-Earth conduction current through the equation:

$$V_I = J_C R_C. \qquad \textbf{Eq. (1.1)}$$

The Ionosphere is positively charged with respect to the Earth's surface under fair-weather conditions. This produces a downward pointing (negative) electric field (E_z), thus by convention potential gradient (PG) is defined as the negative of E_z.

$$PG = -E_z. \qquad \textbf{Eq. (1.2)}$$

Near the Earth's surface, the PG arises because J_C is flowing through the weakly electrical conductive air. It is therefore J_C that permits the effect of the Global Electric Circuit (GEC) circuit to be measured at the surface, either directly through the measurement of J_C itself or by PG.

However, PG is also a function of the local atmospheric air conductivity (σ_T). Away from sources of charge separation, the atmospheric electrical conductivity (σ_T), potential gradient and conduction current density are related by Ohm's Law:

$$PG = \frac{J_C}{\sigma_T}. \qquad \textbf{Eq. (1.3)}$$

In the fair-weather part of the circuit, small ions dominate the charge transport since they have a large electrical mobility. Therefore, an increase in small ion concentration will increase the atmospheric electrical conductivity by providing more charge carriers. Aerosols in the atmosphere removes small ions by ion-aerosol coupling. An increase in aerosol number concentration therefore reduces the ion number concentration and decreases the atmospheric electrical conductivity. A change in aerosol number concentration subsequently modifies PG through **Eq. (1.3)**.

The global schematic of GEC and its important processes can be seen next on **Figure 1.14**:

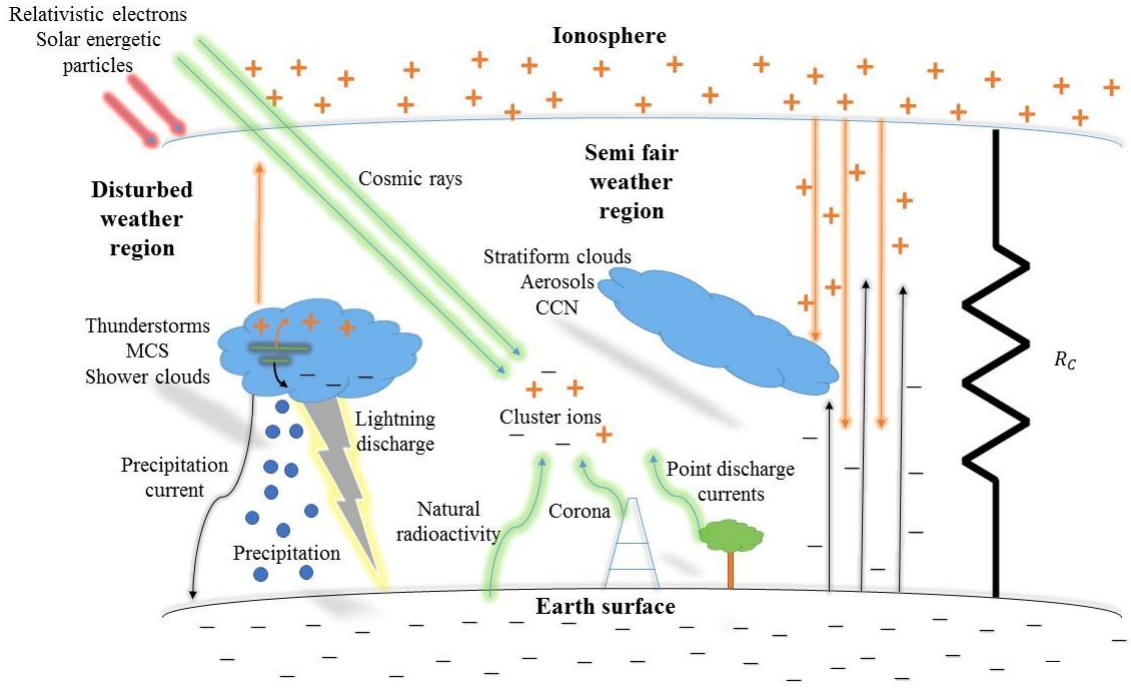

Figure 1.14 *Processes of interest in the global electric circuit. Charge separation in thunderstorms, which occur in disturbed weather regions, creates a substantial potential difference between the highly conducting regions of the ionosphere and the Earth's surface. The positive potential of the ionosphere (positive with respect to the Earth's surface) is distributed to fair-weather and semi-fair-weather regions, where a small current (whose density is J_C) flows vertically. When this current flows through clouds it generates charge near the upper and lower cloud edges, which can influence cloud microphysical processes. (In this diagram, Mesospheric Convective Systems, which are large scale thunderstorms late in their evolution and which favor sprite generation above them, are indicated by MCS; sprites are one example of Transient Luminous Events (TLEs); Cloud Condensation Nuclei are shown as CCN).*

Thunder clouds, which generate potential differences exceeding 100 MV between the positive charges at their top sand the negative charges near their bottoms (Wormell, 1930), are one important source of upward currents through the atmosphere. They are both a DC ‘‘battery’’ and an AC generator in the circuit. Each one of the approximately 1000 thunderstorms active at any time generates an upward DC (Wilson) current of 1 A to the ionosphere, which is an excellent conductor, at an equipotential of 250 kV with respect to the Earth (e.g. Rycroft et al., 2000; Singh et al., 2011). The conduction current flows down in areas far from thunderstorms, termed regions of fair-weather (i.e. non-cloudy) and semi-

fair-weather (non-precipitating layer clouds). These currents flow through the partially conducting atmosphere where ionization is produced by galactic cosmic rays (GCRs); the vertical conduction current density is termed J_C. Near the land surface, but not the oceans, escaping radon determines the ion concentration and hence the electrical conductivity of the atmosphere in the planetary boundary layer, at heights up to 2 km (Pulinets, 2007; Kobylinski and Michnowski, 2007).

At sub-auroral latitudes, there is some extra ionization at 70 km altitude produced by relativistic (1 MeV) electron precipitation from the magnetosphere. Within the polar cap, polewards of the auroral oval, occasional energetic solar proton events (SPEs) of 100 MeV produce extra ionization at 60 km altitude. The circuit closes through the highly conducting land and sea, and via point discharge currents from pointed objects on the Earth's surface up to the bottom of the thunderclouds. The increase by seven orders of magnitude of the electrical conductivity of the neutral atmosphere, from the Earth's surface up to the lower ionosphere at 80 km altitude, has been modelled by Rycroft et al.(2007) and Rycroft and Odzimek (2010). It is emphasized here that the conductivity profile is the most important parameter in establishing the global circuit (Holzworth, 1987; Rycroft et al., 2008).

There is another important DC current generator in the global circuit; this is due to electrified rain/shower clouds (**Figure 1.14**) which generally bring negative charge to the Earth's surface. The shower cloud contribution is believed to be a significant fraction (up to about a half) of that of thunderstorms.

Of the quantities, which can be measured at the surface, the air-Earth conduction current density (J_C) presents one of the most fundamental parameters of the Global Electric Circuit (Chalmers, 1967). In fair-weather regions, a positive current density occurs when positive charge moves downward and negative charges move upwards. The conduction current density is one of several components contributing to the total current density, J_S, received by a horizontal flat plate, conducting electrode, at the Earth's surface, electrically isolated from the ground, like a *PG* measurement sensor. J_S comprises contributions from turbulence J_T,

conduction J_C, displacement J_D and precipitation J_P. Based on Maxwell's equations, the displacement current density is given by:

$$J_D = \epsilon \frac{dE_z}{dt}, \qquad \textbf{Eq. (1.4)}$$

where ϵ is the electric permittivity of air.

All precipitation particles carry positive or negative electric charges from the atmosphere to the ground. Precipitation current is very important from a global point of view, since it is one of the mechanisms for the maintenance of the negative electric charge on the Earth's surface. Some measurements were made and amounts of ±0.2 up to 5×10^{-12} Am^{-2}, (Reiter, 1976), were found. Bear in mind that this current depends strongly on the type, rate and physical state of the precipitation and weather conditions.

Finally fast electrons ionizing gas molecules induce point discharge current, which causes a strong local ion concentration increase. It can happen on the leaves of trees when a highly charged cloud is above them or it can happen by means of corona discharges.

1.4 Atmospheric Ions and interaction with aerosols

Aerosols can be defined as an assembly of liquid and/or solid particles suspended in the atmosphere and when they are substantially big, we can notice them as they scatter and absorb sunlight. The size distribution of these particles ranges from r > 3 nm, that corresponds to large ions (usually referred as charged aerosol particles) up to 100 μm, which is characteristic of large organic matter. Usually the aerosols can be divided into 2 groups accounting to their size: fine particles, d < 2.5 μm, and coarse particles, d > 2.5μm. Aerosols may be originated by several ways, being the most important ones affecting the Earth's environment, volcanic aerosols, desert dust and anthropogenic aerosols, essentially from industry heating systems and traffic. These ones are referred as primary aerosols, because they are directly injected into the atmosphere. There are also secondary aerosols, which result from chemical interactions between several constituents of the atmosphere, which can be derived mainly by two methods: Gas-to-Particle Conversion, (GPC), which consists in gas

molecules becoming clustered together, creating a macroscopic particle; Ion-Induced nucleation, which is a process based on aerosol formation and growth by vapor condensing onto an ion (CCN).

Atmospheric small ions both positive (n_+) and negative (n_-) are small clusters, which carry electric charges through the air. Small ions have electric mobilities between 1 and 3 cm/s for 1 V/cm; large ions, between 3×10^{-3} and 3×10^{-4} cm/s for 1 V/cm; intermediate ions have electric mobilities between the values of the other two.

Small ions are the most important type of ions for atmospheric electricity; this is because they have high electric mobility, allowing them to take a more active part in charge transfer through the atmosphere. The electric mobility of ions is of great importance since it determines how much an ion contributes to the electric conductivity of the air. The positive and negative contribution of all particles to the atmospheric electric conductivity can be expressed in a general form by:

$$\sigma_+(z) = e\mu_+(z)n_+(z) + \sum^{p} K_+^p(z)N(z)_+^p v_+^p e,$$
$$\sigma_-(z) = e\mu_-(z)n_-(z) + \sum^{m} K_-^m(z)N_-^m(z)v_-^m e, \qquad \textbf{Eq. (1.5)}$$

where z represents the height, μ represents the small ion electric mobility for both polarizations, n is the number density of positive and negative ions, K is the electric mobility of all larger ions (which goes from intermediate ions to charged aerosol particles), N corresponds to the number of large ions, p and m to the different diameters of particles and v, $v=1$ for small ions, is the number of elementary charges e per ion size (larger particles can bear more than 1 elementary charges, instead, small ions have always v = 1).

Nevertheless, the equation for the total atmospheric electric conductivity is commonly simplified considering only small ions (as they have the greatest effect on it) and charged aerosol particles are assumed to have a negligible contribution (Wright et at., 2014a). Using this simplification and considering the total atmospheric electric conductivity, which means

the sum due to positive and negative ions and that both type of ions have the similar mobilities and number density we arrive at:

$$\sigma_T(z) = \sigma_+(z) + \sigma_-(z) \cong 2\mu(z)n(z). \qquad \textbf{Eq. (1.6)}$$

Woessner et al. (1958) made several measurements of ion conductivity of both polarization with respect to height, *z*, up to 26 km and found the following relations:

$$\sigma_+(z) = 3.33 \times 10^{-14} \exp(0.254z - 0.00309z^2),$$
$$\sigma_-(z) = 5.34 \times 10^{-14} \exp(0.222z - 0.00255z^2). \qquad \textbf{Eq. (1.7)}$$

A plot of **Eq. (1.7)** is shown here:

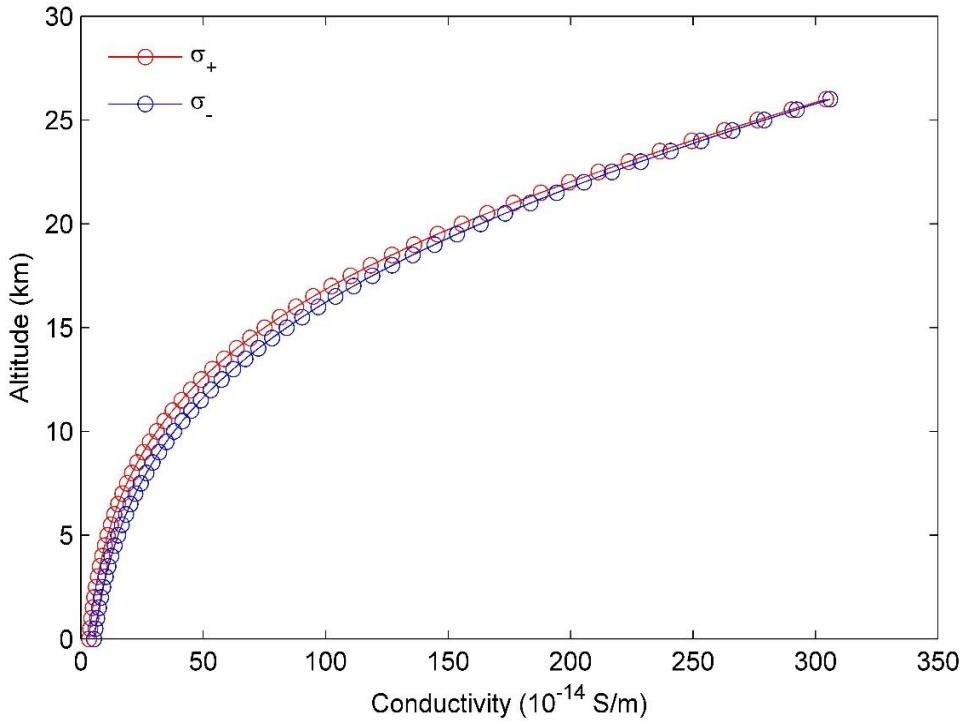

Figure 1.15 *Conductivity profile.*

Primary ions, singly charged positive ions and free electrons, are mainly produced by ionization of molecules in the air and quickly form small ions clusters, through the clustering of water molecules, because it is energetically favorable for primary ions to react rapidly with water molecules. The sources attributed to play a role in atmospheric ionization are cosmic radiation and radon decay through gamma, alpha and beta radiation.

The process of small ion cluster formations is explained as follows: upon a molecule or atom being hit by those ionization agents, it loses an electron per impact, leaving them positively charged and thereby forming a positive primary ion with one elementary charge. The free electron will be captured within ~10^{-8} seconds by a neutral molecule or atom forming a negative primary ion. The primary ions keep colliding with other molecules and atoms in the air for about 10^{10} times/s. The ones that are not removed by mutual recombination tend to form small ion clusters when water vapor is present (Reiter, 1976). The all process is represented schematically in **Figure 1.16**:

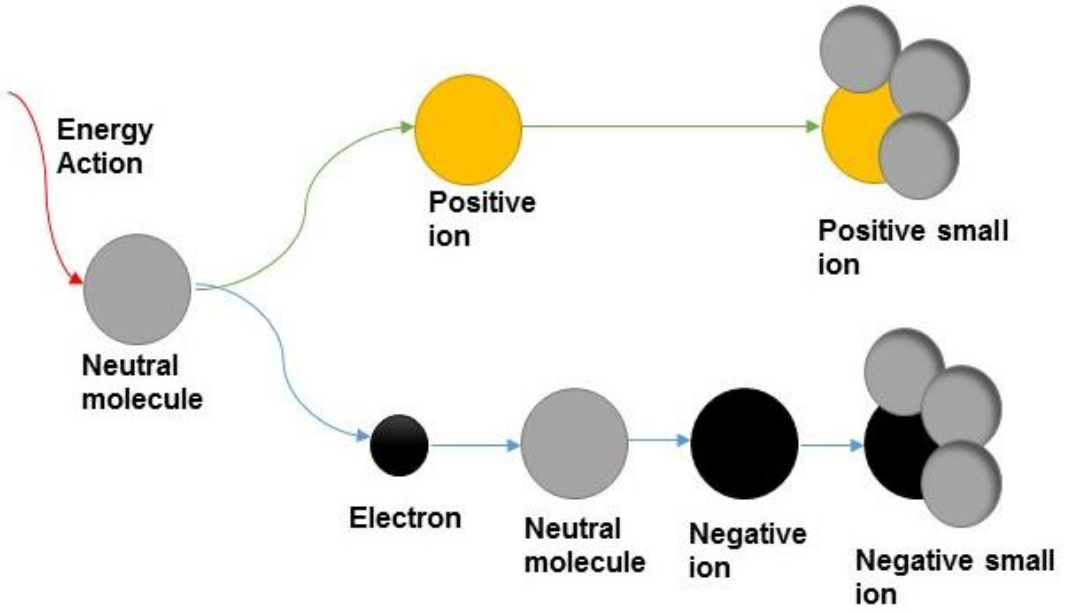

Figure 1.16 *Schematic representation of small ion clusters formations.*

Without exception, small ion clusters only carry one elementary charge and their life-time depends on aerosol particle concentration. Since both small ions and aerosol move in the air they can both collide with each other. The very important concept of "ion equilibrium" is composed by three basic components: 1) small ion production rate, q; 2) the recombination of the polar small ions, which then dissipate, expressed by the recombination coefficient α; 3) the attachment between small ions and air aerosols, expressed by the coefficient β_a.

Equilibrium equations are shown next:

$$\frac{dn}{dt} = q - \alpha\bar{n}^2 - \beta_0\bar{n}N_0 - \beta_{1e}\bar{n}N_1 - \beta_{1u}\bar{n}N_1 - \beta_{2e}\bar{n}N_2 - \beta_{2u}\bar{n}N_2$$
$$\frac{dN_0}{dt} = 2\beta_{1u}\bar{n}N_1 - 2\beta_0\bar{n}N_0$$
$$\frac{dN_1}{dt} = \beta_0\bar{n}N_0 + \beta_{2u}\bar{n}N_2 - \beta_{1u}\bar{n}N_1 - \beta_{1e}\bar{n}N_1 \qquad \textbf{Eq. (1.8)}$$
$$\frac{dN_2}{dt} = \beta_{1e}\bar{n}N_1 + \beta_{3u}\bar{n}N_3 - \beta_{2u}\bar{n}N_1 - \beta_{2e}\bar{n}N_1$$
$$\frac{dN_3}{dt} = \beta_{2e}\bar{n}N_2 + \beta_{4u}\bar{n}N_4 - \beta_{3u}\bar{n}N_3 - \beta_{3e}\bar{n}N_3,$$

where $n=n_+ + n_-$, $\bar{n} = (n_+ + n_-)/2$, $N=N(R_a)$ corresponds to the concentration of all particles with radius R_a. $N_0(R_a)$ corresponds to the concentration of uncharged particles with radius R_a. $N_\upsilon=N_\upsilon(R_a)$ corresponds to the concentration of positive and negative charged particles where the index, υ, determines the amount of elementary charges. $\beta_0 = \beta_0(R_a)$ is the combination coefficient between small ions and uncharged particles, $\beta_{\upsilon e}=\beta_{\upsilon e}(R_a)$ is the combination coefficient between small ions and charged particles with equal sign, *e*, with υ elementary charges and $\beta_{\upsilon u}=\beta_{\upsilon u}(R_a)$ is the combination coefficient between small ions and charged particles of unequal sign, *u*, with υ elementary charges.

Considering that all aerosol particles have an "effective radius", i.e they form a representative monodisperse population, that no charged aerosol particles are present, the number of positive and negative ions is equal, expressed by *n*, $\beta_a$is the effective ion-aerosol attachment coefficient, Z_a is the aerosol number concentration, Z_a is the aerosol number concentration, **Eq. (1.8**) can be simplified to a single formula for ion balance:

$$\frac{dn}{dt} = q - \alpha n^2 - \beta_a Z_a n. \qquad \textbf{Eq. (1.9)}$$

From this equation, it is possible to calculate the evolution of the number of ions in an environment containing aerosols varying with time. The formalism developed by (Hoppel, 1985) uses effective parameters to simplify the equation for ion balance in the presence of a more realistic case that should consider the aerosol size distribution. This formalism gives theoretical support to the assumption made in **Eq. (1.9)** of a monodisperse aerosol

distribution by using an "effective" ion-aerosol attachment coefficient β_a as representative of a polydisperse aerosol population. Thus, the steady-state equation for ion formation and loss in the presence of aerosols can be written as:

$$q - \alpha n^2 - \beta_a Z_a n = 0. \qquad \textbf{Eq. (1.10)}$$

It is worth to mention here that **Eq. (1.10**) is a simplification because it neglects the positive to negative ion concentration unbalance which is crucial in highly perturbed regions where space charges form (Matthews et al., 2010). Nevertheless, the present formulation assumes a quasi-equilibrium state perturbed by the presence of aerosols. The solution of **Eq. (1.10**) is straightforward:

$$n = {}^{1}/_{2\alpha}\left[\sqrt{(\beta_a Z_a)^2 + 4\alpha q} - \beta_a Z_a\right]. \qquad \textbf{Eq. (1.11)}$$

Further developments regarding this matter are discussed in the following chapters.

1.5 Dissertation structure

- Chapter 2 provides an insight of mathematical techniques and instruments used through the dissertation and a briefing about other formulations useful for Engineering, such as the Discrete Fourier Transformation and primitive instruments like Lord Kelvin' Electrometer.

- Chapter 3 approaches a very important thematic, which is the effect of pollution on atmospheric electric field of Lisbon, where a daily and weekly cycle were identified on *PG* records. (This is a study, which is in vogue nowadays, since pollution is one of the major problems affecting society in several and problematic ways).

- Chapter 4 includes a deeper thematic, which is the relation between relative humidity, which can be an indicator of fogs, for instance, and the atmospheric electric field. A new model, according to some simplifications, is presented and shows a very close relation between *PG* and relative humidity when aerosols grow hygroscopically. (This information can maybe in the future be used for fog detection).

- Chapter 5 corresponds to the study of one of the most severe tragedies that occurred in the recent history of Lisbon. This event was the Chiado's fire and this study demonstrates the later effect of fire plume in the atmospheric electric field. This is the first study able to make a connection between the smoke plume dynamics and the *PG* response to it, which is very important not only because it is the first, but also it may enable, in the future, the study of smoke plume's motion with *PG* records as an extra tool for fire fight or any other idea that may arise.

- Chapter 6 presents a simple circuit model of the Global Electric Circuit coupled with a local circuit, measuring *PG* in fair-weather conditions. This is a first attempt to connect both things in order to separate the global effects from the local ones and to find values that are suitable to compare literature values for the Global Electric Circuit parameters with real data. This chapter is a preliminary work and is referenced for future work and development.

- Chapter 7 presents the conclusions of the thesis and future work is outlined.

2 Instrumentation and Signal Processing Techniques

2.1 Introduction

This chapter englobes the explanation of mathematical techniques and instruments used along the dissertation and a briefing about them.

2.2 Lord Kelvin's Water Dropper apparatus

A fundamental atmospheric electrical measurement is to acquire the electric potential at a known height, from which the vertical potential gradient (*PG*) can be obtained. This requires that minimal distortion of the potential occurs from the measurement apparatus, or that a correction can be applied for the distortion, since objects disturb the electrical field.

Lord Kelvin developed two *PG* sensors but only one of his instruments will be briefed here. Kelvin water dropper equaliser instrument comprised an insulated tank of water from which a continuous stream of water is allowed to flow (for example, out of a window), finally breaking into water drops: The water tank and an electrometer to measure the tank's potential would typically be installed on an upper floor of a building (**Figure 2.1**). At the stream to spray transition, droplets will polarize if their potential (which is that of the tank, via the connection provided by the water stream), differs from the local potential of the air. The effect of this polarization at the moment of drop release is to cause charge transfer between the water stream and the air, which continues until the potential of the water stream equals the potential of the air at the stream-spray transition point. Because the tank is connected through the water stream to the spray formation point, the formation point potential can be measured more conveniently at the tank. If the height of the stream-spray transition point is also determined, the vertical potential gradient can be found.

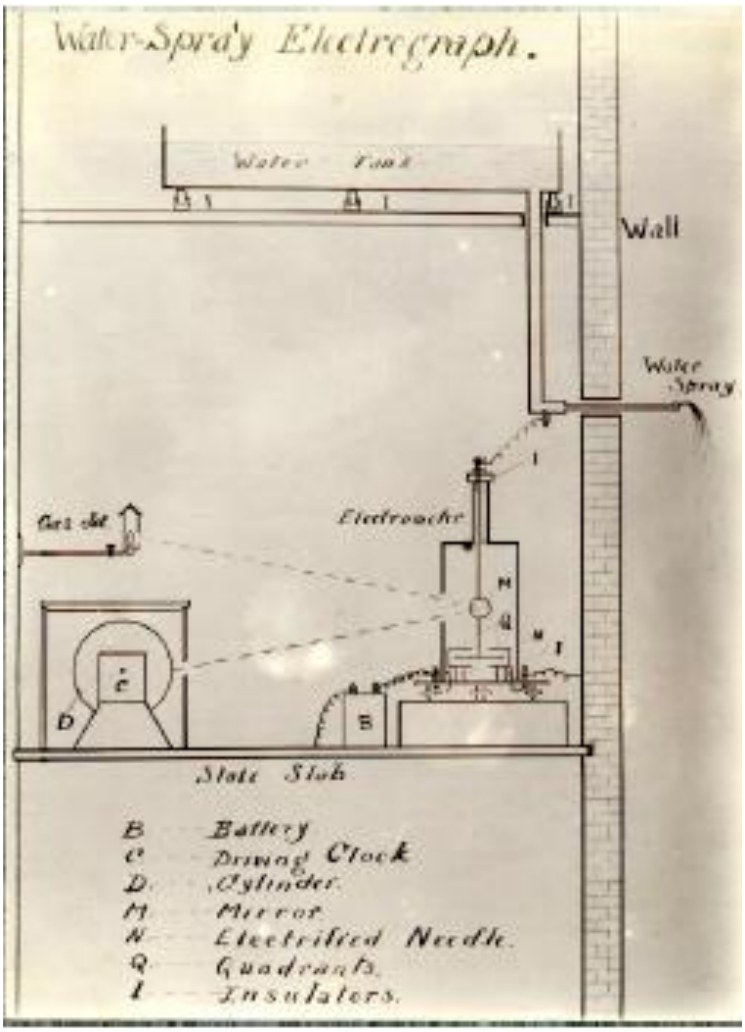

Figure 2.1 *Schematic of water dropper equaliser (Gendle, 1912).*

Lord Kelvin got even further and developed an automatic measurement system with the help of photographic paper and reflexion of light. A beam of light was reflected on a mirror, which was connected to the vane, which rotated based on the potential it acquired from air and the electrodes enclosing the vane. That beam of light was then reflected to photographic paper, where there was already a time and *PG* scale.

The zero was set as seen in **Figure 2.2** and the basic scheme can be visualized on it.

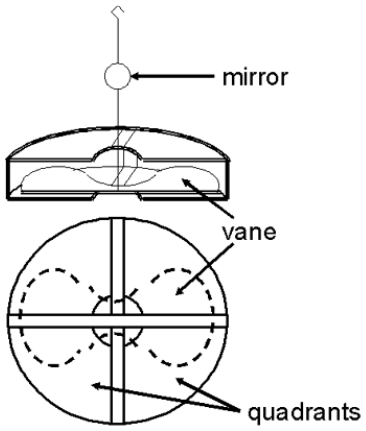

Figure 2.2 *Lord's Kelvin Electrometer schematic (www.orau.org).*

2.3 Benndorf Electrograph

A Benndorf electrograph was coupled to a radioactive probe to secure equality of potential between the sensor and the air and also improving the time response of the electrograph, since the radioactive decay impose an increase in ionization, allowing the sensor to measure small value fluctuations and at the same time a faster response . It was installed at 1 m above ground in a cement base recorded the *PG* at Portela meteorological station (Lisbon Airport, Portugal). Its sensitivity was checked using an electronic electrometer with standard voltage source between ± 200 V and the same calibration procedure was used in all periods of operation, from 1950's to 1990's. The analog records of the electrograph were digitalized afterwards (Serrano, 2010). Further details on the dataset can be found in (Serrano et al., 2006 and Serrano, 2011). Measurements with similar devices were made worldwide, e.g. (Shigeno et al., 2001).

This instrument was portable which is an advantage compared with the one from Lord Kelvin and data writing process was achieved through a telegraph technique.

Figure 2.3 *Benndorf's Electrometer (http://physik.uibk.ac.at).*

Sensor schematics can be seen next:

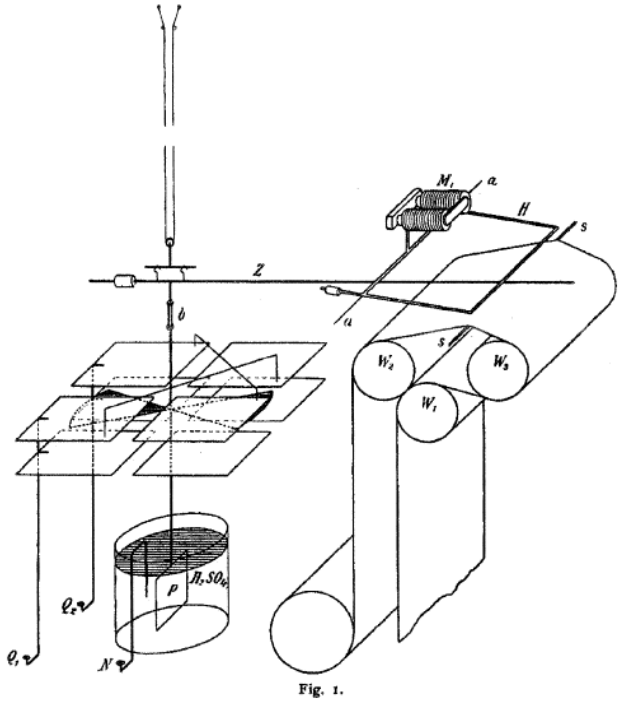

Figure 2.4 *Benndorf's Electrometer schematic (Klemens R., 2003).*

The 20 cm long pointer Z of aluminum wire is rigidly connected with the needle of the quadrant electrometer. It swings across a 12 cm wide paper strip, which is moved about 4 cm

per hour through a clockwork. The pointer will be pressed down from time to time and marks its position. For this purpose it lies a knitting needle s below the paper strip, above the paper strip lies a strip of "blue paper". If the stirrup H pressed the pointer down, a blue dot forms on the paper. Such so-called point recorder has the advantage of an almost non-existing hysteresis, therefore such recorders have been manufactured and distributed until the end of the 20th Century.

The clockwork drives the roll W1 for the paper transport. The print roll W2 prohibits the slippage of paper; W3 is only a deflector roll. Batteries supplied the electromagnet. The core of the electrometer has been isolated from the pointer Z by a piece of amber b. The supply line to the needle was through the contact N and the platinum sheet p in sulphuric acid, which served for damping the system.

If the quadrant pair Q_1, Q_2 have been put to the potential V_1, V_2 and the moveable needle to the potential V_N, there was a deflection of the pointer Z, where its intensity was determined by the torsional moment of the needle mounting was equally and opposing the moment evoked by the electrostatic forces. The measurements of the diagrams (paper roll) were carried out by glass scales.

2.2 Electric field mill JC 131/F

Because weather conditions are constantly changing, there exists a need to measure the strength of the electric field constantly, which translates into the need to alternately read the charged state of the sensor plate, discharge it, and read again, repeatedly. This is accomplished by repeatedly exposing the sensor plate to the external electric field to charge it, **Figure 2.5**(a), then shielding the plate to allow it to discharge, **Figure 2.5**(b). When the plate area is shielded, the charge on the plate must flow out, causing a current i_s to flow to ground.

This current is proportional to the atmospheric field as:

$$q_s(t) = \epsilon E_z A_s(t),$$
$$i_s(t) = \epsilon E_z \frac{dA_s}{dt}, \qquad \textbf{Eq. (2.1)}$$

where, A_s is the effective exposed area of the sensing electrode at the time t and ϵ is the permittivity of air. If the induced signal is rectified by a phase-sensitive detector (relative to the shutter motion), the DC output signal will indicate both the polarity and magnitude of the electric field.

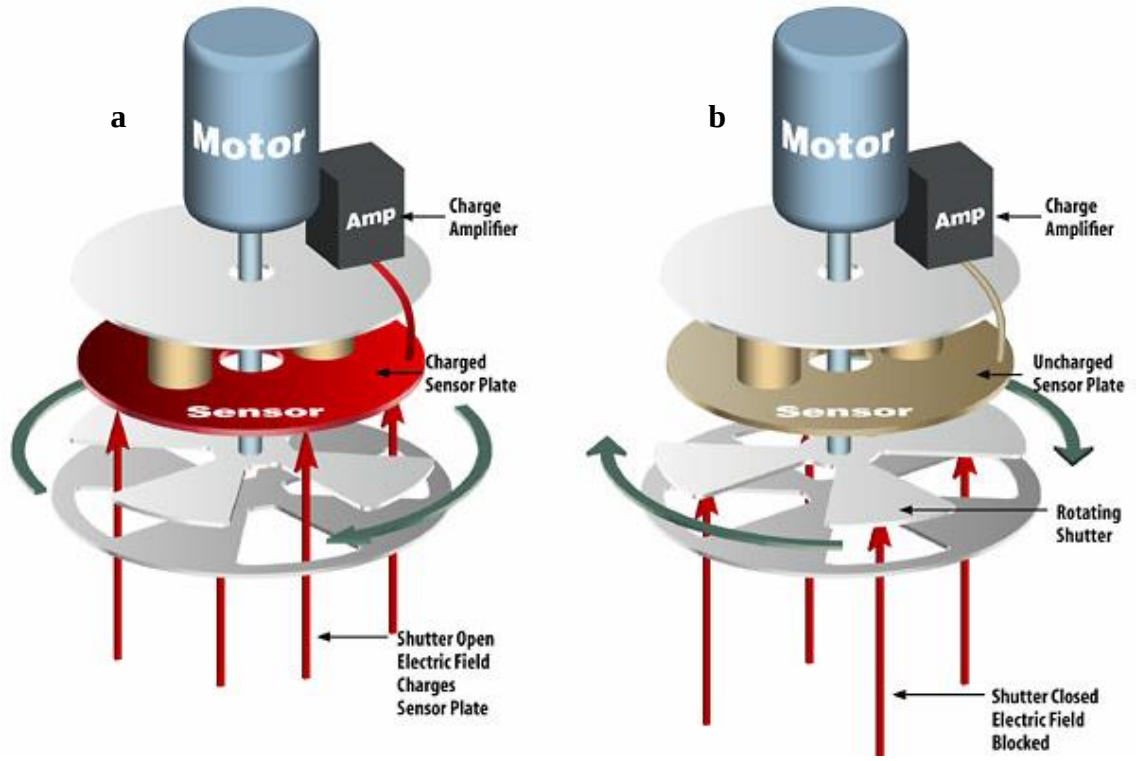

Figure 2.5 *Field mill operating principle (http://www.missioninstruments.com).*

One of the problems of this kind of sensor from **Figure 2.5** is that the rotor connected to the chopper, needs to be connected to the ground to discharge, so the measurements are not disturbed by any potential created by on the unearthed rotor on the sensing plate. Late models used a system with brushed to ground the rotor, which is expensive at long terms and obviously the sensor needs to be stopped so the brushed can be replaced, leaving some data unrecorded. The JC1 131 uses a new system, called back to back, where the rotor does not need to be earthed. The 'back to back' fieldmeter approach, (Chubb, 1990) is based on two

sensing plates. The secondary sensing plate is in a fully shielded enclosure. The signal arises just from any voltage on the rotor assembly. By backing off the signal of the primary fieldmeter by an appropriate fraction of the signal observed by the secondary fieldmeter signal it is possible to fully compensate for any net charge held on the rotor assembly.

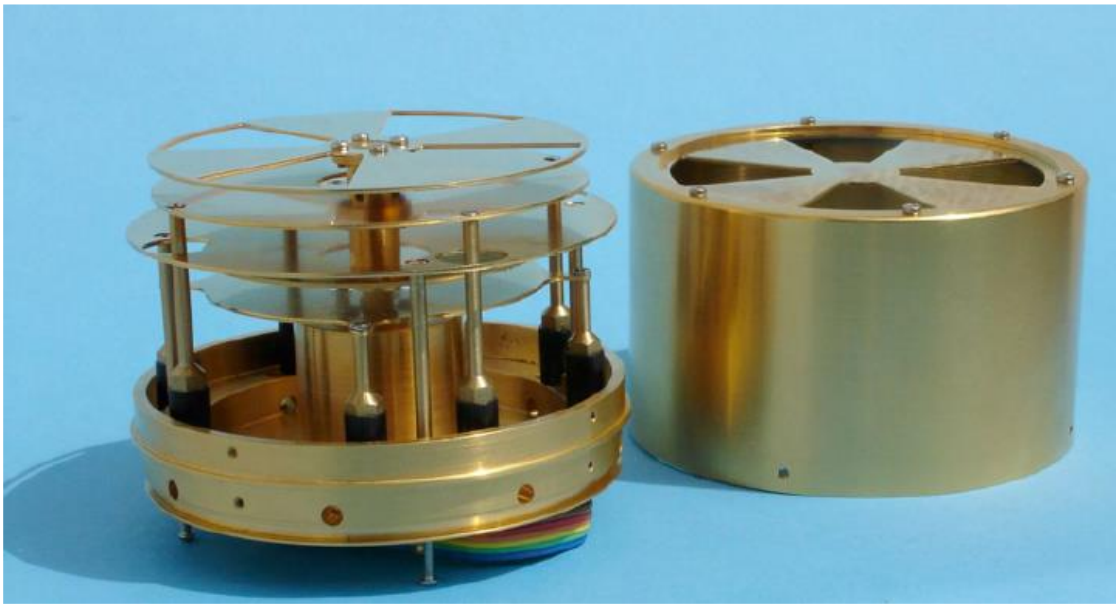

Figure 2.6 *JCI 131/F internal design.*

The JCI 131 Electrostatic Fieldmeter and JCI 131F, faster response version, is a compact and robust instrument for the precise measurement of electric fields in adverse environmental conditions. It is particularly suitable for long term continuous monitoring of atmospheric electric fields - such as those associated with thunderstorms, volcanic activity or power-lines.

Electric field measurement sensitivities of 2, 20, 200 and 2000 kV/m are provided with high precision (<1.5%), low noise. When used as a potential probe, well away from nearby structures, the sensitivity is about 10 kV/m for 1kV of local space potential, although critical applications should be underwritten by in-situ calibration. The basic chopping frequency is set close to 275 Hz. This frequency is chosen to be well away from harmonics of possible 50 or 60 Hz mains power supply signals. For the fast response version, the chopping frequency is 465 Hz.

If the sensitivity of a fieldmeter to the local voltage (or an applied calibration voltage) is *S* kV m^{-1} per kV, and at a height *z* in a local atmospheric electric field E_z shows an electric field E_o, then:

$$E_a = \frac{E_0}{Sz}. \qquad \textbf{Eq. (2.2)}$$

One problem with the use of electric field mills is that strong concentrations of ions can cause extra currents to be created in the field mill due to ions impacting on the vanes of the field mill. Field meters are often affected in an ion-filled environment by ion currents causing false results. The JCI 131 and JCI 131F are designed to be immune to the presence of ionized air by using phase sensitive detection. Ionization currents are out of phase with electric field signals in a rotating blade system and can therefore be removed.

Analogue output signals are provided from the JCI 131 and their observations may be recorded for analysis and re-display using computer based signal processing systems. A convenient approach is to use the Picoscope ADC-212, which has a resolution of 12 bits. It has a sample rate of 3 MS/s, which means three Mega samples per second, 3 MHz. It has a maximum range of ±20 V, which with 12 bits gives ~ 10 mV per step. In practice, this means that it can measure signals with frequencies to 1.5 MHz, although the signal will be very distorted. It should be used for lower frequencies data, like *PG*. In these kind of ADC it is warned that the sampling rate should be at least not two but five times the maximum frequency that needs to be measured.

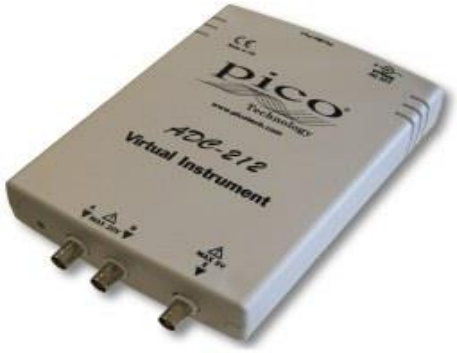

Figure 2.7 *Photograph ADC-212 (http://www.picoauto.com/).*

2.4 Discrete Fourier Transformation

The Discrete Fourier Transformation (DFT) is a very interesting tool with usage in signal processing for instance to retrieve frequency information about a time domain input. Fourier formulation is based on a projection of a discrete signal, with equally spaced samples, onto a basis made up of sinusoidal functions of varying frequencies. Its formulation is presented as:

$$X(\omega_k) = \frac{1}{N_s}\sum_{n=0}^{N-1} x(t_n)e^{-j\omega_k t_n}, \quad k = 0,1,2,\dots,N_s - 1, \qquad \textbf{Eq. (2.3)}$$

where $x(t_n)$ corresponds to the input signal amplitude at the time t_n, N_s the number of samples of the input signal, ω_k is the frequency sample and $X(\omega_k)$ is the spectrum of x at k^{th} frequency sample, ω_k. Some terms of **Eq. (2.3)** can be further expanded as:

$$t_n = nT, n\text{th sampling instant}, n \geq 0, \qquad \textbf{Eq. (2.4)}$$

$$\omega_k = \frac{k2\pi}{NT}, k\text{th frequency sample}, \qquad \textbf{Eq. (2.5)}$$

where T is the sampling interval. Implementing **Eq. (2.4)** and **Eq. (2.5)** in **Eq. (2.3)** and using Euler's identity it is found that:

$$X(\omega_k) = \frac{1}{N}\left[\sum_{n=0}^{N-1} x(nt)\cos\left(\frac{2\pi kn}{N}\right) - j\sum_{n=0}^{N-1} x(nt)\sin\left(\frac{2\pi kn}{N}\right)\right]. \qquad \textbf{Eq. (2.6)}$$

Looking at **Eq. (2.6)** it can be seen that this method projects the input signal $x(nt)$ within cosine and sine waves, resulting in a real and imaginary part, respectively. Indeed, each time the process runs, it projects each sample of the input signal within the corresponding sample of the basis functions at k cycles per N_s samples, meaning that k tells in which sinusoid the signal us being projected. Note also that the result of the first iteration, dot product between each sample of input signal and basis functions, is called DC component, since it is the average of the input signal.

Also note that if a time-varying signal is periodically sampled at a rate of at least twice the frequency of the highest-frequency sinusoidal component contained within the signal, then

the original time-varying signal can be exactly recovered from the periodic samples. Nowadays this concept is sometimes misinterpreted and mistakes like the next one usually happen: "I want to study the power lines which work at for instance 60 Hz, so I need a sample frequency of 120 Hz." As you might initially think, this is quite right according to the concept stated before. The thing is that this idea is completely wrong, because of the fact that power lines contain several harmonics of the fundamental frequency. For instance, one usually present is the fifth harmonic, which has 300 Hz, meaning that a sample rate of 120 Hz would not be even close to reconstruct the original sign in terms of frequency. This was just to state that the theorem itself can be very misleading and obviously, people need to be aware of the problem they are dealing with.

The result, $X(\omega_k)$, is usually reworked as the absolute value of the complex number and converted to decibels, dB, as shown:

$$\text{power spectrum} = 20\, log_{10}|X(\omega_k)|. \qquad \textbf{Eq. (2.7)}$$

The frequencies bins are given by:

$$f = \frac{k}{N_s} f_s. \qquad \textbf{Eq. (2.8)}$$

One problem of the method described in this section is what is called spectral leakage, caused when the input signal has different frequencies multiples of f_s/N_s, and the number of periods is not integer, generating discontinues at the end points. One technique to minimize this is to a priori multiple the time domain signal by a windowing function. Windowing functions approach zero at the beginning and end of the time domain signal, leading to a continuous wave form without sharp transitions. The operation of multiplying in the time domain the signals is equivalent of a convolution in frequency domain. This means that each peaks and side lobs on the input signal in the frequency domain will be shaped like the peak and sides lobs of the windowing function. However, how does this helps reducing the spectral leakage? Well, if the chosen windowing function can obliterate side lobs, meaning that it reduces their amplitude, it will lead to a decreasing, amplitude wise, of the artificial side lobs (spectral leakage) of the original input signal. However, the true frequencies that are hidden since the beginning will not appear but the spectrum will be much clear in terms of artificial

frequencies created by DFT approach. Other approach is known as Interpolated Discrete Fourier Transform (IpDFT), which based on the leakage spectrum, makes new calculations for frequencies and amplitudes, in order to be closer to the true solution.

2.5 Lomb-Scargle Periodogram

Another tool that is very useful in signal processing is the Lomb-Scargle Periodogram (LSP) since it permits the analysis of unevenly space data, which is a common phenomenon in real life measurements. Sometimes the sensors have problems and cannot measure for long periods of time, which results in missing data. This leads to the idea of padding the missing data with zeros or use some kind of interpolation and then use (DFT). The problem here is that if the data is very irregular, amplitude wise, due to anomalies or some other effects, the missing data that was filled with some method will end in very poor results.

This technique was developed for interrupted data sets in astrophysics (Lomb, 1976; Scargle, 1982), and has been extensively used in atmospheric science (Schulz and Stattegger, 1997; Hocke and Kampfer, 2009). The Lomb-Scargle Periodogram (LSP) is similar to the Discrete Fourier Transform, but it estimates the frequency spectrum based on a least squares fit of the sinusoids. In fact, the LSP spectrum converges to Fourier transform spectrum in the limit of evenly spaced observations. The LSP provides the significant frequencies and their respective amplitudes (in a statistical sense) enabling a proper evaluation of the dominant periods that influence the data. In this context, fair-weather *PG* is an unevenly distributed time series and for that reason, its spectral analysis must be made using the LSP technique, e.g. (Xu et al., 2013). The program used in the present study is an LSP implementation (Press et al., 1992), which was developed in MATLAB® (Brett, 2001).

The LSP is a method that does not fill any gaps, it analyses the data *x(t)* only where exists, from $i= 1,2,3\ldots N_s-1$, not leading to error due to padding.

The LSP Spectral Power (P_N) as a function of angular frequency $\omega=2\pi f$ is formulated as:

$$P_N(\omega) = \frac{1}{2\sigma^2}\left[\frac{\left(\sum_i (h_i - \bar{h_\iota})\, cos\left(\omega(t_i - \tau)\right)\right)^2}{\sum_i cos^2\left(\omega(t_i - \tau)\right)} + \frac{\left(\sum_i (h_i - \bar{h_\iota})\, sin\left(\omega(t_i - \tau)\right)\right)^2}{\sum_i sin^2\left(\omega(t_i - \tau)\right)}\right], \qquad \textbf{Eq. (2.9)}$$

where σ^2 is the data variance, $\bar{h_j}$ corresponds to the mean of the data and τ, value that makes the basis orthogonal at time i, is formulated as:

$$\tan(2\omega\tau) = \frac{\sum_i \sin(2\omega t_i)}{\sum_i \sin(2\omega t_i)}. \qquad \textbf{Eq. (2.10)}$$

The number of different frequencies (Press et al., 2002) N_f returned by the program is given by:

$$N_f = \frac{\text{ofac} \times \text{hifac}}{2} N_s. \qquad \textbf{Eq. (2.11)}$$

Where hifac is the higher frequency tested and ofac an oversampling factor and are used in the algorithm. Note that differently from DFT this algorithm uses statistical confidence tests to check a when peaks are from signal or artificial, for instance from leakage.

2.6 Adjusted boxplot

The boxplot is a very popular graphical tool to visualize the distribution of continuous univariate data. First, it shows information about the location and the spread of the data by means of the median and the interquartile range. The length of the whiskers on both sides of the box and the position of the median within the box are helpful to detect possible skewness in the data. Finally, observations that fall outside the whiskers are pinpointed as outliers, hence the boxplot also includes information from the tails. However, when the data are skewed, which is normally the case when analyzing *PG* records, usually too many points are classified as outliers. The adjusted boxplot (Vanderviere and Huber) is a generalization of Tukey's method (Tukey, 1977), which allows a robust outlier detection for skewed distributions.

Thus, the original boundaries, Upper boundary (U_b) and Lower boundary (L_b), for an outlier to be actually an outlier are not longer given by:

$$L_b = Q_1 - 1.5IQR;\ U_b = Q_3 + 1.5IQR, \quad \textbf{(2.1)}$$

where Q_1 represents the first quartile, Q_3 is the third quartile and *IQR*, (Q_3-Q_1), corresponds to the interquartile range. Instead, according to Vanderviere and Huber formulation the new boundaries are:

$$L_b = Q_1 - 1.5\exp(-3.5MC)\,IQR;\ U_b = Q_3 + 1.5\exp(4MC)\,IQR, \quad \textbf{(2.2)}$$

where *MC*, MedCouple, is a measure of the distribution skewness.

2.7 Dormand-Price Method

The Dormand–Prince method is a member of the Runge–Kutta family of ODE solvers. It uses six function evaluations, k_s ,as shown next, to calculate fourth and fifth order accurate solutions to initial value problems (IVP) such as:

$\dot{y} = f(t, y)$ with initial condition: $y(t_0) = y_0$. **(2.3)**

Here are the equations for k_s:

$$\begin{aligned}
k_1 &= hf(t_k, y_k),\\
k_2 &= hf\left(t_k + \frac{1}{5}h, y_k + \frac{1}{5}k_1\right),\\
k_3 &= hf\left(t_k + \frac{3}{10}h, y_k + \frac{3}{40}k_1 + \frac{9}{40}k_2\right),\\
k_4 &= hf\left(t_k + \frac{4}{5}h, y_k + \frac{44}{45}k_1 - \frac{56}{15}k_2 + \frac{32}{9}k_3\right),\\
k_5 &= hf\left(t_k + \frac{8}{9}h, y_k + \frac{19372}{6561}k_1 - \frac{25360}{2187}k_2 + \frac{64448}{6561}k_3 - \frac{212}{729}k_4\right),\\
k_6 &= hf\left(t_k + h, y_k + \frac{9017}{3168}k_1 - \frac{355}{33}k_2 - \frac{46732}{5257}k_3 + \frac{49}{176}k_4 - \frac{5103}{18656}k_5\right),\\
k_7 &= hf\left(t_k + h, y_k + \frac{35}{384}k_1 + \frac{500}{1113}k_3 + \frac{125}{192}k_4 - \frac{2187}{6784}k_5 + \frac{11}{84}k_6\right).
\end{aligned} \quad \textbf{(2.4)}$$

Then the next step value, y_{k+1}, is calculated as:

$$y_{k+1} = y_k + \frac{5179}{57600}k_1 + \frac{7571}{16695}k_3 + \frac{393}{640}k_4 - \frac{92007}{339200}k_5 + \frac{187}{2100}k_6 + \frac{1}{40}k_7. \quad \textbf{(2.5)}$$

This is a calculation by Runge-Kutta method of order 4, since the error over multiple steps (total accumulated error), is $O(h^4)$. Next, we will calculate the next step value, z_{k+1}, by Runge-Kutta method of order 5, since the error is $O(h^5)$,as:

$$z_{k+1} = y_k + \frac{35}{384}k_1 + \frac{500}{1113}k_3 + \frac{125}{192}k_4 - \frac{2187}{6784}k_5 + \frac{11}{84}k_6. \quad \textbf{(2.6)}$$

Calculate the difference between these two values:

$$|z_{k+1} - y_{k+1}| = \left|\frac{71}{57600}k_1 - \frac{71}{16695}k_3 + \frac{71}{640}k_4 - \frac{17253}{339200}k_5 + \frac{22}{525}k_6 - \frac{1}{40}k_7\right|. \quad \textbf{(2.7)}$$

The result in **Eq. (2.7**) is considered the error in y_{k+1}. Finally we calculate the optimal time interval h_{opt} as:

$$h_{opt} = h\left(\frac{\varepsilon h}{2|z_{k+1} - y_{k+1}|}\right)^{\frac{1}{5}}, \quad \textbf{(2.8)}$$

where ε is the error allowance in one step calculation. In MATLAB® relative tolerance, *reltol*[2] and absolute tolerance, *abstol* are used in a different ways to calculate h and to ensure the next step. The iterative process is based on the final simulation time point. One small note to take is that since the algorithm is step adaptive it may not end on the predetermined final point. Therefore, at the last stage of the algorithm, it rearranges h so that the final step ends on the final point in terms of abscissa.

[2] MATLAB ® has a different step, which is the calculation of an error with relative and absolute tolerance given by user as:

$$\text{error} = \frac{h(z_{k+1} - y_{k+1})}{\max(\max(abs(y_{k+1}), abs(y_k)), abstol)} < reltol;\ h_{opt} = 0.8\left(\frac{reltol}{error}\right)^{\frac{1}{5}}$$

3 PG measurements affected by pollution in Lisbon

3.1 Overview

The weekly dependence of *PG* with respect to pollutant aerosols in the urban environment of Lisbon (Portugal) was inferred from the records of atmospheric electric field at Portela meteorological station (38°47'N, 9°08'W). Measurements were made with a Benndorf electrograph. The data set ranges from 1955 to 1990, but due to the contaminating effect of the radioactive fallout during 1960's and 1970's (Pierce, 1972), only the period between 1980 and 1990 was considered. Using a relative difference method a weekly dependence of the atmospheric electric field was found in these records, which shows an increasing trend between 1980 and 1990. This is consistent with a population growth in the Lisbon metropolitan area and consequently urban activity, mainly traffic. Complementarily, using the Lomb-Scargle periodogram technique, the presence of a daily and weekly cycle was also found. Moreover, to follow the evolution of theses cycles, in the period considered, a simple representation in a color surface plot of the annual periodograms is presented. Furthermore, a noise analysis of the periodograms was made, which validates the obtained results. Two datasets were considered: all days in the period, and fair-weather days only.

3.2 Introduction

As discussed in the Introduction, in clean air, the global effect of thunderstorm activity can be apparent in *PG*, more precisely in the daily cycle known as the *Carnegie curve* (Harrison, 2013). Local effects arising from aerosol pollution contribute to additional variation in *PG* that may be very significant, when in a polluted environment. Thus, in an urban environment it is expected that the *PG* at the ground, where the measurements are carried out, to be predominantly influenced by the combination of the effects of local pollution with those of the Global Electric Circuit (GEC). Pollution affects the *PG* through the following mechanism: pollutant aerosols remove small ions from the air that are very important to the atmospheric electric conductivity because they have the highest electric

mobility. This removal causes the conductivity to decrease and therefore Ohm's law, **Eq. (1.3**), implies that the *PG* must increase (assuming that a constant electric current is present between the ionosphere and the Earth's surface, J_C). In fact, for a constant aerosol size distribution it is shown that the *PG* is positively and linearly related with the aerosol particle mass concentration (Harrison and Aplin, 2002). Such relation was further confirmed with measurements at Kew Observatory (Harrison, 2006), where there is a long record of simultaneous measurements of *PG* and pollution levels. Bearing this in mind, it was discussed the possibility of using *PG* data to retrieve pollution levels (Manes, 1977). Actually, such possibility is of great importance in sites that have historical *PG* data sets, like Lisbon, but where no pollution records are available, like the case of western Scotland (Aplin, 2012), where smoke emissions from industrial activity was inferred from Lord Kelvin's atmospheric electricity measurements. A similar situation occurs with the city of Lisbon, Portugal (**Figure 3.1**):

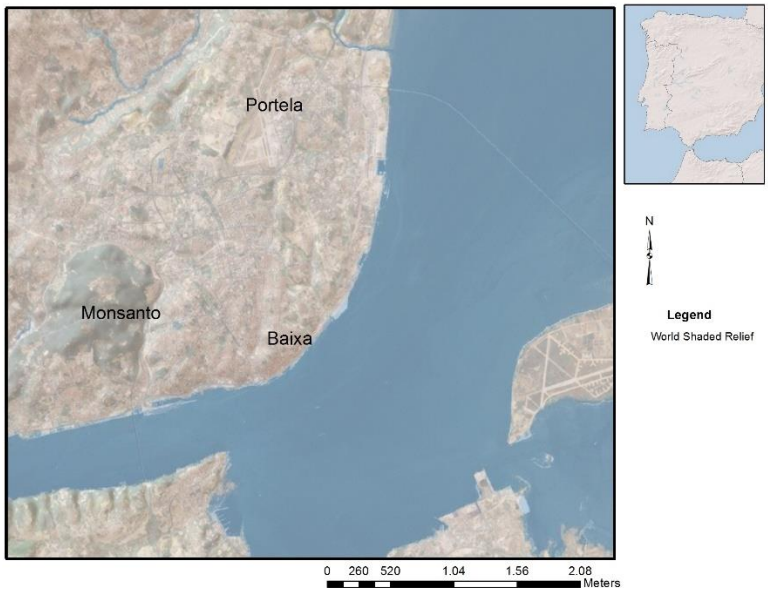

Figure 3.1 *Left figure, geomorphology of Lisbon region with three main features marked: Serra de Monsanto, Baixa (city center), and Portela Airport (location of the PG sensor). Right figure, the rectangle marks the geographical location of Lisbon in Portugal*

Lisbon is a polluted city and has a characteristic Mediterranean climate with fresh/rainy winters and a drought period during the summers (Andrade, 1996). It is geographically located near the coast and presents topographical features, marked by a slightly rugged relief,

associated with *Serra de Monsanto* with altitude of order 200 m on the west side, marked in **Figure 3.1**.

Moreover, to consider the effect of pollution in urban measurements of *PG*, as it is the objective of this chapter, it is important to clarify the main cycles that affect pollutant aerosols. These cycles are imposed by the city dynamics and are expected be present in the *PG* records too, since they are related to each other. Three main possible cycles are listed:

- *Daily cycle*: Two maxima are expected to appear, which correspond to the combined influences of urban pollution daily cycle and planetary influences (Harrison and Aplin, 2002; Harrison, 2009). One maximum shall develop in the early morning with the steep increase in city daily activities, followed by a decrease with the development of the planetary boundary layer[3] while another maximum shall occur in the evening, when the planetary influences intensify and then boundary layer convection weakens. Because local *PG* is affected by the global variation of the electric field, it is necessary to remove this variation in order to properly observe the effect of the urban daily cycle.

- *Weekly cycle*: During weekends urban activities decrease, causing less pollution than in workdays (Mondays to Fridays). This notation will be used throughout. Thus on weekends the *PG* is expected to be lower as compared with workdays, especially on Sundays (because pollutant aerosols generated during the workdays are significantly reduced by dry and wet depositions). In this way, this cycle can be linked exclusively to urban activities and for that reason it can be most useful to retrieve pollution historical records in the location where the *PG* measurements are made (Manes, 1977).

[3] Defined to be the lowest portion of the atmosphere, between 100 and 1000 m, directly influenced by the Earth's surface through its forcings within a timescale less than 1 hour. As the result of transport processes such as turbulence, due temperature changes in the surface, the PBL has a characteristic diurnal variation over land (Stull, 1950)

- *Annual cycle*: the spring/summer months are expected to have lower concentration of pollution near the ground, because of the reduction in traffic levels (especially during the holiday time, like in Lisbon), but also the increase of altitude of the planetary boundary layer. In fact, this cycle is dominated by seasonal variations (Reddell et al., 2004) related with the development and weakening of the convective layers in spring/summer and fall/winter, respectively. Such variations mask the effect of urban activity changes and one way of overcoming this is to look for seasonal variation in the weekly cycle.

In fact, the influence of weekly pollution dependence in urban environmental processes is now receiving a significant research effort (Williams and Mareev, 2014). The verification of the weekend effect in lightning (Bell et al., 2009), rainfall (Bell et al., 2008), both hail and tornadoes (Rosenfeld and Bell, 2011), and diurnal temperature (Forster and Solomon, 2003) reveals the importance of studying this cycle and the necessity of further research.

With that in mind, this chapter shows the signature caused by the weekly cycle in pollution on the *PG* recorded at Portela. Other effects have been previously studied with this set of data: cosmic radiation, artificial radioactivity, and aerosol concentration (Serrano et al., 2006a); relative humidity and wind intensity (Serrano et al., 2006b); seismic activity (Silva et al., 2012); but this is the first study addressing pollution.

3.3 Data

Mean hourly *PG* values were registered at the Portela meteorological station. In the present study two situations are studied: all weather *PG* (AW), which includes the entire *PG* dataset; and fair-weather *PG* (FW), selected as those hours with cloudiness less than 0.3, wind speed less than 20 km/h and absence either of both fog or precipitation. More details of the dataset can be found in the study of Serrano et al., 2006a.

It is important to mention that FW dataset has two drawbacks: it has significantly less data than the AW dataset (number of days given in **Table 3.1**), and it is difficult to find FW values of *PG* for a complete week and for this reason we had compared values for workdays and weekends that do not necessarily correspond to the same week. This implies that the results for FW data are not so statistically reliable compared with AW in respect to the study of the weekly cycle.

3.4 Methodology

- *Relative difference method:* An initial comparison was made between the normalized distributions of the *PG* for workdays and weekends for both AW and FW datasets. Furthermore, to quantify the effect of the weekly cycle the relative difference between the mean *PG* for workdays (Mondays to Fridays), $PG_{workdays}$, and for weekends (Saturdays and Sundays), $PG_{weekends}$, is calculated using the formulation:

$$\Delta PG\ (\%)\ = \left(\frac{PG_{workdays}}{PG_{weekends}} - 1\right) \times 100. \qquad \textbf{Eq. (3.1)}$$

  This formula is similar to the one used by Sheftel et al., 1994 which considers the ratio of the *PG* for workdays and for Sundays. Such a formulation was used previously to study the weekly effect on the electric conductivity of air (Tammet, 2009). Three average procedures for $PG_{workdays}$ and $PG_{weekends}$ were made: average per month (monthly means); average values that correspond to the same month for all years, e.g. the values of all Januaries in 1980-1990 (annual behavior); average per year (annual means).

- The periodogram, using LSP, for the entire data sets has been calculated. Moreover, to follow the evolution of the dominant periods (less than a year) the LSP is calculated for each year (with a two hour resolution that is twice the sampling time, according to Nyquist theorem), and the periodograms plotted in a color surface plot. To do this, estimations of the spectral amplitudes with respect to the same periods for all the years were considered. Thus, a vector was created with logarithmically spaced values from the initial period (always above the inverse of the Nyquist frequency) until the

final period (always below one year) and interpolated the values of the smoothed periodograms (moving averages of 5 values) using cubic spline interpolation. In this way, dominant periods appeared as horizontal lines across the plot.

3.5 Results and Discussion

The monthly mean values for the *PG* in AW and FW conditions for the period of study is presented in **Figure 3.2**(a).

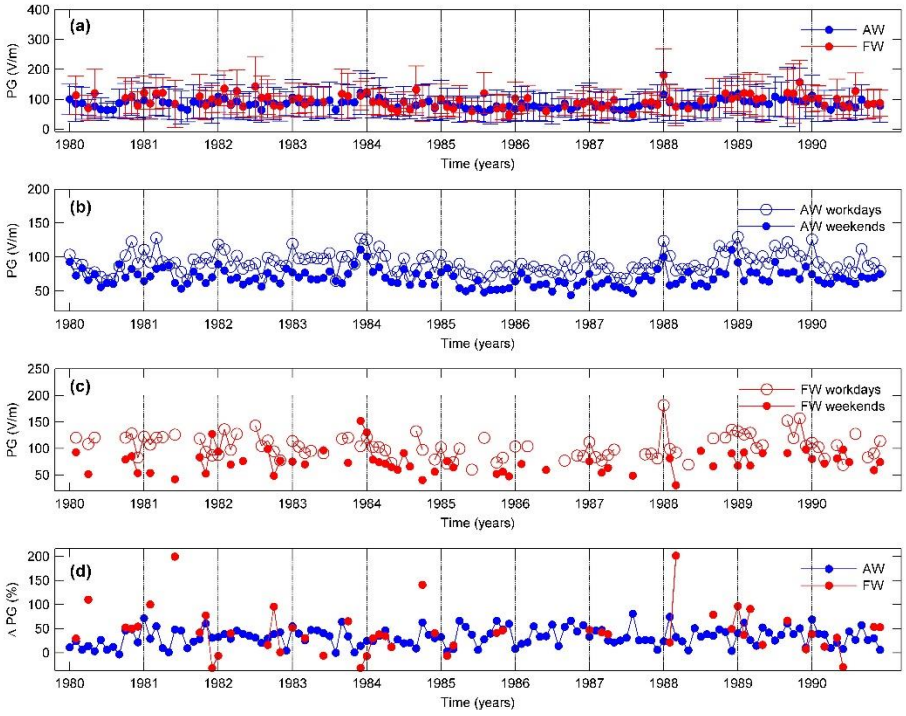

Figure 3.2 *Monthly mean values of PG measured from Portela during the period from 1980 until 1990: a) PG for AW and FW (error bars represent standard deviations); b) AW week and weekends PG; c) FW week and weekends PG; d) AW and FW-PG relative difference between workdays and weekends, ΔPG.*

Moreover, **Figure 3.2**(b) and (c) demonstrate that *PG* values at the weekends tend to be lower than the values for workdays, both for AW and FW. Actually, the monthly values of Δ*PG*, (d), are generally positive. This observation is confirmed by the distributions of *PG* values for workdays and weekends. The boxplots, **Figure 3.3**(a) and (b), show that the weekends have inter quartile ranges smaller than the ones for workdays, for both AW and FW.

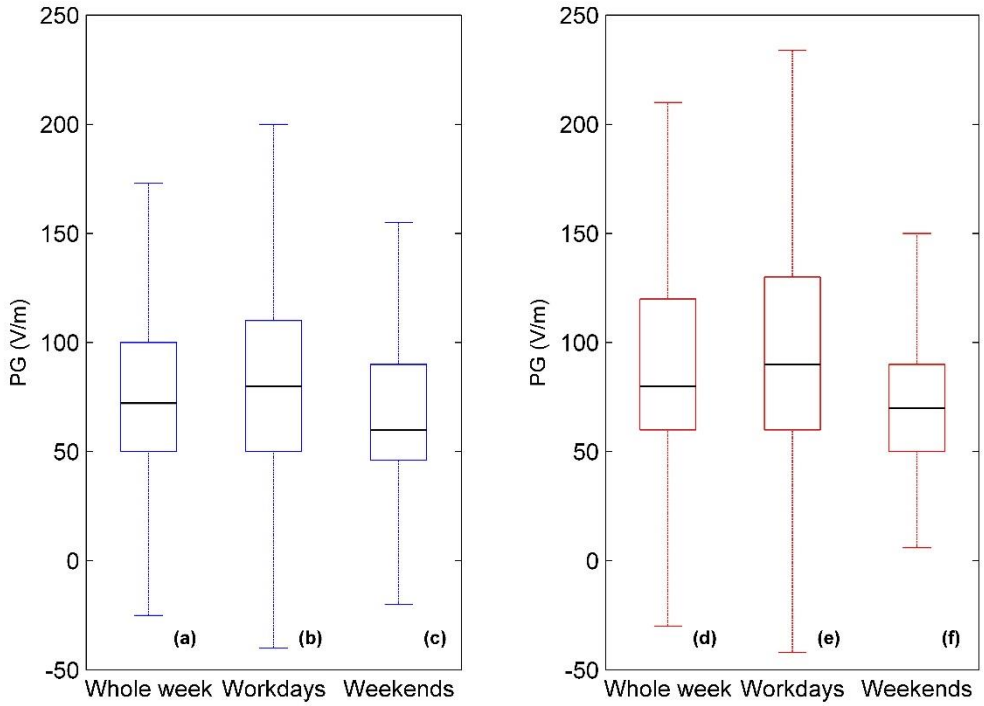

Figure 3.3 *Boxplot of hourly PG values for AW (blue): a) whole week, b) workdays, and c) weekend; boxplot for FW (red): d) whole week, f) workdays, and g) weekends. A black line in all boxes marks median and the outliers are not presented.*

Descriptive statistical parameters are presented in **Table 3.1**. These show the following:

- AW, mean values of *PG* for workdays, (90.87 V/m), is higher than for weekends, (69.39 V/m), the relative difference is 31.00 %. *PG* for workdays has a broader distribution, is more positively skewed and less prone to outliers than weekends.
- FW, *PG* shows a similar tendency, mean values for workdays, 101.72 V/m, higher than for weekends, 73.49 V/m, the relative difference is 38.41 %. Workdays *PG* has a boarder distribution, is more positively skewed and more prone to outliers than weekends.

Table 3.1 *Mean, median, standard deviation, skewness, kurtosis, and number of hours for the period between 1980 and 1990. The atmospheric electric field measurements are divided in: AW whole week, AW workdays, AW weekends, FW whole week, FW workdays, and FW weekends.*

	AW whole week	**AW workdays**	**AW weekends**	**FW whole week**	**FW workdays**	**FW weekends**
Mean (V/m)	84.73	90.87	69.39	94.27	101.72	73.49
Median (V/m)	72.32	80.00	60.00	80.00	90.00	70.00
Standard deviation (V/m)	54.81	58.64	39.88	54.96	59.35	32.11
Skewness	1.031	1.039	-0.1790	1.725	1.549	1.023
Kurtosis	13.364	11.180	29.25	7.710	6.671	4.972
Number of days	4018	2870	1148	356	262	94

The high relative differences statistically prove the existence of a week dependence of the *PG*, both for AW and FW. Actually, Israelsson and Tammet (2001) at Marsta Observatory, located in a rural region (10 km north of Uppsala, Sweden), measured air conductivities and calculated the relative differences using Sheftel's formulation (Sheftel et al., 1994). The relative differences they found are much lower than the relative differences found here for *PG*. Such disparity reveals the importance that urban pollution has on *PG* measurements.

The annual behavior of the *PG* for AW and FW conditions (shown in **Figure 3.4**(a)) demonstrate that summer months have the lowest mean values and standard deviations (August for AW and June for FW) and January has the highest for both AW and FW. Additionally, **Figure 3.4**(b) reveals that Δ*PG* has an annual behavior different from *PG* (AW and FW). Interestingly, Δ*PG* shows a minimum in December which is the month of the year with less urban activity (especially traffic) because of Christmas holidays. During the rest of the year, Δ*PG* behavior for AW appears to be more consistent with urban activity. Actually, it decreases from January until August (summer holidays) and increases again until October (a month with significant urban activity) decreasing again until December. On the contrary, Δ*PG* for FW has an increasing tendency from January until August and after that decreases. The reason for this is probably lack of FW data, as discussed above.

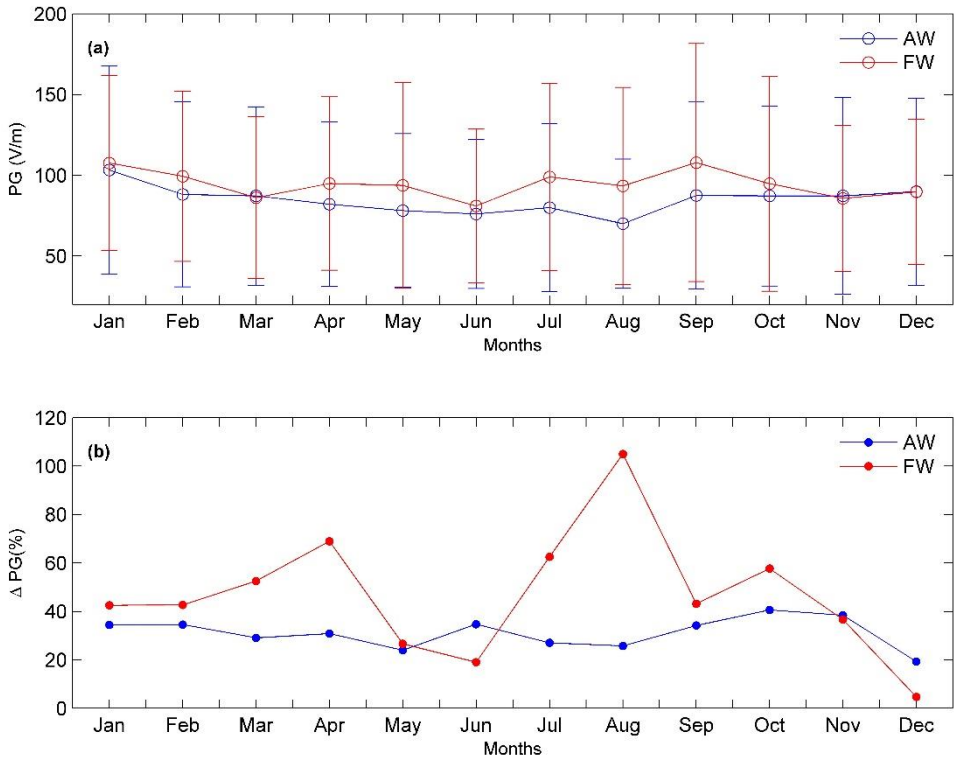

Figure 3.4 *Annual behavior of: a) PG for AW and FW; (b) ΔPG for AW and FW. Error bars represent standard deviations.*

Finally, the trend for annual averages of Δ*PG* (AW and FW) is shown in **Figure 3.5**(b) and year behavior in (a). Again, the behavior of AW and FW values of *PG* differs; AW shows an increasing trend and no trend is evident for FW. The tendency of Δ*PG* for AW is in accordance with the population growth in the Metropolitan Area of Lisbon in the considered period. According to the Portuguese National Statistics Institute (INE, 2011), the population in the Metropolitan Area of Lisbon has grown until the 1980's and stabilized in the 1990's. Actually, the most significant population growth occurred in the 1970's and the reason for that was the Portuguese democratic revolution of 25th of April 1974. Thus after it and until 1976 an important growth in the Portuguese population occurred due to the return of many immigrants from the former Portuguese colonies of Africa, as those nations claimed their independence (Moreira and Rodrigues, 2008). Because of such increase in population, there was an increase in urban pollution; which was mainly due to traffic intensification and industrial activity. In fact, the social processes involved in this relation of population growth

and pollution level was intensively studied, e.g. (Constant et. al, 2014) and links the demographic growth of the 1980's in Lisbon region with the development of the weekly cycle in the *PG* values. This relation adds a socioeconomic dimension to the studies of *PG* in urban regions as discuss in other works (Aplin, 2012).

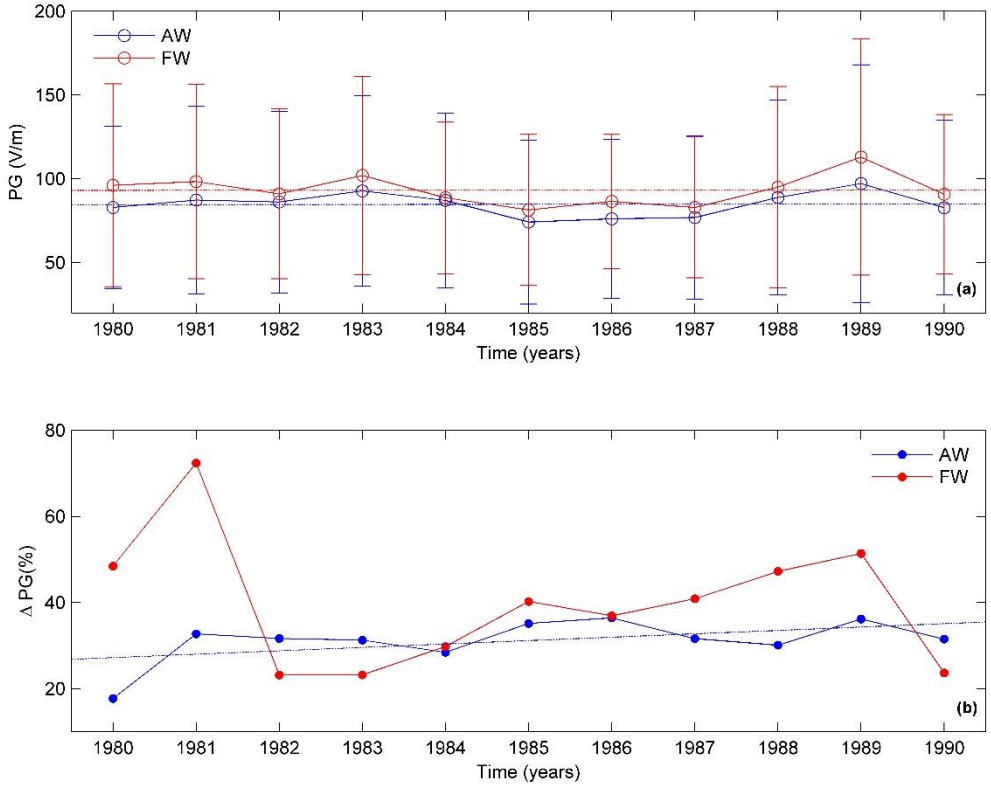

Figure 3.5 *Annual averages from 1980 until 1990: a) PG for AW and FW; ΔPG for AW and FW. Error bars represent standard deviations.*

Figure 3.6 (a) and (b) show Lomb-Scargle Periodograms calculated from *PG* data for AW and FW, respectively. As expected, the periodogram for AW contains more harmonic components than the FW one, especially for lower periods. The occurrence of two main cycles, daily, and weekly cycles, is evident in both data sets. Additionally, *PG* for AW shows two other cycles: an annual cycle caused by the seasonal meteorological variations, and half-day cycle (12 h period) likely to be related to traffic pollutant aerosols. Tchepel and Borrego (2010) have shown the presence of a significant influence of short-term fluctuations (12 h and 24 h periods) to the variance of both CO and PM_{10} measured in urban environments.

Those authors confirmed the contribution of traffic as the pollutant source using cross-spectrum analysis; which showed a correlation percentage from 45 to 70% between the pollutant concentrations and traffic dynamics (Tchepel and Borrego, 2010). Besides the main peaks mentioned, LSP in the AW case presents a myriad of other smaller peaks between the main ones; which are their sub-harmonics (Xu et a., 2013).

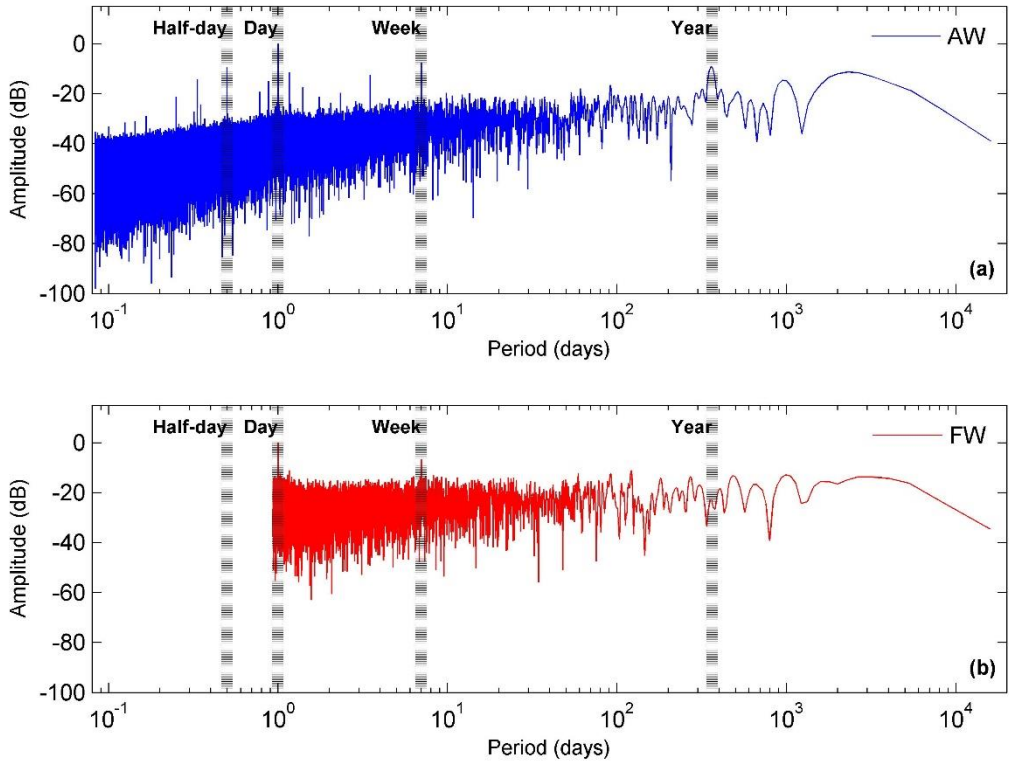

Figure 3.6 *Lomb-Scargle periodograms calculated using the LSP implementation in MATLAB (Brett, 2001) for 1980-1990: a) AW; b) FW. The following parameters were used hifac=1 (that defines the frequency limit as hifac times the average Nyquist frequency), ofac=4 (oversampling factor).*

To further clarify the evolution of the weekly cycle during the period of study, **Figure 3.7**(a) and (b) show color surface plots of the LSP using the procedure described previously. It is important to mention that due to the variation in the number of FW days, the band of periods observable in each year varies considerably; in the worst case, the periods accessible were above 1.63 days. For that reason the color surface plot for FW, **Figure 3.7**(b), is restricted to periods above 3.162 days. In the AW case, periods start at ~ 0.316 days (an order of magnitude lower). The amplitude is represented in a color map as a function of the period (*y*

axis) for the 11 years of analyzed data (*x* axis). For AW, **Figure 3.7**(a), the daily and weekly cycles are clearly seen by two horizontal red lines (labelled with the respective cycle) and confirm the persistence of the weekly cycle during the 1980s and beginning of the 1990s. In contrast, the color surface plot for FW, **Figure 3.7**(b), does not show the weekly cycle so clearly. Nevertheless, it enables us to see that the spectrum for 1986 responds most appreciably to low periods as compared to the other years (red blurs below the weekly cycle). This behavior can be tentatively related with the impact of Chernobyl nuclear accident (26 April 1986) on the global electric circuit (Takeda et. al, 2011); study of this effect is out of the scope of the present work.

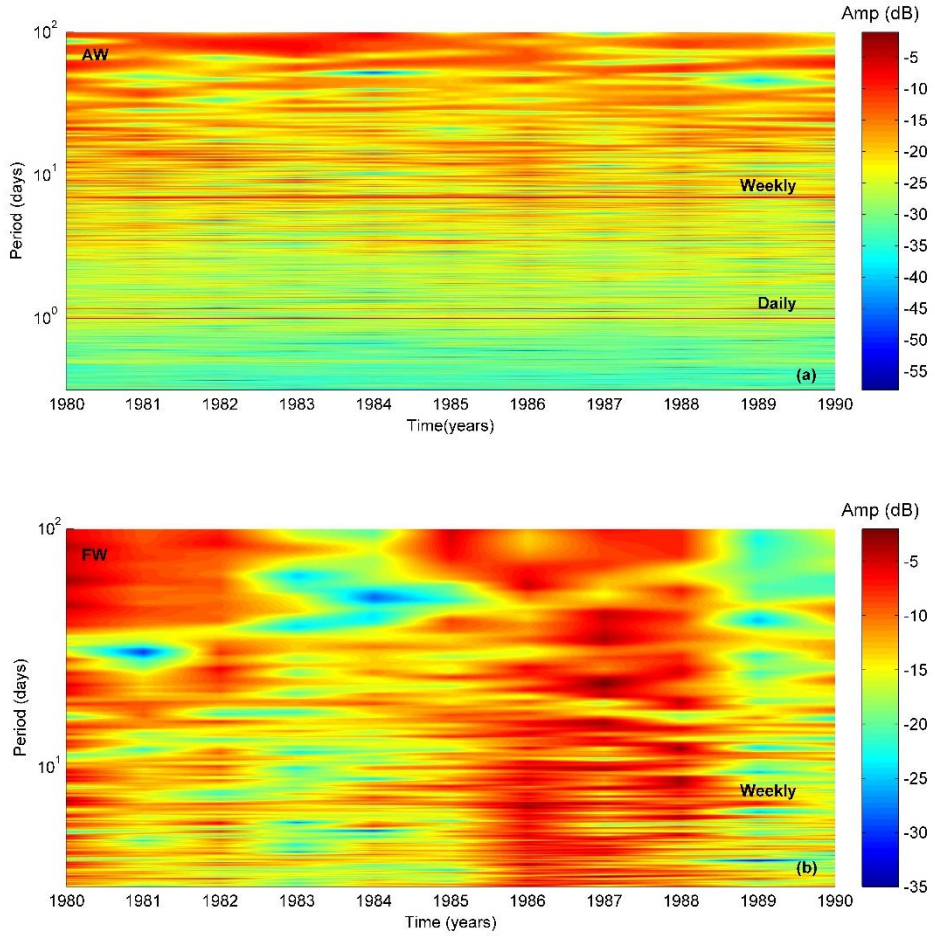

Figure 3.7 *Color surface plot of Lomb-Scargle periodograms for each year: a) AW; b) FW.*

The consistency of the color surface plots is confirmed by noise analysis of the LSP (Tuzlukov, 2002). This calculates, for each LSP, the *n*-exponent defined as a power law dependence of the power spectral density, $S(T)$, with the period, T, of the type, $S(T) \propto T^n$ .The

spectra are split into two parts: periods shorter than two days (twice the dominant 1 day period), and periods longer than two days. The exponents for periods shorter than T_c = 2 days are shown to be higher than exponents that correspondent to longer periods.

For AW, **Figure 3.8**(a), the *n*-exponents for $T < T_c$ are close to the 1/f noise (pink noise); this type of noise is present in many systems in nature and is of special interest (Dutta and Horn, 1981). Complementary, the *n*-exponent for $T > T_c$ diminishes over the studied years down to 0.5.

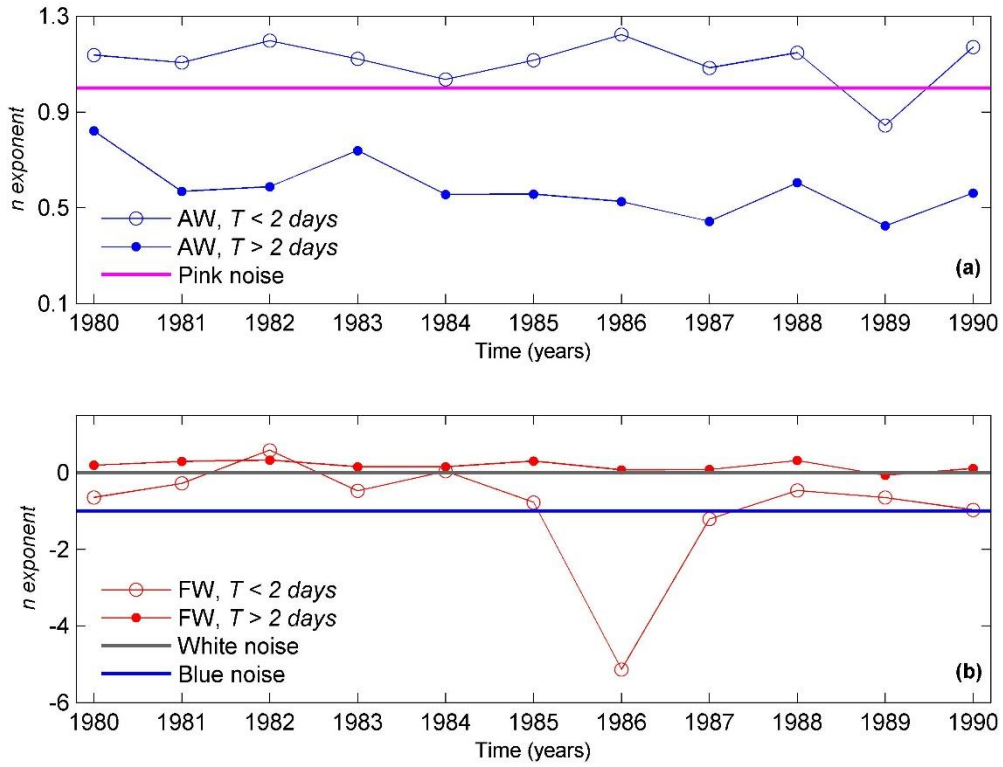

Figure 3.8 *Noise Upper panel: Evolution of the n-exponent from the Lomb-Scargle periodograms shown in Figure 3.6 and* ***Figure 3.7*** *along the years for period below T_c = 2 days (empty circle) and above 2 days (full circle): a) AW; b) FW.*

It is argued that such decreasing tendency (the opposite trend of ΔPG for AW) must be related with the increase in Lisbon pollution levels. Seen in this way, pollution causes a spread of spectral power for periods longer than T_c and tends to flatten the spectra. In fact, it is known that long-range transport of the pollution contributes to pollutant aerosols spectra at high

periods (Tchepel and Borrego, 2010). Additionally, because of the mentioned variation in the number of FW days per year it is difficult to properly study the evolution of the *n*-exponent for periods shorter than T_c = 2 days in this case. For these periods *n* tends to be negative, around −1 (blue noise), and has an anomalously low value for 1986. The negative values of *n* reveals that the *PG* responds better to processes with lower-periods and contradicts the behavior found for AW; this could be related with local perturbations that have typically small periods, e.g. the half-day cycle (Xu et. al, 2013). Nevertheless, the analysis of *n* for periods above T_c is found to have values near from, but not zero (white noise, $n = 0$). This is consistent with the behavior found in the AW case for periods above T_c. Again, this fact can be interpreted by a spread of power in the complete spectral band.

4 Aerosol hygroscopic growth and the dependence of atmospheric electric field measurements with relative humidity

4.1 Overview

A simple formulation is developed to model the influence of the aerosol hygroscopic growth in the dependence of the atmospheric electric field measurements with relative humidity. The formulation uses the Petters and Kreidenweis's model for the hygroscopic growth factor of aerosols with relative humidity and assumes that the ion-aerosol attachment coefficient is linearly proportional to the particle radius according to Gunn's formulation. A formula, which describes the atmospheric electric field increase with relative humidity in the regime expected for the aerosols to grow hygroscopically, between 60 % to 90 %, was found. It also relates the microphysical parameter of aerosol hygroscopicity, κ, with the macrophysical measure of the atmospheric electric field. Due to the high pollution levels in Lisbon (as discussed in the preceding chapter) the atmospheric electric field measurements were divided in four wind sectors, NW, NE, SE, and SW. The sector least affected by pollutant aerosols, NW, was used in the fitting and the following parameters were found: $r^2 \sim 0.97$, the aerosol concentration number is ~ 3280 cm^{-3} and the hygroscopic growth parameter $\kappa \sim 0.094$. These are very reasonable values consistent with an urban environment, which typically has high aerosol number concentration with small hygroscopicity. The limitations of the model are presented throughout the sections.

4.2 Introduction

Radiative forcing caused by aerosols (e.g. Li, 1998; Kaufman et al., 1998; Charlson et al., 1999; Markowicz et al., 2002; Lyamani et al., 2006; Foster et al., 2007; Obregón et al., 2014) is of relevance to the Earth's radiation balance and consequently to the Earth's climate. Special emphasis has been given to the direct radiative effect, in which aerosols scatter and

absorb radiation, and the indirect effect, in which aerosols as cloud condensation nuclei (CCN) are able to modify cloud droplet number concentration, size, and distribution (Pruppacher and Klett, 2010). Moreover, in CCN processes the increase in aerosol size with relative humidity (RH) through particle hygroscopic growth is of fundamental importance. For instance, as aerosol particles become larger in size than their dry equivalents, they scatter more light because of the increase in the particle cross-section, e.g. (Pilat and Charlson, 1966; Seinfeld and Pandis, 1998; Koloutsou Vakakis 2001; Carrico et al., 2000; Fierz-Shmidhauser et al 2010a; Titos et al., 2014a,b). Considering the hygroscopic growth patterns, aerosol particles can be divided into three categories. Some aerosol species like soot or mineral dust are insoluble; therefore do not grow significantly in size with increasing RH (Weingartner et al., 1997; Sjogren et al., 2007). On the contrary, some aerosol species like H_2SO_4 and some organics are hygroscopic, thus being able to take up water and grow or shrink smoothly as the RH increases or decreases. Finally, some aerosol species, e.g. sea salt, are also hygroscopic, but show hysteretic behavior and are called deliquescent aerosols. In fact, aerosol hygroscopic growth has been a research topic of considerable interest. Work has been done in field campaigns, e.g. (Duplissy et al., 2011), laboratorial experiments, e.g. (Rickards et al., 2013), and modeling, e.g. (Petters and Kreidenweis, 2007). In this context, it is usual to refer to the aerosol growth factor, $GF = R(RH)/R_0$, where $R(RH)$ stands for the particle wet radius for a given RH and R_0 is the particle dry radius. Various models have been used to describe GF; Petters and Kreidenweis's model (Petters and Kreidenweis, 2007) is commonly used in literature. This model is a key aspect of the formulation that will be presented below and is given by:

$$GF(rh) = \left(1 + \kappa \frac{a_w}{1-a_w}\right)^{1/3}. \qquad \textbf{Eq. (4.1)}$$

In **Eq. (4.1)** a_w is the water activity (related with RH) and κ is the hygroscopicity parameter. According to (Petters and Kreidenweis, 2007) the hygroscopicity of atmospheric particles is in the range from 0.1 to 0.9. Moreover, the authors show that if κ of each of the components is known it is possible to calculate the hygroscopicity of the mixture by weighting the component κ with the correspondent volume fractions. This implies that the κ of the mixture can also be obtained from measurements in the absence of information on its chemical composition. Such "effective hygroscopicity parameter" can then be used in modelling CCN

activity. In this context, the possibility of assessing κ from historical records of the Potential Gradient (*PG*) seems highly likely. In fact, *PG* records go back to the mid-nineteen century in different places of Europe, e.g. London (Harrison, 2006), Paris (Harrison and Aplin, 2003), and Glasgow (Aplin, 2012). Valuable historical information about aerosol properties (not only concentration) can be accessed this way. On one hand, the sensitive of atmospheric electric parameters to pollutant aerosols has long been proven, e.g. (Retails, 1977; Manes, 1977), and widely used to retrieve pollution dynamics in urban environments (Silva et al., 2014). On the other hand, it was previously shown that marine aerosol size increase with relative humidity is responsible for the decrease in Atmospheric Electric Conductivity (AEC), e.g. (Kamra et al., 1997; Deshpande and Kamra, 2004). To relate aerosol hygroscopic growth and *PG* measurements, a simple model is proposed here. In the literature, simple models relating aerosols and *PG* exist, e.g. Harrison and Aplin (2002) and Harrison (2012), and give very useful information about the atmospheric processes under study. As discussed in the Introduction, *PG* is a result of the action of the Global Electric Circuit (Wilson, 1920; Odzimek et al., 2010; Williams and Mareev, 2014) and the local joint effect of ions, aerosols and water droplets (Harrison, 2012). Ions act as charge carriers in the atmosphere and are the major contributors to electric conduction (Matthews et al., 2010; Wright et al., 2014b). In the lower troposphere the most representative negative ions are O_2^-, CO_3^-, NO_3^-, HSO_4^- while the positive ones are: H_3O^+, H^+, NO^+, NO_2^+, NH_4^+ (Harrison and Carslaw, 2003). These are known to form small ion clusters, like $O_2^-(H_2O)_n$, via hydration by water molecules (Harrison and Carslaw, 2003). This process reduces ion mobility and consequently decreases the AEC, which causes the *PG* to increase with *RH*. This is a possible mechanism explaining the *RH* dependence of the *PG*, at least in low *RH*, *RH* ~ 20 %. The change in the local ionization rate with *RH* is another mechanism to explain the dependence of the electrical parameters with *RH* (Israël, 1970; Israël, 1973); these two works go deep into the complexity of the processes being discussed here. Nevertheless, in urban environments the presence of aerosols alters significantly the electrical proprieties of the atmosphere (Manes, 1977). This is because aerosols scavenge conducting atmospheric ions and reduce AEC that, through Ohm's law (for a constant conduction current), causing an increase in *PG* (Retails, 1977). It should be mentioned here that this is a simplistic view in the sense that the charge is still present, but is carried by larger and less mobile charged aerosols, which contributes much less to

conductivity (Wright et al., 2014a). Besides, it is known that the ion-aerosol attachment coefficient (β_a) depends on the radius (R_a) of the particles (Gunn, 1954) as:

$$\beta_a = \frac{4\pi k_B T_e \mu}{e} R_a, \qquad \textbf{Eq. (4.2)}$$

where k_B is the Boltzmann constant, T_e is the ambient temperature (considered here as 293 K), μ ion electric mobility and e electron charge. Thus it is expected that the increase in the aerosol size with RH would imply the scavenging of more ions and consequently the decrease in AEC and increase in PG; such process is expected to dominate the relative humidity dependence of the PG mainly in the RH range where aerosols grow hygroscopically (Kamra et al., 1997). Different types of aerosols would give different contributions according to their hygroscopicity; only the aerosols that grow hygroscopically would contribute. In particular, soot, a common pollutant aerosol in urban environments does not grow hygroscopically and for that reason, it would not contribute to the PG dependence with RH. This is an important aspect and will be discussed in the next sections. Moreover, RH between ~60 % and ~90 % can be considered as a reasonable range where aerosols grow hygroscopically (Kamra et al., 1997; Petters and Kreidenweis, 2007; Rickards et al., 2013). For high RH, especially close to saturation, CCN processes will dominate and droplet formation will start (Nicoll and Harrison, 2010). In this context, Harrison (2012) explored the induced effect of aerosols on the atmospheric electric field in cases of reduced visibility with the presence of water droplets. However less attention was given to the formulation of models describing the role that aerosol hygroscopic growth has in the atmospheric electricity (Deshpande and Kamra, 2004), in particular in the Potential Gradient. A simple model was developed here to describe the contribution of hygroscopic aerosol growth in the Relative Humidity dependence of the Potential Gradient.

4.3 Formulation

Keeping in mind these arguments a basic formulation of the influence that aerosol hygroscopic growth has in PG is presented. The RH range of validity of the model is between ~60 % and ~90 % (as discussed above) and the limitations of the model will be pondered during the formulation. The first step in the formulation is to consider the equation for ion

balance in an environment containing aerosols with the formalism developed by (Hoppel, 1985). Starting with a variable change in **Eq. (1.11**), the next equation is obtained:

$$n = n_\infty \left(\sqrt{x^2 + 1} - x\right), \qquad \textbf{Eq. (4.3)}$$

where $n_\infty = \sqrt{q/\alpha}$ is the steady state ion concentration when no aerosols or droplets are present (Harrison and Carslaw, 2003), and x is given by:

$$x = \frac{\beta_a Z_a}{2\sqrt{\alpha q}}. \qquad \textbf{Eq. (4.4)}$$

It is assumed that the AEC is given by $\sigma_t = 2\mu e n$; here the contribution of charged aerosols to the total atmospheric electric conductivity is neglected. This is an approximation required to maintain the simplicity of this model, but it is reasonable to do so, as it is known that charged aerosols contribute less to conduction due to their lower mobility, as compared with atmospheric ions (Wright et al., 2014a). Actually, this contribution is often neglected in similar models, e.g. (Harrison and Aplin, 2002; Harrison, 2006; Harrison, 2012). Thus, using Ohm's law it is possible to relate σ_t and PG:

$$PG = \frac{J_C}{\sigma_T} = \frac{J_C}{2\mu_m e}\left[n_\infty \left(\sqrt{x^2 + 1} - x\right)\right]^{-1}, \qquad \textbf{Eq. (4.5)}$$

where J_C is the air-Earth conduction density current. Using standard values of $J_C \sim 2$ pA m^{-2}, $\mu \sim 1.2$ cm^{-2} V^{-1} s^{-1}, $\alpha \sim 1.6 \times 10^{-6}$ cm^3 s^{-1} and $q \sim 10$ cm^{-3} s^{-1} (Harrison and Carslaw, 2003) and assuming a typical $PG \sim 100$ V/m, it is found that $x \sim 2.3$. In fact, in cases with high aerosol number concentration it is expected that $x \gg 1$ and **Eq. (4.3)** can be written as:

$$n = n_\infty x \left(\sqrt{1 + x^{-2}} - 1\right) \approx \frac{n_\infty}{2x} = \frac{q}{\beta_a Z_a}. \qquad \textbf{Eq. (4.6)}$$

The approximation in **Eq. (4.6)** was accomplished by a Taylor series expansion of the square root, neglecting $O(x^{-4})$. Hence **Eq. (4.5)** simply becomes:

$$PG \approx \frac{J_C}{2\mu_m e q}\beta_a Z_a = \frac{2\pi J_C k_B T_e}{e^2 q} R_a Z_a. \qquad \textbf{Eq. (4.7)}$$

In **Eq. (4.7)** the ion-aerosol attachment coefficient β_a was substituted by the formula derived by Gunn (1954) and presented in **Eq. (4.2)**. Notice that the particle radius should not be seen as a real particle size of a monodisperse aerosol size distribution, rather as an "effective

attachment radius" representative of a polydisperse aerosol size distribution subjected to electrostatic forces (Hoppel, 1985). In the formulation that was developed here, the attachment coefficient is modeled to retrieve "effective aerosol proprieties" from *PG* values, in particular aerosol concentration. Equation **Eq. (4.7)** reveals that the *PG* is proportional to the product of aerosol radius and concentration, $R_a Z_a$, and does not depend on the ion mobility. This is a significant result from the model as the reduction in ion mobility with RH can be a possible cause for AEC decrease (*PG* increase) with RH in clean environments. Obviously, it is important to remark that this is only valid for the high aerosol concentration regime, e.g. an urban environment (Silva et al., 2014) or a fire (Conceição et al., 2015). Actually, **Eq. (4.7)** is similar to the one found by Harrison and Aplin (2002). The last step in the formulation is to describe the R_a growth with RH. To do that **Eq. (4.1)** is used and a simplification is made assuming that water activity is given by $a_w = rh = RH/100$. This is a good approximation in the regime of validity of the present model where RH is restricted from 60 % to 90 % (Rickards et al, 2013). Similarly to the discussion presented for the "effective aerosol radius", in real atmosphere GF will vary accordingly to the dry size and composition of the aerosols, thus here the hygroscopicity parameter, κ, should be interpreted as an "effective hygroscopicity parameter" representative, in a statistical sense, of the actual polydisperse aerosol size distribution. Finally, the equation relating *PG* and RH through aerosol growth is found:

$$PG \approx \frac{2\pi J_C k_B T_e}{e^2 q} Z_a R_{a,0} \left(1 + \kappa_a \frac{rh}{1 - rh}\right)^{1/3}. \qquad \textbf{Eq. (4.8)}$$

In **Eq. (4.8)** Z_a, $R_{a,0}$ and κ_a are the number concentration of aerosols, the dry radius, and the hygroscopicity parameter, respectively. This equation relates, in a simple formulation, three significant microphysical aerosol parameters: number concentration, dry radius and hygroscopicity parameter with two macrophysical measurements: Potential Gradient and Relative Humidity. Obviously, the microphysical parameters must be considered as "effective parameters" in the statistical sense described above and not "precise parameters". Here the significant point is that in macrophysical radiative modelling the "effective parameters" are more relevant than the precise measurements of those microphysical parameters (Petters and Kreidenweis, 2007).

4.4 Data

In the present analysis, only non-negative values of *PG* were selected because negative *PG* values are not a consequence of *RH* as they are linked to rain and shower clouds. On the contrary, positive values of *PG* ~ 400 V/m, are found under high *RH* condition, for example, in the case of fogs (Deshpande and Kamra, 2004). Thus when studying the dependence of the *PG* with *RH*, it is important to include these cases, that are usually rejected under the fair-weather conditions, Voeikov (1965). This is the reason why a strict fair-weather selection is not fully appropriate to the present study. It should be mentioned that positive charged clouds also exist and affect the *PG*, though less statistically significant in Lisbon with low cloud cover percentages (ranging from 28 % in summer and 61 % in winter). A wind rose and location of measurement site and surroundings is shown in **Figure 4.1**.

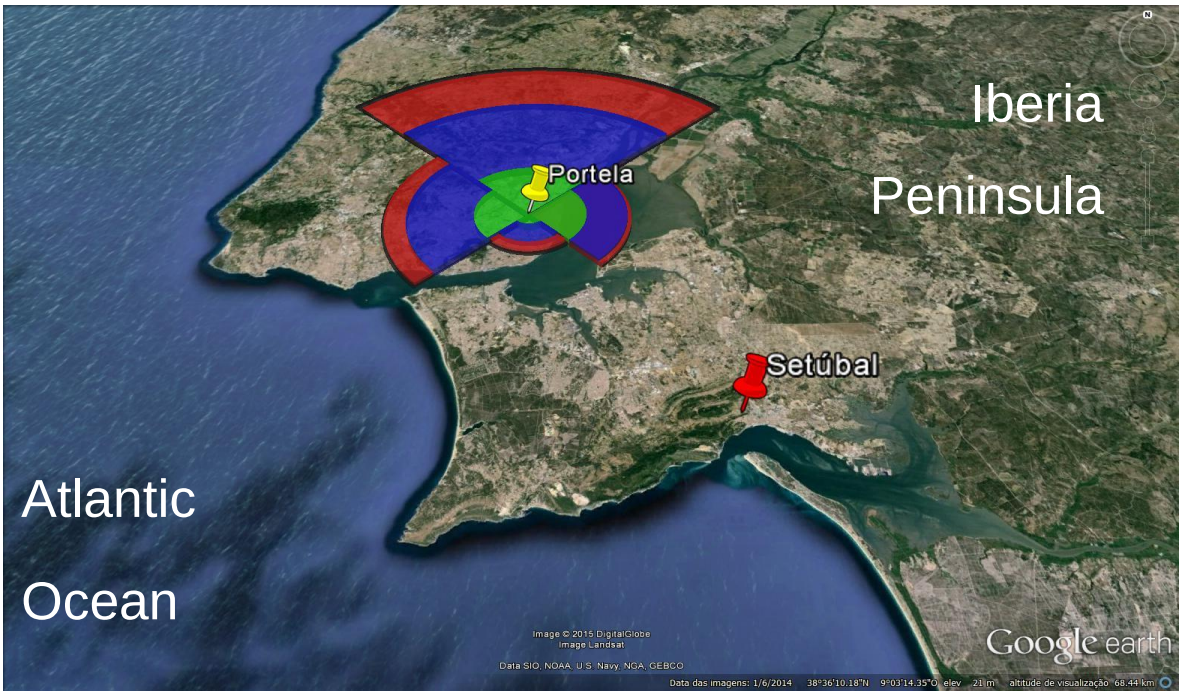

Figure 4.1 *Location of the Portela meteorological station (yellow pin) and the industrial region of Setubal (red pin) are marked. The Atlantic Ocean and Iberian Peninsula are also indicated. A wind rose measured at Portela is also shown.*

Precipitation and snow further perturb the *PG* and for that reason "manually observed present weather", (MW) was used. *PG* values having MW in the range of 50 - 99, which corresponds to "precipitation at the station at the time of observation", were excluded. Relative humidity

was calculated from air temperature and dew point measured in Portela meteorological station.

During the 1980s most of the industries and main pollution sources in the region were located to the south of Tagus River, in Setubal region. Therefore using the station as a geographic reference, the mentioned main pollution sources can be found in the southern sector while in the northern sector, such sources are scarcer (and population is lower). The Tagus river basin and the Iberian Peninsula are located to the East whereas the Western sector is covered by the Atlantic Ocean. Pollution has the effect of increasing the *PG* (Silva et al. 2014, and the references therein), thus it is expected that south winds correspond to higher *PG* values than northern ones. Furthermore, westerly winds are able to transport marine aerosols, which are known to have higher electrical mobility than those transported from continental regions (Wilding and Harrison, 2005). For that reason lower *PG* values are expected to be associated to winds from the west as compared with those from east. These features were observed in Silva et al. (2015) and according to that procedure *PG* is divided into four wind sectors:

1) NW, $270^{\circ} \leq \theta \leq 360^{\circ}$;

2) NE, $0^{\circ} \leq \theta \leq 90^{\circ}$;

3) SE, $90^{\circ} \leq \theta \leq 180^{\circ}$;

4) SW, $180^{\circ} \leq \theta \leq 270^{\circ}$.

Matthews (2012a,b) previously applied this methodology to study the impact of high voltage power lines on the local *PG*. It is worth to mention that the prevailing winds in Lisbon are from NW (**Figure 4.1**) and result from the Iberian thermal depression (Costa et al., 2010). From the considerations presented this far it is expected that the NW sector corresponds to lower *PG* values than those associated to the NE and SE sectors; regarding the SW sector, where winds bring both marine and polluted air, the *PG* values are expected to be higher than in the NW, but smaller than in the SE. These results are depicted in the histograms of **Figure 4.2** and further statistical parameters are presented in **Table 4.1**.

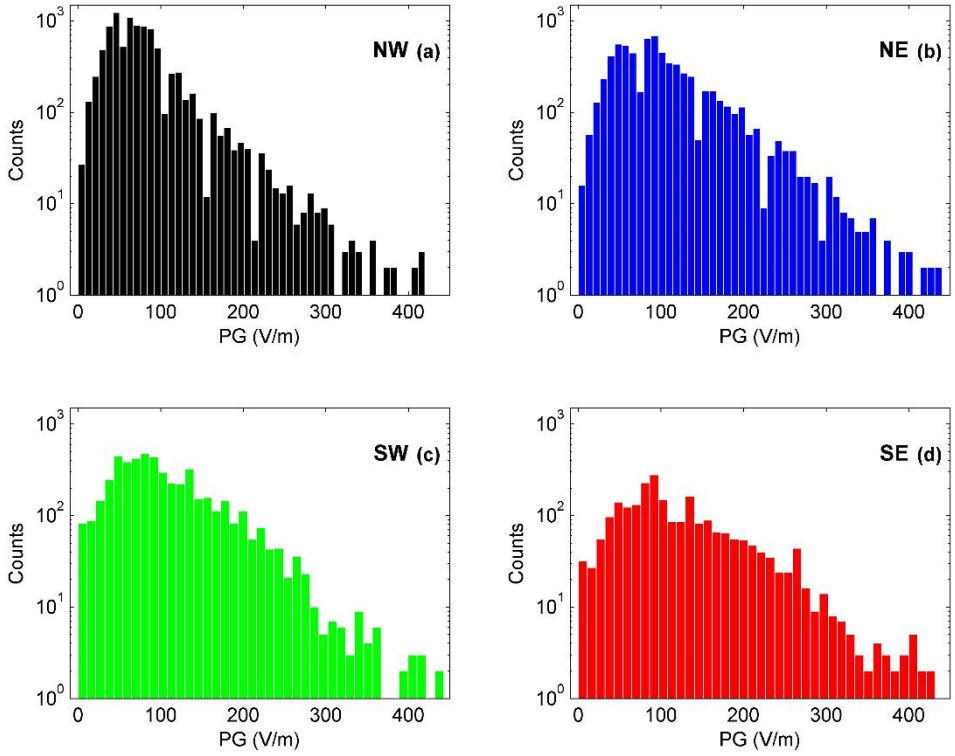

Figure 4.2 *Distributions of the hourly PG values, in logarithmic scale, for the four wind sectors: NW, NE, SE, and SW.*

Table 4.1 *Mean, median, Median Absolute Deviation (MAD), skewness, kurtosis, and number of hours for the period between 1980 and 1990. The atmospheric electric field measurements are divided in: NW, NE, SE, and SW.*

	NW	**NE**	**SE**	**SW**
Mean (V/m)	75.4	101.1	119.5	104.1
Median (V/m)	67.0	90.0	100.0	90.0
MAD (V/m)	30.7	43.7	54.7	47.4
Skewness	2.03	1.34	1.13	1.20
Kurtosis	9.81	5.48	4.61	5.10
Number of days	385	283	95	204

The median *PG* values are consistent with the previous arguments: NW, 62.3 V/m; NE, 80.0 V/m; SE, 91.1 V/m; and SW, 90.0 V/m. Additionally, the daily variation of *PG* corresponding to the four wind sectors is presented in a boxplot[4] representation, **Figure 4.3**, and show similar behavior.

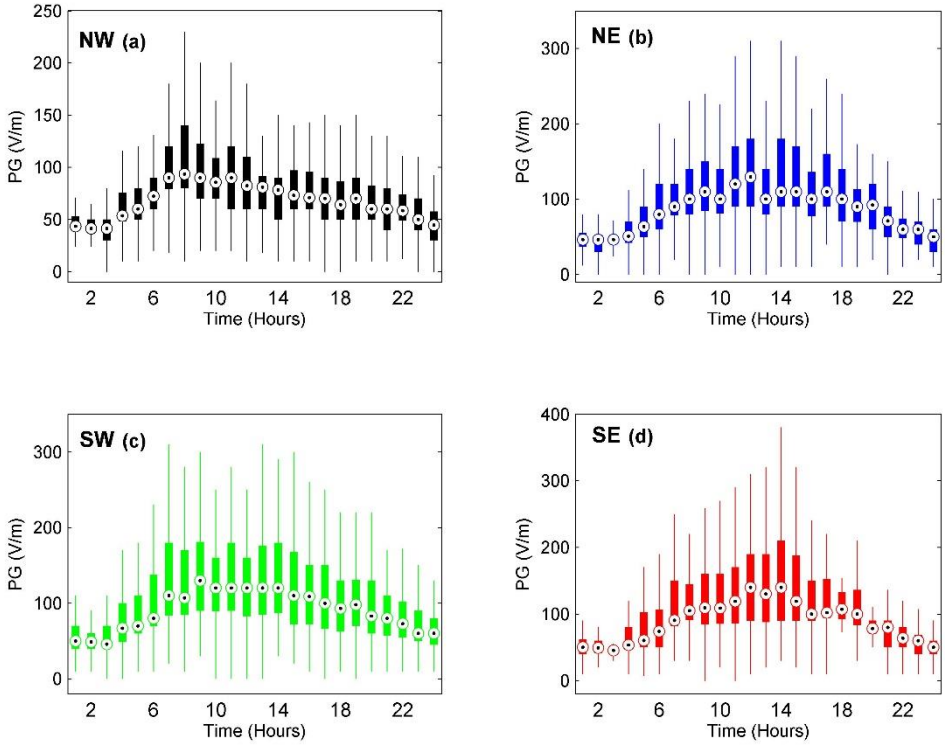

Figure 4.3 *Daily behavior of hourly PG values in a boxplot representation. The four wind sectors are considered: NW, NE, SE, and SW.*

It is verified that in the beginning and end of the day low values of *PG* are observed, around ~ 50 V/m. Daily *PG* curves measured inland often differ from the Carnegie curve mainly due the action of local phenomena, for example, convective currents (Tacza, 2014). Convective currents due to the presence of the Atlantic Ocean could, in fact, be a reason explaining such

[4]On each box, the central dot is the median, the limits of the box are the 25th (first quartile, q_1) and 75th (third quartile, q_3) percentiles and the whiskers (solid lines) extend to the most extreme data points not considered outliers. Maximum whisker length (w) is set to 1.5 and outliers are defined to be larger than $q_3 + w(q_3 - q_1)$ or smaller than $q_1 - w(q_3 - q_1)$.

low values measured at Portela; nevertheless, investigation of such mechanism is out of the scope. Even though, the daily behavior for the NW is slightly different from the other three sectors as it shows less variability and the peak observed in the other wind sectors at 18:00 h is reduced in this one. In fact, for *PG* measurements carried out in urban environments, the peak at 18:00 h is a combination of the maximum of the Global Electric Circuit activity, Carnegie curve (Harrison, 2013) and of the air pollution generated at the end of the workdays (Harrison, 2009). Also winds from the NW sector are most likely to occur during this time of the day (known as *Nortada*, Alcoforado et al. 2006). Hence, the reduction of the 18:00 h peak for NW sector can be an indication of a more efficient removal of air pollution. Finally, daily averages, **Figure 4.4**, are calculated for both *PG* and *RH*, reducing the variability of these parameters.

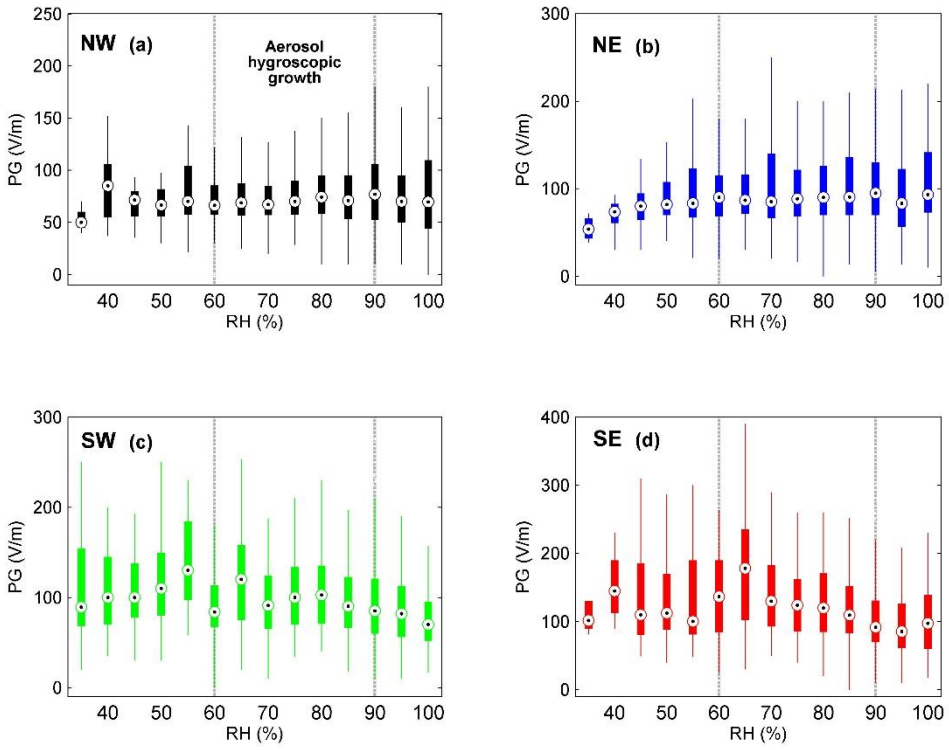

Figure 4.4 *RH dependence of daily averaged PG values of all sectors: NW, NE, SE, and SW. Bins with ΔRH = 5 % in the RH range from 30 % to 100 % were used. The label attributed to a bin corresponds to its upper limit. Vertical lines mark the hygroscopic growth region, in which the analysis is focused.*

4.5 Results and discussion

PG as a function of RH is shown in a boxplot representation in **Figure 4.4** for the four wind sectors. *PG* values were separated into RH bins with a given width, ΔRH = 5 %, from RH = 35 % up to 100 %. The condition for each i-bin is:

$$RH_{ini} + (i-1)\Delta RH < RH(i) \leq RH_{ini} + i\Delta RH. \qquad \textbf{Eq. (4.9)}$$

The choice of the ΔRH was made as a trade-off between statistical representatively of each bin and sufficient number of bins to have enough values to guarantee the validity of the analysis. It is seen in **Figure 4.4** that for low RH the *PG* values tend to fair-weather values around ~ 80 V/m and a diversity of behaviors is observed for higher RH. Mainly in the heavily polluted southern sectors, SW and SE, it is observed that the *PG* tends to decrease with RH; which is an unexpected result, but could result from the presence of high levels of pollutant aerosols that influence the *PG* with a different mechanism than the one explored here. Such mechanism may be air pollution particles precipitation by charged water aerosol (Balachandran et al., 2001). The northern sectors show an increase in the *PG* with RH in the region of aerosol hygroscopic growth. The *PG* for NE sector shows a slightly lower increase with RH as compared with the NW sector. This is an important result because these sectors are known to be the least polluted (Silva et al., 2015) and more hygroscopic marine aerosols, coming from the Atlantic Ocean influence, the NW sector. Marine aerosols are known to have high hygroscopicity (Carrico et al., 2000; Titos et al., 2014b) and will dominate the non-hygroscopic behavior of the pollutant aerosols. To progress with the analysis the median values of the *PG* corresponding to the northern sectors, for each RH bin, are represented against the median RH of the respective bin. The data was fitted to the model in **Eq. (4.8)** in the RH region defined for aerosol hygroscopic growth between ~ 60 % and ~ 90 %, **Figure 4.5**(a) and (b).

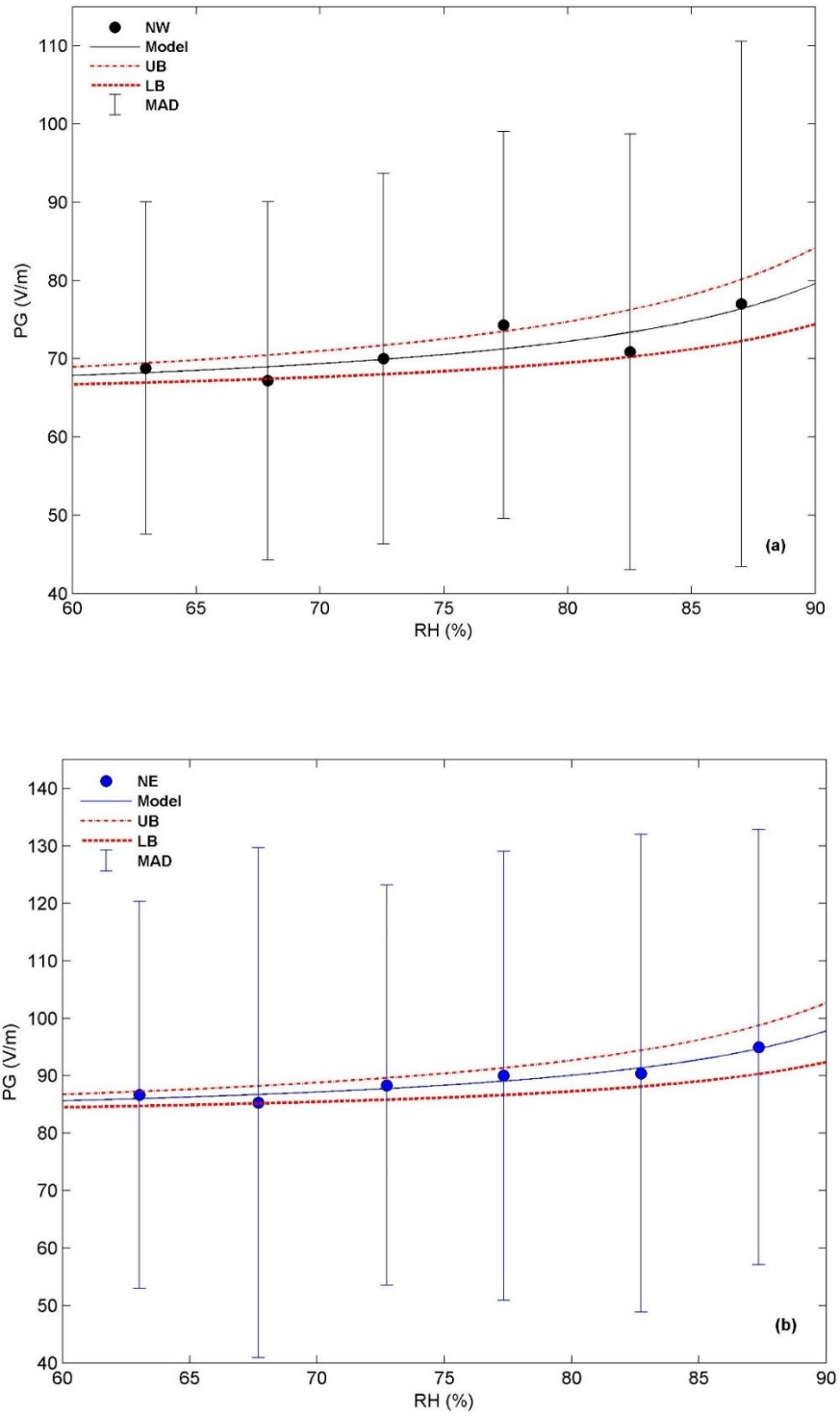

Figure 4.5 *Fits of the model to the wind sectors: a) NW; b) NE, The error bars represent the median absolute deviation (MAD), the solid-line the fitted curve and the dashed-lines the model function but with a variation in* κ *of 40 % above and below the fitted valued.*

In the fitting it was assumed that the dry size of the aerosols is $R_{a,0} \sim 0.1$ μm, and the following parameters are used: $J_C \sim 2$ pA m^{-2}, $T_e \sim 293$ K, and $q \sim 10$ cm^{-3} s^{-1} (Harrison and Carslaw, 2003). The fits are presented in **Figure 4.5**(a) and (b). The error bars represent the median absolute deviation (MAD), the solid line is the fitted curve and the dashed lines are the model curve using κ 40 % above (upper limit) and bellow (lower limit) of the fitted valued, respectively. The model describes well the *RH* evolution of the *PG* for the northern wind sectors in the region of aerosol hygroscopic growth. The results are presented in **Table 4.2**.

Table 4.2 *Results from fitting the model to the PG in the northern wind sectors: aerosol number concentration (Z_a) and aerosol hygroscopic growth parameter (κ_a). The goodness of the fit is also given (r^2). It is assumed that particle dry radius is $R_{a,0} = 0.1$ μm.*

	NW	**NE**
$\mathbf{Z_a}$ (cm^{-3})	3280	4179
$\boldsymbol{\kappa_a}$	0.094	0.072
$\boldsymbol{r^2}$	0.970	0.997

These are very reasonable values consistent with an urban environment; which has high aerosol concentration number with small hygroscopicity. They are probably a result of the mixture between the non-hygroscopic pollutant aerosols resulting from the activity of the city of Lisbon and the hygroscopic marine aerosols. This is more evident for the NW sector. The fitting procedure is robust against the $R_{a,0}$ used and would only affect the value estimated for Z_a because these two quantities appear as a product in **Eq. (4.8)**. It is important to mention that $R_{a,0}$ is expected to be small as it is the dry radius instead of the typical values measured in real atmospheric conditions where the aerosol particles are already hydrated to some extent (Deshpande and Kamra, 2004).

4.6 Potential Gradient modulation by wind effect

Considering that, a division was made by wind sectors and our argument was that southern winds are more polluted then northern winds in this section we to use the *PG* weekly cycle to confirm such assumption. To that end, analysis of the weekly cycle (caused by anthropogenic pollution related with urban activity) were undertaken for each wind sector. A boxplot method and Lomb-Scargle spectra are used as in the previous chapter. In fact, it is shown that NW sector was the least affected by this cycle and the daily variation of NE sector for weekends reveals a similar behavior to the Carnegie curve. As discussed above, *PG* measurements in urban environments are affected by anthropogenic action. The main agents of these influences are pollutant aerosols from traffic, heating and industrial activity. According to the geographical position of pollutant sources around a measurement point, different winds bring different ion and aerosol contents; for that reason, a significant modulation of *PG* is expected with wind direction.

In this section, only non-negative values of *PG* were selected as negative values often correspond to precipitation and cannot be considered. Otherwise, high positive *PG* values can occur as a consequence of pollution, as in case of fires. This occurred during the historical Chiado's fire in Lisbon downtown (Conceição et al., 2015) as will be discussed in the next chapter. Lisbon is situated on the north margin of the Tagus River and Portela station is located to its northeast. Traffic and urban heating are the predominantly cause of pollution in the city. In the 1980's the south margin of the river contained most of the industry (Setubal region), which were then significant pollution sources. At the east of Lisbon is the Tagus river basin and Iberian Peninsula; while to the west is the Atlantic Ocean. Thus, it is expected that winds from different directions should modulate the *PG* as they contain different air contents. At Portela, south winds bring pollution from the city mixed with the pollution from industry, west winds transport some pollution from the city mixed with marine aerosols, north winds carry less pollution and the east winds carry mainly continental aerosols.

PG was separated into workdays, Mondays to Fridays, $PG_{workdays}$ (WD) and weekends, Saturdays and Sundays, $PG_{weekends}$ (WK). It is expected that *PG* for workdays would have

higher values as compared with the *PG* for the weekends, because workdays have more pollution. Thus, to evaluate the difference between workdays and weekends, the relative difference equation for the ΔPG is used again. Please, refer to the previous chapter **Eq. (3.1)**. The comparison of the daily behaviour for workdays and weekends is also very informative and such method is used here. The LSP technique was used to identify the presence and importance of the weekly cycle in each wind sector.

Figure 4.6 shows the boxplots of the *PG* values for each wind direction separated by workdays (WD) and weekends (WK), for clarity outliers are not represented. It is evident that:

- NW sector shows small differences between workdays and weekends having a small relative difference of the medians for workdays, 70 V/m, and for weekends, 60 V/m, ΔPG ~17%, consistent with low levels of anthropogenic pollution.

- NE sector presents more variability in the workdays as compared to the weekends, the median for workdays is 87 V/m and for weekends is 60 V/m, this corresponds to ΔPG ~45%, which is a high value and is mainly due to the low median value for the weekends.

- SE sector shows the higher variability of *PG* for workdays of all sectors, again the median for the weekends, 80 V/m, is lower than that of the workdays, 104 V/m, having ΔPG ~30%, this behavior shows evidence of the presence of a significant influence of anthropogenic pollution.

- SW sector has a median *PG* value for the workdays of 98 V/m, and for the weekends, 80 V/m, this implies ΔPG ~23%. These results show that all the sectors are affected by the weekly cycle; nevertheless, the NW tends to be the least affected. This can be interpreted as a consequence of lower pollution levels and the presence of marine air brought by the western winds from the Atlantic Ocean. In fact, marine air is known to increase atmospheric conductivity (Wilding R.J., Harrison R.G, 2005) and consequently reduces *PG*.

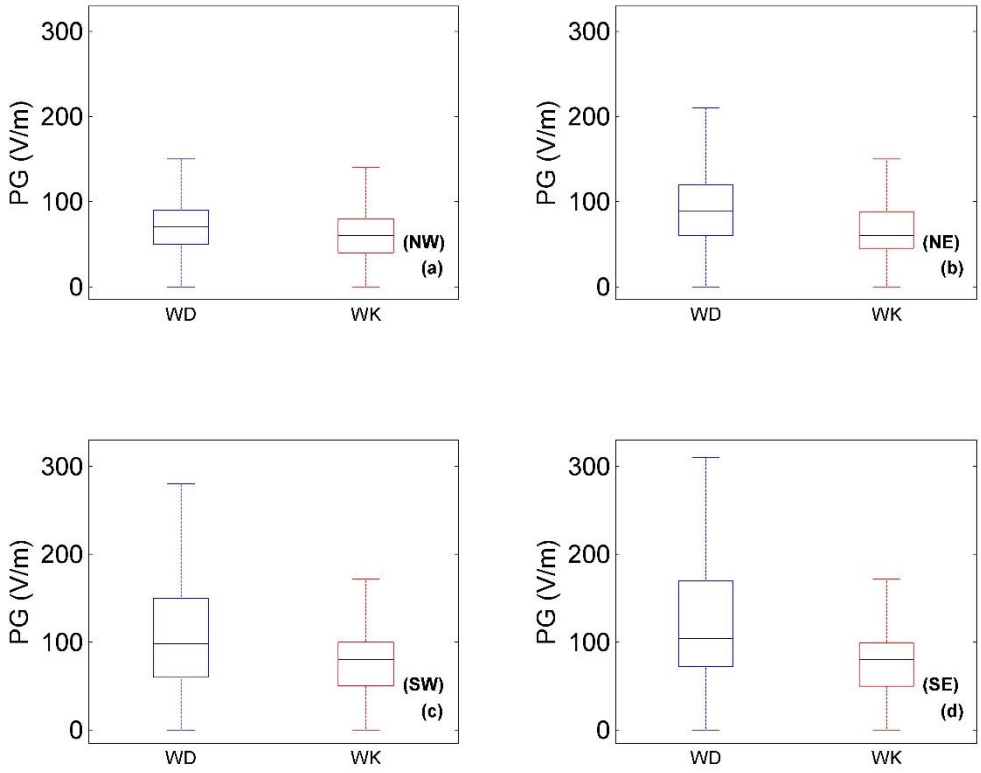

Figure 4.6 *Boxplots of the four wind sectors: a) NW, b) NE, c) SW and d) SE, divided in workdays (WD) and weekends (WK).*

Figure 4.7 presents the daily behaviour of the median *PG* values from the studied period divided into workdays and weekends. On one hand, the northern sectors, NW and NE, show little difference between the daily behaviour of the workdays and the weekends. Actually, the NW sector shows the lowest values of the sectors. On the other hand, the southern sectors show the most significant difference from the workdays to weekends, in particular, the SE and SW sectors show a prominent disparity in the period 08:00 h – 20:00 h, the moment of greatest activity. This aspect may be interpreted as the signature of pollution coming from industries in the south margin of Tagus River, which were most active in that period. Lastly, the daily variation of NE sector for weekends reveals a similar behavior to the Carnegie curve (Harrison, 2013).

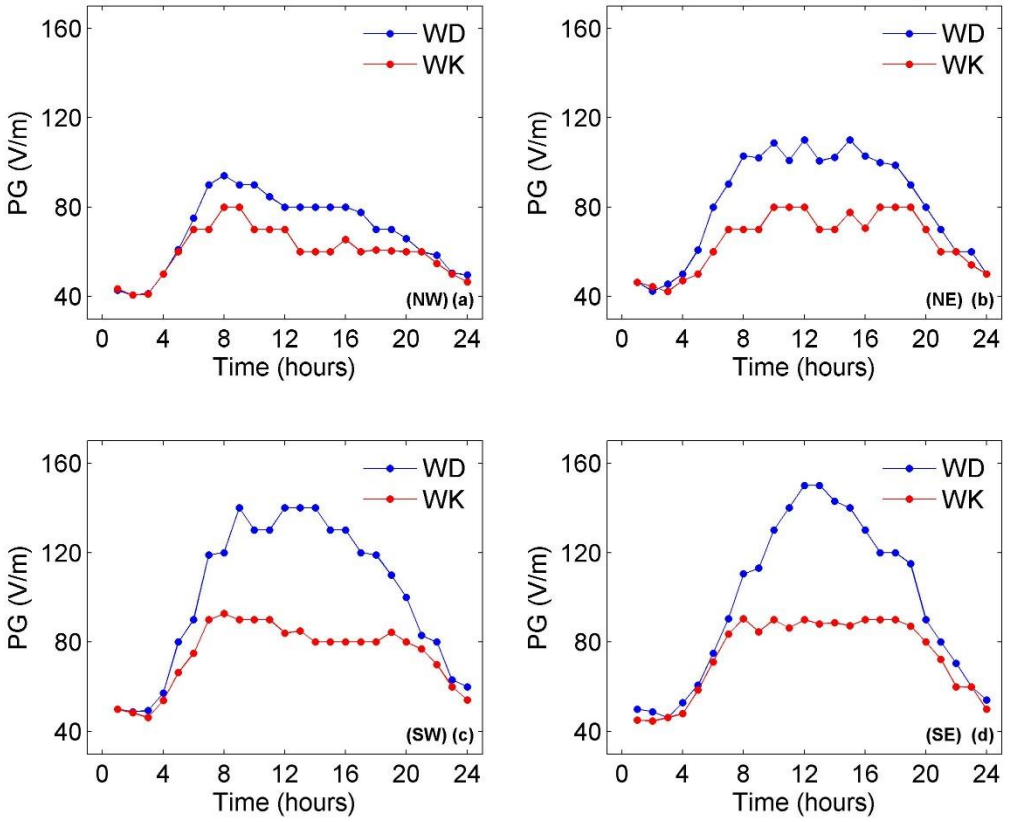

Figure 4.7 *Daily behavior of the median PG values for 1980 to 1990 separated in workdays (WD) and weekends (WK) for each wind sector: a) NW, b) NE, c) SW and d) SE.*

Figure 4.8 displays the Lomb-Scargle Spectra for each of the four wind sectors, a clear modulation with wind direction is observed. The most revealing feature is the *n*-exponent values found for each wind sector. This exponent is defined from the asymptotic spectral amplitude, *S*, with the frequency, *f*, usually written as $S \sim f^{-n}$. The NW and NE have higher slopes with *n*-exponents around, 6.1 and 5.0, correspondingly. The SW and SE have lower *n*-exponent values, 3.9 and 3.3, respectively. These lower values are compatible with measurements taken under more polluted air as pollution tends to induce spectral dispersion that flattens the spectra as discussed in the preceding chapter (Silva et. al., 2015 and Tchepel O., Borrego, C.). Moreover, the presence of the weekly cycle peak, but apparently less pronounced in the NW sector. This observation is compatible with the low *ΔPG* found for this sector and could be another indication of the effect of marine air as it tends to increase the conductivity in contrast to the effect of pollution that tends to cause it to decrease.

Interestingly, the NE sector shows a marked weekly cycle even though the pollution levels should be lower as compared with the sectors from the south. This can be as indication that pollution from traffic should be the main cause of pollution in this sector as traffic is considerably affected by this cycle. Otherwise, pollution from the south is a result of industrial activity and, in principle, less affected by the weekly cycle as many industries continue to labour at the weekends. Finally, all sectors, except the SE, clearly show a daily cycle and a half-day cycle.

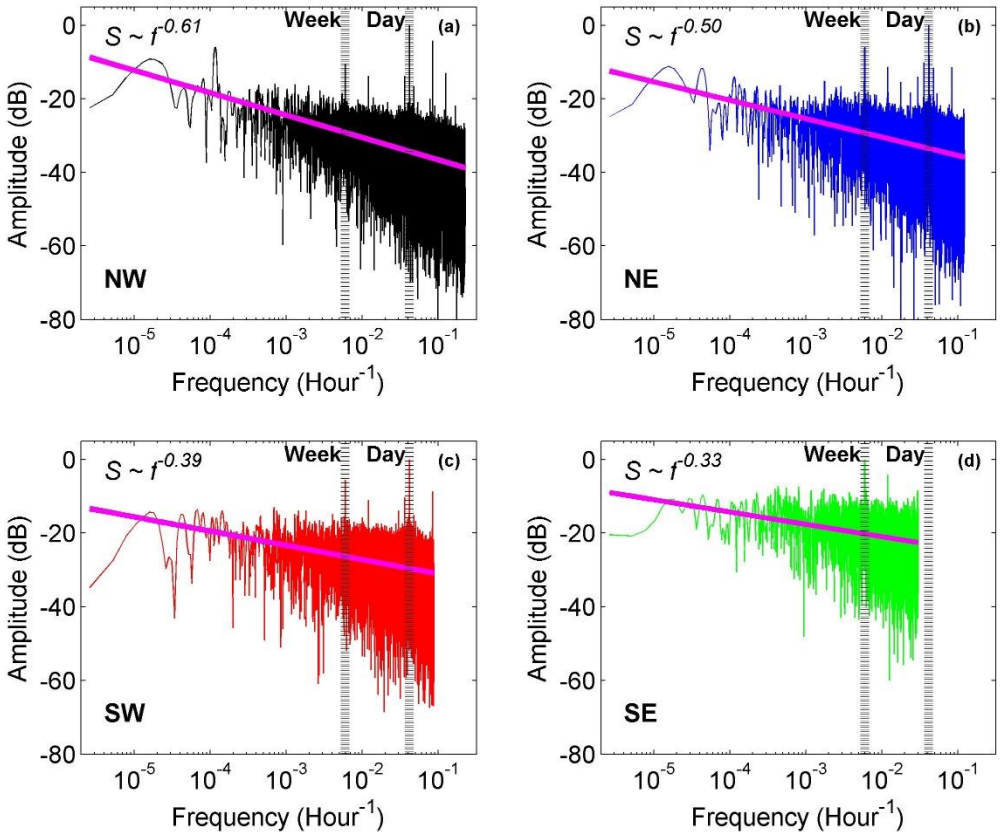

Figure 4.8 *Lomb-Scargle Spectra corresponding to the four wind sectors. The following parameters were used hifac=1 (that defines the frequency limit as hifac times the average Nyquist frequency), ofac=4 (oversampling factor).*

5 Transport of the smoke plume from Chiado's fire in Lisbon (Portugal) sensed by atmospheric electric field measurements

5.1 Overview

The Chiado's fire that affected the city center of Lisbon (Portugal), **Figure 5.1**, occurred on 25th August 1988 and had a significant human and environmental impact. This fire was considered the most significant hazard to have occurred in Lisbon city center after the major earthquake of 1755. A clear signature of this fire is found in the atmospheric electric field data recorded at Portela meteorological station about 8 km NE from the site where the fire started at Chiado. The atmospheric electric field reached 510 V/m when the wind direction was coming from SW to NE, favorable to the transport of the smoke plume from Chiado to Portela. Such observations agree with predictions using Hysplit air mass trajectory modelling and have been used to estimate the smoke concentration to be ~0.4 mg/m^3.

It is demonstrated that atmospheric electric field measurements were therefore extremely sensitive to Chiado's fire. This result is of particular current interest in using networks of atmospheric electric field sensors to complement existing optical and meteorological observations for fire monitoring.

Figure 5.1 *Image of the Chiado's fire that took place at Lisbon city center; courtesy of the Municipal Archive of Lisbon.*

5.2 Introduction

Among its different uses, sensing pollution with *PG* measurements is one of the most significant ones (Harrison 2006). Historical *PG* records have been used to infer pollution dynamics since the first reliable *PG* measurements were done in the mid-nineteenth (Aplin 2012, and references therein) to late twentieth century (Silva et al., 2014) when particulate matter measurements became abundant as part of routinely air quality control (Krzyzanowski and Cohen 2008). In this context, AEC was also proven to be very sensitive to air pollution (Retails et al. 1991; Sheftel et al. 1994). These studies show a decrease in AEC with the increase of air pollution; which does relate, through **Eq. (1.3)**, to the increase of *PG* (Retalis and Retalis, 1997; Silva et al. 2014). Actually, the reduction of the number of small ions caused by air pollution (Retails 1977) is the main mechanism behind these observations as it reduces considerably AEC. Details on the theory will be given below.

Due to its sensitive to air pollution a possible application of *PG* measurements is the detection of fires. These hazards represent an immense threat to public health and impose a strong environmental impact; which makes all possible tools available to their monitoring of fundamental importance. In the context of atmospheric electricity, initial interest in fires was related with lightning from fire-clouds (Vonnegut et al. 1995). It was found that the plumes

of hot gas, moisture, and smoke formed by the fires originate anomalous lightning (Lang and Rutledge 2006) and disturb significantly the local *PG* (Phalagov et al. 2009). This perturbation is caused by the action of two distinct factors (Gopalakrishnet al. 1996): 1) the atmospheric ions created by the burning flame increasing AEC and decreasing *PG*; 2) the smoke spread with the plume scavenge the atmospheric ions decreasing AEC and increasing *PG*. The second factor dominates over the first (Ippolitov et al. 2013).

Presently, the use of *PG* measurements in sensing smoke plumes derived from fires is gaining vigor with the development of networks of *PG* sensors worldwide. In particular, in South America, a *PG* network is operating (Tacza et al. 2014); this region comprises the Amazon rainforest (largest tropical rainforest in the world) and the use of this network could be of significant value in complementing visual and meteorological measurements.

In this perspective, the urban fire that occurred in Lisbon (Portugal) on 25th August 1988, known as Chiado's fire, represents a rare opportunity to study the effect of smoke particles on *PG*, as such measurements were made in the suburbs of Lisbon at Portela meteorological station (Serrano et al. 2006 and Silva et al. 2014). Chiado's fire was considered the most significant hazard to have occurred in Lisbon city center since the 1755 earthquake. It had a significant economical and human impact due to the destruction of many buildings, 2 people lost their lives, 73 were injured, and around 300 people lost their homes, while nearly 2000 lost their jobs. The fire started about 05:00 h (local time) at the Grandella store in Carmo Street (Chiado). Highly flammable and explosive materials were stored in the buildings affected by the fire, which contributed to its rapid spread and great magnitude. Firefighters fought this urban hazard until 16:00 h on 25th August 1988 while smoke emissions last for several days (firefighters work in the zone went to 5th September). In the end, Chiado's fire affected about 8000 m², which corresponds to approximately 3.4% of Lisbon's downtown.

Here it is discussed the impact that Chiado's fire had on the *PG* at Lisbon. The analysis of these records is complemented with air mass trajectory modelling, using Hysplit model (as no aerosol measurements or satellite monitoring was available during that period) and the

examination of local meteorological conditions to evaluate the sensitivity of the *PG* to this urban fire.

5.3 Results and Discussion

The hourly values of *PG* measured during 1988 are presented in **Figure 5.2**; the vertical green line marks the period in which Chiado's fire occurred, on 25th August.

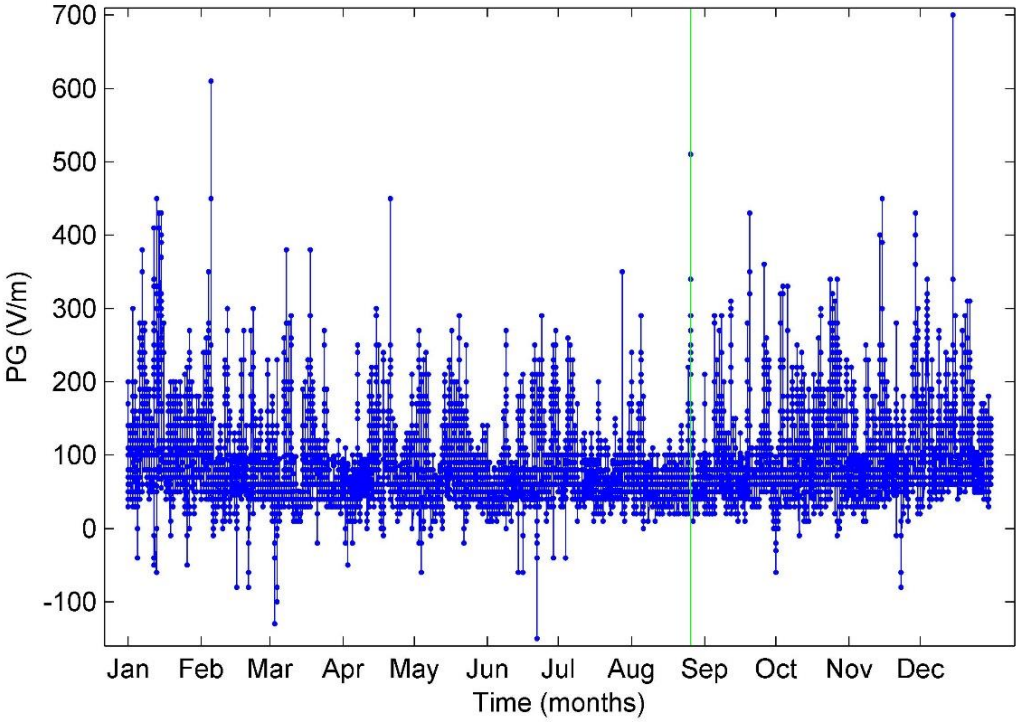

Figure 5.2 *PG data measured at Portela during 1988 (the green line denotes the PG peak of Chiado's fire on 26th August).*

Examination of **Figure 5.2** shows that on the 26th August the *PG* at Portela was significantly enhanced, reaching a maximum value of 510V/m at 19:00 h. **Figure 5.3**(a) and (b) show the annual and summer *PG* histograms (in logarithmic scale) for 1988, respectively. This is because seasonal variations affect considerably the *PG* distribution.

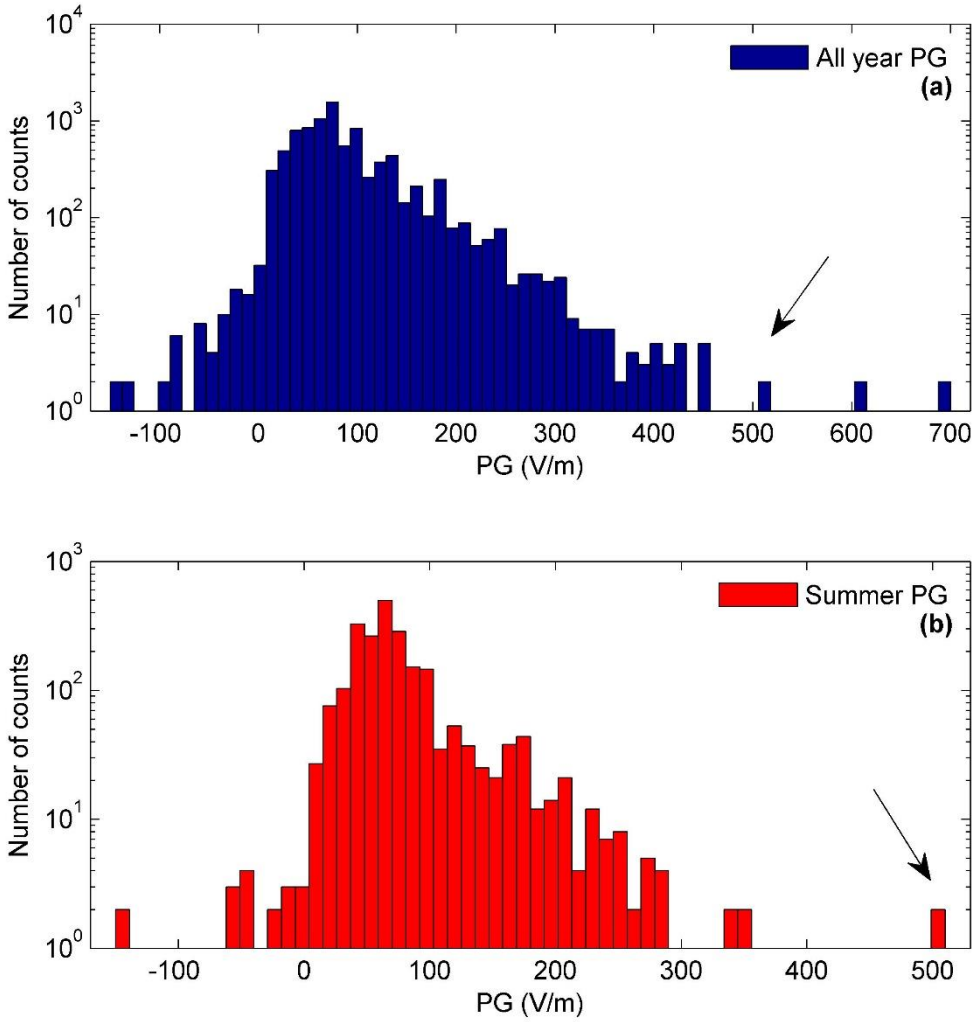

Figure 5.3 *a) distribution of PG values for all the year of 1988; b) distribution of PG values for the summer of 1988. The arrows point to the anomalous PG value in study.*

In **Figure 5.3**(a) and (b) it is seen that the *PG* distributions are not normal and are positively skewed (to the right), due to the predominantly positive *PG* values during fair-weather. Descriptive statistics for both distributions are presented in **Table 5.1**.

Table 5.1 *Mean, median, standard deviation, skewness, lower whisker, lower adjacent value, upper whisker and upper adjacent value for all year of 1988 (Annual) and Summer of 1988 (Summer). The last four statistical parameters were calculated trough adjusted boxplot method (Vanderviere and Huber, 2004).*

	Annual	**Summer**
Mean (V/m)	88.9	75.4
Median (V/m)	80.0	70.0
Standard deviation (V/m)	58.2	46.1
Skewness	1.76	1.92
Lower whisker (V/m)	0.0	10.0
Lower adjacent value (V/m)	50.0	49.0
Upper whisker (V/m)	110.0	90.0
Upper adjacent value (V/m)	160.0	150.0

The reliability of the 26th August *PG* value as an outlier it is checked by the skewness of *PG* and by the statistics in **Table 5.1**. Additionally, taking into account that in the summer the mean *PG* is 75.4 V/m and standard deviation is 46.1 V/m, this means that the *PG* anomaly was above the summer mean value more than 9 times its standard deviation. It was so large that such a value was only exceeded on two days in that year (recorded during foul-weather winter days). A stronger indicator is the estimation of the probability that such anomalous *PG* have to occur. To do so the distributions in **Figure 5.3** are fitted to t Location-Scale distributions (using maximum likelihood estimation) to calculate the probability of a value of 510 V/m to occur. The results show that the probabilities are low: ~0.13 % in all the year and ~0.08% in the summer.

Further analysis of the *PG* data can be achieved by considering its average diurnal variation; which is due to a combination of local and global effects. The black curve in **Figure 5.4** shows the average diurnal variation in *PG* at Portela for 1988 having two maxima at approximately 08:00 h and 16:00 h.

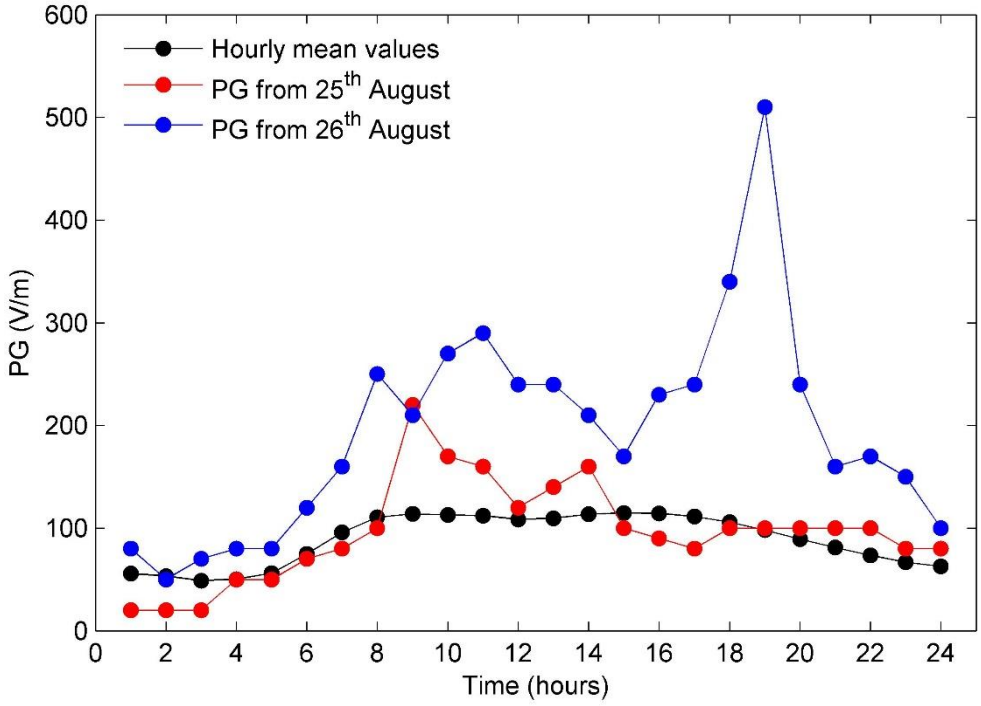

Figure 5.4 *Hourly mean behavior of the PG at Portela calculated from all year of 1988 (black curve), PG during 25th (red curve) and 26th of August 1988 (blue curve).*

This is consistent with daily particulate matter variations in urban environments (Harrison 2009). Plotted alongside is the *PG* data measured during the period of Chiado's fire: in red for 25th and in blue for 26th August. The large difference between the average diurnal *PG* variation and the one measured on 26th August (which is much larger than the typical values) suggests the presence of an external factor driving the unusual *PG* changes. Therefore, such effect is attributed to the increase in smoke particle concentration generated by Chiado's fire. In fact, assuming that the smoke from Chiado's fire caused the large *PG* values over Portela, it is possible to estimate the concentration of smoke particles directly from the *PG* measurements through the theory developed by (Harrison 2006). This is briefly derived from the ion balance equation **Eq. (1.10)** . In the case of heavy pollution, $n\beta_a Z_a \gg \alpha n^2$, **Eq. (1.10)** simply becomes:

$$n = q/\beta_a Z_a \qquad \textbf{Eq. (5.1)}$$

Substituting **Eq. (5.1)** in the equation for AEC, **Eq. (1.6)**, and the result included in the formula for the *PG*, **Eq. (1.3)**, it is found the relation:

$$PG = \frac{J_C \beta_a Z}{2q\mu e}. \qquad \textbf{Eq. (5.2)}$$

It is possible to substitute Z in **Eq. (5.2)** by smoke mass concentration, M, through the relation, $Z = M/m$, with m the mean mass of a single particle. Thus it is obtained the relationship:

$$PG = \frac{J_C \beta_a}{2q\mu em} M. \qquad \textbf{Eq. (5.3)}$$

This equation links the PG directly to M. Finally, the measured PG is written as the sum of two components: the one caused by the action of smoke particles, **Eq. (5.3)**, and the one conforming to clean air, PG_0. This results in:

$$PG = \frac{J_C \beta_a}{2q\mu em} M + PG_0. \qquad \textbf{Eq. (5.4)}$$

Substituting the coefficient of M in **Eq. (5.4)** by C and isolating M, the smoke concentration can be retrieved as a function of PG and PG_0:

$$M = C^{-1}(PG - PG_0). \qquad \textbf{Eq. (5.5)}$$

The constant C was estimated by (Harrison, 2006) for Kew (London) to be ~1082.6 (V/m)/(mg/m^3). Using **Eq. (5.5)** it is possible to make a reasonable estimation of M at the *PG* maximum (510 V/m). The mean *PG* values for the Sundays of August 1988 is used as corresponding to clean air, PG_0 ~ 53 V/m. Sundays were chosen because they are the less polluted days of the week (Silva et al. 2014). The estimation indicates a maximum smoke concentration of M ~ 0.4 mg/m^3 at Portela (8 km from the origin of the fire) which is consistent with high smoke concentration scenario as expected for this fire. It is important to bear in mind that this is an indicative value. Moreover, it is expected that the value of C for Lisbon might not differ significantly from London's, as both cases consider a high pollution scenario. Finally, using **Eq. (5.5)** a simple estimation for the threshold smoke concentration needed for a fire to be detected by *PG* measurements would be around ~0.2 mg/m^3; this assumes that a *PG* ~ 300 V/m is anomalous and PG_0 ~ 53 V/m (the one used above).

5.4 Meteorological considerations

PG is drastically affected by local weather conditions. It is therefore important to determine whether the anomalous *PG* values measured on 26th August were in fact due to the increase in smoke concentration, caused by the fire, or resulted from local meteorological factors. Meteorological parameters at Portela meteorological station (the same location of *PG* records) were obtained from NNCD Climate Data Online website supported by NOAA. These include visibility, wind speed and direction, air temperature, and dew point (used to calculate relative humidity). **Figure 5.5** shows the time series of the meteorological variables over Lisbon for the period 25th and 26th August 1988: (a) *PG*; (b) visibility; (c) wind speed; (d) wind direction; (e) relative humidity (*RH*).

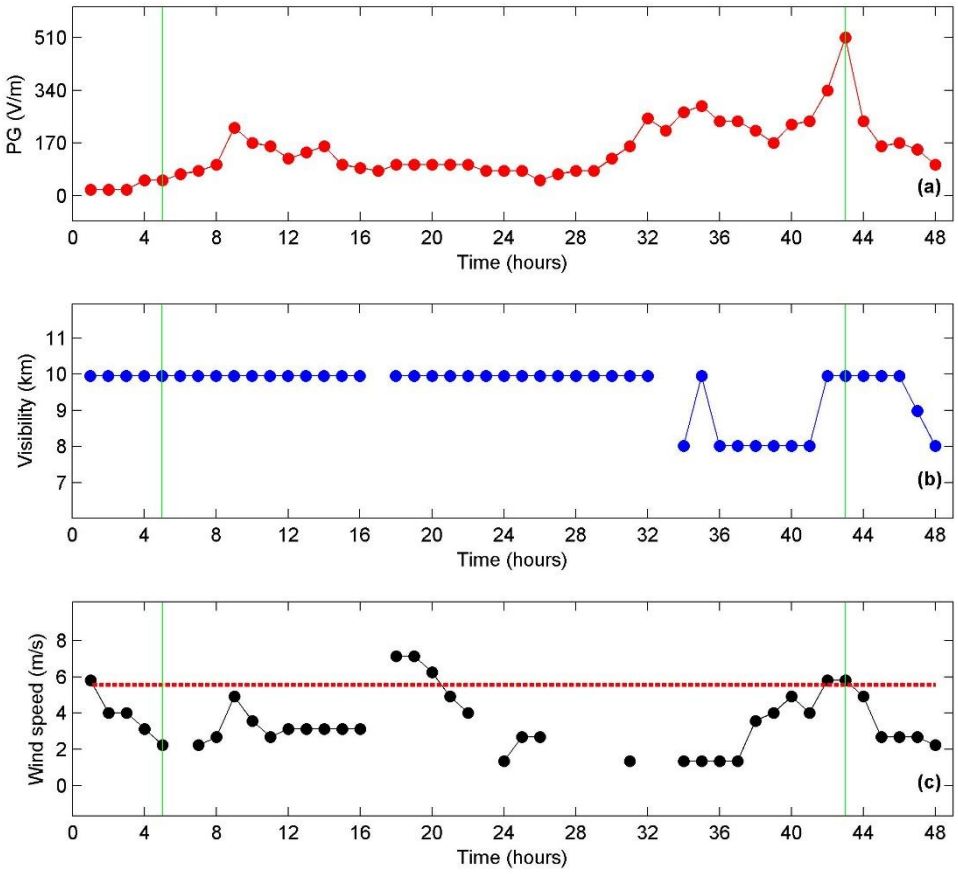

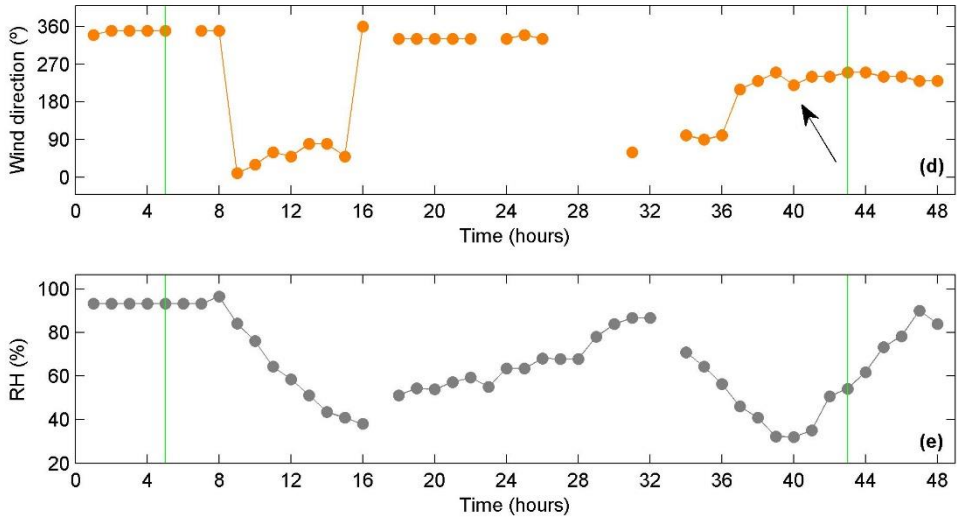

Figure 5.5 *Meteorological conditions from 25th and 26th of August 1988 for Portela meteorological station (Lisbon airport): a) Potential Gradient; b) Visibility; c) Wind Speed; d) Wind Direction; e) Relative Humidity (RH). The vertical lines denote the start of the fire (first green line) and the PG peak hour (second green line). The horizontal red dash line in c) marks the fair-weather limit for wind speed, 6 m/s, according to Voeikov (1965). The black arrow in d) marks the moment when the smoke plume started travelling to Portela.*

These demonstrate that during the period of the fire there were fair-weather conditions, according to (Voeikov, 1965). Some high cloud (above 5km) was present on 26th and 27th, though. Such clouds, due to their high altitude (well above the boundary layer) cannot account for the large *PG* values measured at the time of the fire. The synoptic situation (not shown) during this period was characterized by a high-pressure system over Portugal with mostly clear skies and no precipitation corresponding to quiet atmospheric conditions. Such conditions in summer are characterized by intense solar radiation that causes significant air convection. It is expected that the smoke plume due to its high temperature would have been injected well above the ground, but air convention would cause vertical dispersion of smoke particles. These would reach the ground during the travel time from Chiado to Portela. In fact, the increased smoke particle concentration from the fire could last for several days.

It can also be seen in **Figure 5.5**(b) and **Figure 5.5**(e) that visibility and *RH* have values that exclude the possibility of fog formation; this is important because fogs tend to increase the *PG* (Piper and Bennett 2012) and could be a possible cause for the anomalous *PG* discussed

here. Besides, to account for the smoke plume transport from the fire's site to the *PG* measurement location, it is important to consider the wind direction on 25th and 26th August, **Figure 5.5**(d). This shows that on the 25th the wind was mainly coming from the north, 360º; whereas on the 26th the wind direction started coming from east and then gradually from southwest, 240º. This process took ~6 hours to stabilize (the black arrow marks the stabilizing moment) and it is clearly seen in **Figure 5.6** (withe arrow marks the wind rotation).

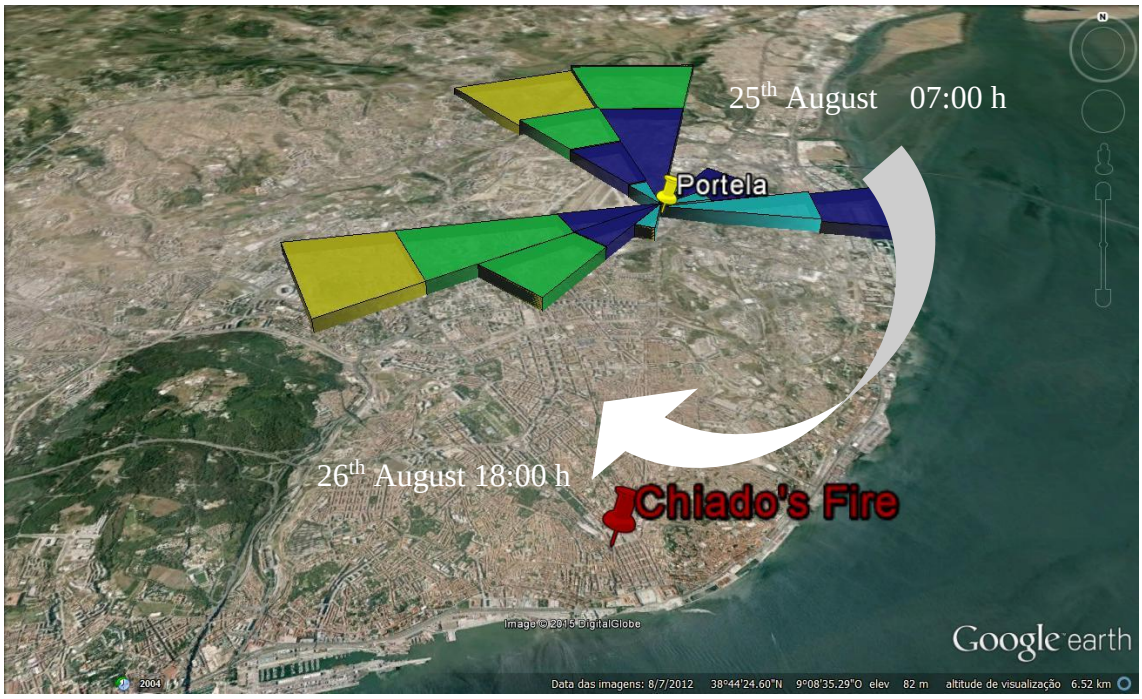

Figure 5.6 *Rose wind representation in Portela during 1988 (a 3D perspective is used). The white arrow marks wind rotation in time from 25th of August at 07:00 up to 26th of August at 18:00 (UTC). These moments are marked in the figure. The wind speed varies according to 4 colors increasing its magnitude from light blue, dark blue, green and yellow. The increasing radius represents an increase in the observations. The Chiado's fire is marked with red pin and Portela station marked with a yellow one.*

After this it is observed that the *PG* starts to increase, up to its peak value ~3 hours later, **Figure 5.5**(a). The smoke plume took roughly ~1 hour to travel from the fire's site to the measurement location. This is estimated dividing the distance from Chiado to Portela, 8 km, by an average wind velocity of ~2 m/s (**Figure 5.5**(c)). This means that there is a delay of ~2 hours between the plume arrival and the *PG* maximum. This delay is attributed to the time that smoke particles took to scavenge enough atmospheric ions to cause the significant decrease in AEC and consequently the anomalous increase in the *PG*. A simple estimation

can be made taking into account that the lifetime of atmospheric ions in highly polluted air is ~20 s (Retails 1991). Assuming that ion concentration before the fire was ~500 ions/cm^3 (Harrison and Carslaw 2003) an increase of the *PG* from a typical ~100 V/m to the anomalous ~500 V/m would imply, through **Eq. (1.6)**, a reduction in atmospheric ions by ~400 ions/cm^3 (assuming that J_C remained constant and the ion mobility did not change). Multiplying this value by the ion life time an estimation of the time needed for the process of ion scavenging to occur is calculate, ~8000 s, which corresponds to approximately 2 hours. Adding this estimation with the time for the smoke plume to travel gives ~3 hours, consistent with the observations. From the evolution of *PG* and visibility, **Figure 5.5**(a) and **Figure 5.5**(b), it can be seen that there was a reduction in the visibility, consistent with the transport of the plume to Portela station.

5.5 Air mass trajectory modelling

Air mass trajectories were calculated using the Hysplit-4 model for air masses that started at the fire site at 05:00 h on the 25th of August 1988 and ended at 20:00 h on the 26th. Despite the fact that the fire ended on 16:00 h of 25th of August smoke emission remained during several days after (firefighters worked in the zone until 5th September as mentioned above). In fact, meteorological conditions also favored a late detection of the smoke plume by the *PG* in Portela. From **Figure 5.7** it is possible to see the time evolution of the smoke particle trajectories between the fire site (marked with red pin) and the location where the *PG* was measured (pointed with a yellow pin).

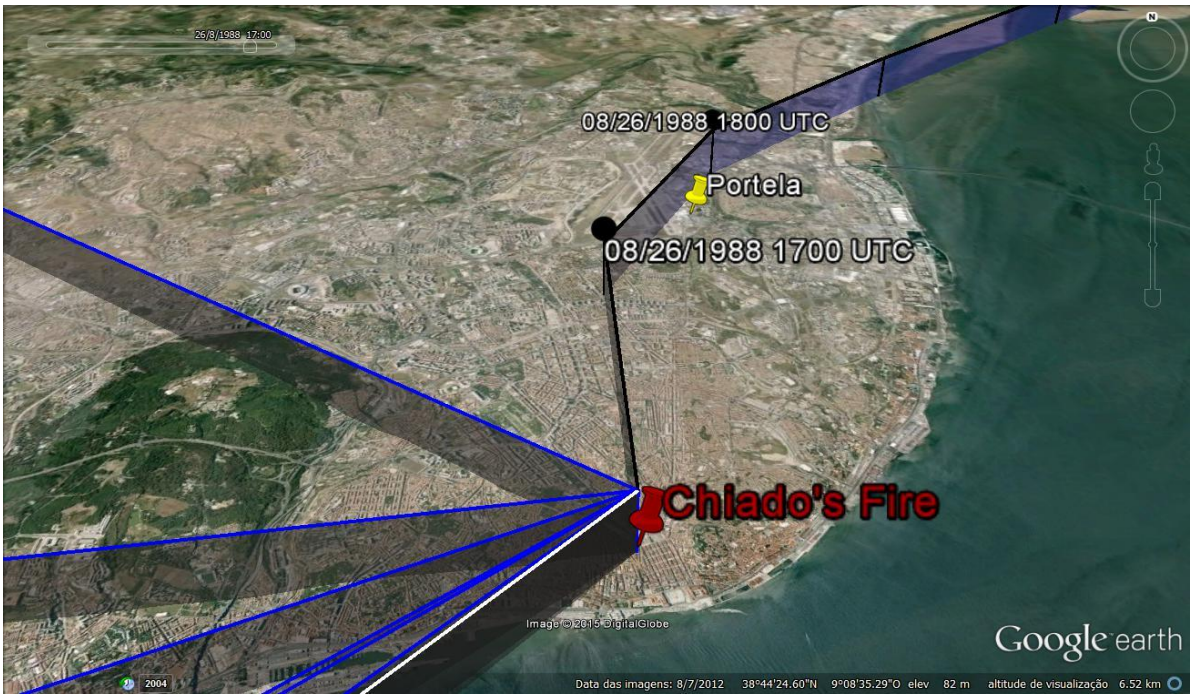

Figure 5.7 *Forward trajectories calculated using Hysplit-4 for air masses at 750 m starting at 05:00 h 25th August (first white trajectory) with a new trajectory created each 5 hours (blue trajectories) until 16:00 h 26th August (last black trajectory). The Chiado's fire is marked with red pin and Portela station marked with a yellow one. NOAA Air Resources Laboratory.*

It is seen that the transport of the smoke plume evolves in a clockwise rotation from SW to the NE, and is estimated to pass over the *PG* measurement site at Portela between 17:00 h and 18:00 h (consistent with the minimum in visibility). Note also that this trajectory started at the source location at 16:00 h, which gives an approximately 1 hour to get to Portela, corroborating the estimation done before.

The Hysplit trajectory shown in **Figure 5.7** is also consistent with the change in wind direction shown in **Figure 5.6**, with the wind blowing from the fire site to the SW on 25th and to the NE (in the Portela direction) on 26th August. Additionally, using the Hysplit dispersion model, which for visualization effect can be more interesting, it was possible to simulate the smoke plume travelling path for 25th and 26th August.

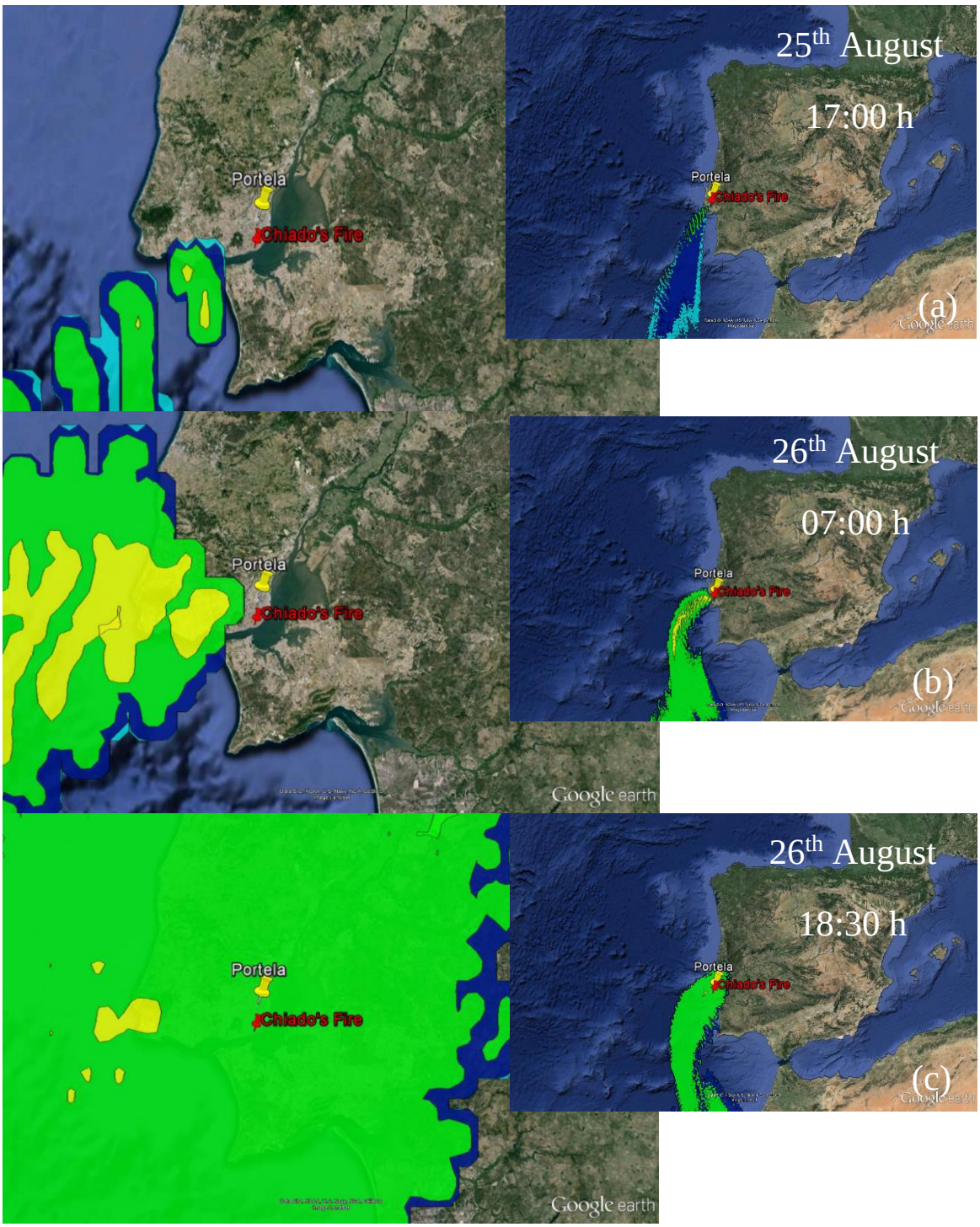

Figure 5.8 *Model projections of the plume spread from Chiado's fire: a) 25th August, 17:00 h; b) 26th August, 07:00 h; c) 26th August, 18:30 h; The smoke particle concentration varies according to 4 colors increasing its magnitude from light blue, to dark blue, green and yellow. The Chiado's fire is marked with red pin and Portela station marked with a yellow one. NOAA Air Resources Laboratory.*

In **Figure 5.8**(a) at 17:00 h on 25th, it is observed that the main concentration of the smoke plume is SW of Portela. By 07:00 h on 26th, **Figure 5.8**(b), the smoke plume had spread W/NW, and by 18:30 h was over Portela region, **Figure 5.8**(c). This effectively demonstrates that when the maximum in PG occurred, the main concentration of the smoke plume was above Portela. This approach was used to complement the trajectory model with improved visualization of the dispersion of the smoke particles by introducing information about the type of deposition (dry deposition), density (1g/cc) and particle diameter (0.1 μm), and approximately 30 hours of emission (counting not only the fire duration but also the period when smoke was still being released). The density was chosen to be consistent with (Harrison 2006). Finally, the results support the argument that during the late afternoon of 26th August a smoke plume from Chiado's fire passed over Portela causing the observed anomalously large PG values.

6 Numerical simulations of the global electric circuit

6.1 Introduction

There are several models that describe the Global Electric Circuit of the atmosphere. It is used the common model and parameters of the Global Electric Circuit to couple it with a local circuit less studied in literature. The first objective is to test different voltage sources describing thunderstorm activity and compare the output, *PG*, with the *Carnegie Curve*. Two sets of parameters are used, the first one from values found in literature and the second one from values tweaked to get the best agreement between the simulated *PG* and the *Carnegie Curve*. This study is a first step in simulations regarding the coupling of the global electric circuit (primary) to local electric circuit (secondary).

The final objective would estimate the aerosol load on the local resistance in a case of aerosol events.

6.2 Overview

The existence of a Global Electric Circuit (GEC) was first recognised by the observation of the so called *Carnegie curve* based on a global daily variation of the surface Potential Gradient (*PG*) aboard of the Carnegie cruises (Harrison, 2013). For that reason, different models have been elaborated to understand the GEC proprieties (Rycroft M.J. et. al., 2015) and its relation with climate (Mareev E.A and Volodin E.M, 2014).

Nevertheless, to our knowledge no attempt has been made to perform simulations coupling the GEC primary circuit to a secondary circuit describing local *PG* measurements. Such simulations are of considerable interest because, for example, in polluted regions the daily variation of the *PG* differs drastically from the *Carnegie curve* (Silva et. al., 2015). Since it

is expected that GEC would impose a similar global daily variation a deviation from the *Carnegie curve* could only be a result from local variation of the electrical components defining the secondary local circuit. If such simulation were successful, it would enable to separate the global effect from local effects on real *PG* data. It would allow, for example, the estimation of the electric resistance load caused by atmospheric pollution from *PG* measurements in polluted cities (Silva. et. al., 2015).

In this chapter a method is described to couple a local circuit to a global one describing GEC. It is assumed that changes in the local circuit would not affect considerably the GEC. The model is presented and adjusted to reproduce the *Carnegie curve*.

6.3 GEC simulations

Two main parts compose the electric circuit considered here. The first part comprises the components defining the primary circuit corresponding to GEC: V_s the voltage generated by the thunderstorms, R_s the resistance associated with the thunderstorms region, R_{FW} the resistance corresponding to fair-weather regions that closes the circuit in parallel with the Ionosphere-Earth capacitance C_{IE}.

Coupled to a secondary circuit that corresponds to local circuit where the *PG* measurements take place it is the primary, global circuit. It is composed by R_{FT} the resistance of the free-troposphere and R_{BL} the resistance of the boundary layer.

To account for space-charge accumulation in the boundary layer a capacitance, C_{BL}, is inserted in parallel with the R_{BL}. The diagram of the circuit is presented in **Figure 6.1**. It is important to mention that with the insertion of C_{BL} it is meant to simulate the space-charge accumulation observed in the boundary layer (Markson R., 1999).

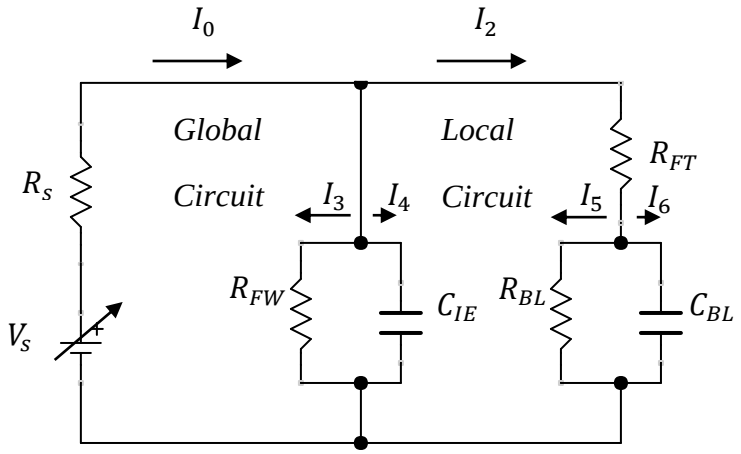

Figure 6.1 *Diagram of the circuit model.*

6.3 Circuit equations

Using Kirchhoff's laws on the circuit of Figure 1, and the notation $I_n = \dot{Q}_n$ (here $\dot{Q}_n$ represents the time derivative) it is obtained the following system of differential equations:

$$
\begin{aligned}
&-V_s + R_s\dot{Q}_0 + R_{FW}\dot{Q}_3 = 0,\\
&-R_{FW}\dot{Q}_3 + \frac{Q4}{C_{IE}} = 0,\\
&-\frac{Q4}{C_{IE}} + R_{BL}\dot{Q}_5 + R_{FT}\left(\dot{Q}_5 + \dot{Q}_6\right) = 0,\\
&{Q_6}/{C_{BL}} - R_{BL}\dot{Q}_5 = 0,\\
&\dot{Q}_0 - \dot{Q}_2 - \dot{Q}_3 - \dot{Q}_4 = 0,\\
&\dot{Q}_2 - \dot{Q}_5 - \dot{Q}_6 = 0.
\end{aligned}
\qquad \textbf{Eq. (6.1)}
$$

Having V_{RB} as the output, $V_{RB}=Q_6\backslash C_{IE}$, it is needed to extract Q_6 from **Eq. (6.1)**. The numerical method used was the algorithm ode45 from MATLAB®, which is based on an explicit Runge-Kutta (4,5) formulation with Dormand-Prince pair, with a relative tolerance of 10^{-6}.

A remark must be made here to explain the use of $I_n = \dot{Q}_n$ and this is because such transformation converts the system above into a system of first-order differential equations

possible to integrate numerically. The result comes in Q_n and time derivation enables the estimation of I_N.

6.4 Results and discussion

The voltage source from the thunderstorms, V_s, was modulated in two different ways: 1) based on the *Carnegie curve*, C_c; 2) based on the *Ionosphere Potential*, V_I, modelled in Mareev, E.A and Volodin, E.M, 2014. For both cases the curves were divided by its mean and multiplied by V_0, amplitude of the voltage source. The expressions are:

$$V_S^{Cc} = V_0 \times \frac{C_c}{\overline{C_c}},$$
$$V_S^{V_I} = V_0 \times \frac{V_I}{\overline{V_I}}. \qquad \textbf{Eq. (6.2)}$$

Two sets of parameters were used for the different components of the circuit. Firstly, parameters according to the literature, (Rycroft et al., 2000): V_0 = 100 MV, R_s = 100 kΩ, R_{FW} = 200 Ω, R_{BL} = 300 PΩ, R_{FT} = 25 PΩ, C_{IE} = 1 F and C_{BL} = 0.01 pF.

Secondly, parameters tweaked to get the closer agreement between the simulations and the observed *Carnegie Curve*: V_0 = 110 MV, R_s = 80 kΩ, R_{FW} = 200 Ω, R_{BL} = 500 PΩ, R_{FT} = 25 PΩ, C_{IE} = 0.7 F, C_{BL} = 0.01 pF. The values of the simulated *PG* were found from $V_{R_{BL}}$ by dividing it by the height of the boundary layer, h ~ 2000 m.

The results obtaining are presented in Figure 2:

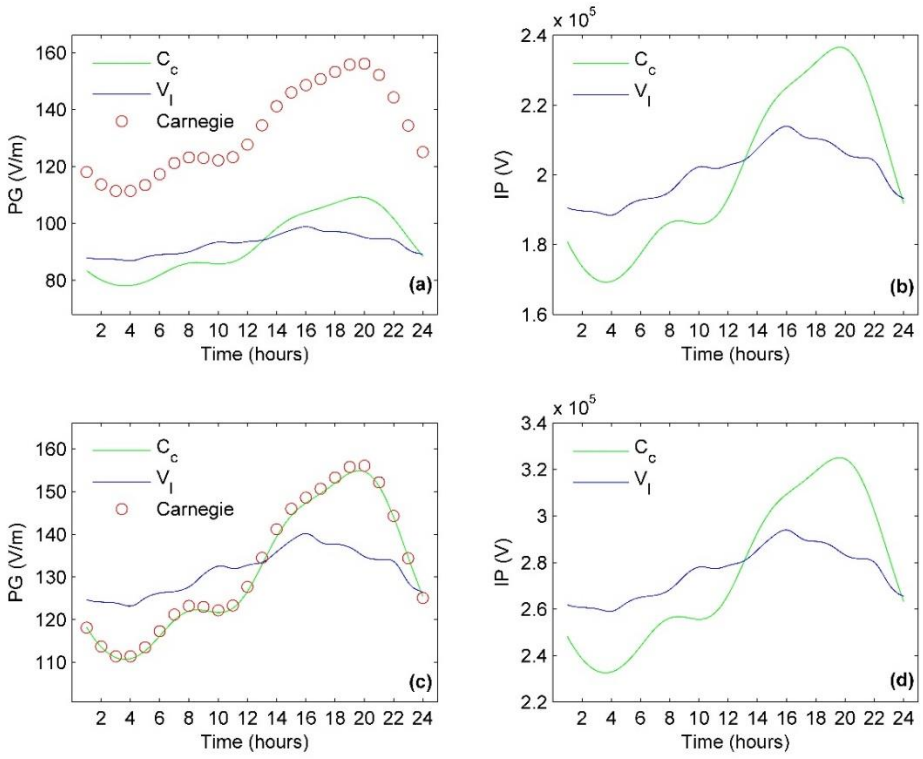

Figure 6.2 *a) PG values simulated with the first set of parameters; b) Ionosphere Potential derived from the thunderstorms voltage source and resistance for the first set of parameters; c) PG values simulated with the second set of parameters; d) Ionosphere Potential derived from the thunderstorms voltage source and resistance for the second set of parameters.*

This is an incomplete attempt to derive several values for the electrical components that are part of GEC. It is part of future try to make a more complex circuit, which can modulate the global and local mechanisms in a realest way. However, it is very important to note that with this circuit, the values found for V_I are much greater than the values found nowadays. This means that V_I is for some reason decaying over time and consequently the *PG*. This is also being in study (Mareev, E.A and Volodin, E.M, 2014) and the *Carnegie* Curve still used today may be, in a very short time, replaced for a new curve. This also means that the circuit exploited here can actually be close from its more realistic model, which can be discovered in the next years.

7 Conclusions and future work

- Chapter 3 clearly demonstrates the existence of a weekly dependence on the *PG* recorded at Portela (Lisbon, Portugal) that is related with the weekly cycle of urban pollution, mainly due to traffic. This dependence was confirmed through a statistical analysis that shows a relative difference of *PG* values for working days and weekends of 31.00 % and 38.41 % for AW and FW, respectively. The annual average of the relative difference shows an increasing trend in the period studied. Additionally, the spectra show a significant peak for the weekly period that confirms the existence of the weekly cycle, as well as a 12 h periodicity present in the *PG* data, attributed to traffic pollution. Spectral noise shows that spectra tend to flatten along the studied period. These aspects are consistent with the evolution of the weekly cycle of pollution due to the rise in pollutant aerosol concentrations caused by the increase of traffic in Lisbon. As a final remark, it is important to mention that this 7-day periodicity is in the range of periods of the known seismic precursors (Silva et al., 2012) and for that reason the effect of urban pollution should be carefully taken into account in those studies.

- Chapter 4 formulation developed here relates in a simple way three microphysical properties of the aerosols: dry radius, concentration number and hygroscopicity; with the macrophysical measurement of Potential Gradient. As a simple formulation, it has several limitations such as neglecting the positive to negative ion concentration unbalance, the effect of electrified aerosols, the influence of aerosol size distribution, and the change in the ionization rate with the relative humidity. Nevertheless, it describes fairly well the dependence of the Potential Gradient with the Relative Humidity for the northern wind sectors (less affected by air pollution) of the measurements done at the Portela meteorological station (Lisbon, Portugal). The values for the aerosol hygroscopicity are low, but consistent with the fact that they are probably a consequence from a mixture between non-hygroscopic pollutant aerosols (resulting from the activity of the city of Lisbon) and the hygroscopic marine aerosols. This point validates the model here developed.

- A clear modulation of *PG* with wind sector is observed also in chapter 4. NW sector has the least affected by this cycle, which has been attributed to the effect of more conductive marine air. The daily variation of NE sector for weekends reveals a similar behavior to the Carnegie curve. Finally, the effect of pollution of industries located to the south of Lisbon on *PG* is found to be strong in the period 8.00 A.M. – 8. 00 P.M.

- Chapter 5 results suggest that the Chiado's fire left a clear signature on the *PG* recorded at Portela. During the late afternoon of 26th August 1988, one day after the fire, the *PG* increased to 510 V/m, which is an anomalously high value in comparison to the annual and summer distributions of *PG* at that site. This value is identified as an evident outlier with a reduced probability to occur, ~0.08 % in the 1988 summer. The analysis of wind speed and direction combined with calculations of forward trajectories using the Hysplit model enabled the assessment of the temporal and spatial evolution of the smoke plume. This analysis shows that the large *PG* values coincide with the approximate arrival time of the smoke plume at Portela. Finally, the analysis of the meteorological and synoptic conditions confirms that the anomaly of the *PG* does not result from meteorological effects. It is therefore likely that not only were the large *PG* values measured at Portela a result of the smoke plume from the Chiado's fire, but also, that measurements of *PG* can be used as a complementary method for fire detection, acting as a smoke proxy.

- Chapter 6 method is described to couple a common model for the Global Electric Circuit (primary circuit) to a Local Circuit (secondary circuit) resembling real PG measurements. Though it is a preliminary approach, a significant discrepancy was found between the PG simulated with a modelled Ionosphere Potential and the Carnegie Curve. Future work would involve different aspects and a major one is to test the contribution of thunderstorm activity as voltage or current source.

8 List of Communications

8.1 Papers in international scientific periodicals with referees

Atmospheric electric field measurements in urban environment and the pollutant aerosol weekly dependence, H.G. Silva, **R. Conceição**, M. Melgão, K. Nicoll, P.B. Mendes, M. Tlemçani, A.H. Reis, and R.G. Harrison, Environment Research Letters 9, 114025 (2014); DOI:10.1088/1748-9326/9/11/114025.

*Transport of the smoke plume from Chiado's fire in Lisbon (Portugal) sensed by atmospheric electric field measurements***, R. Conceição**, M. Melgão, H.G. Silva, K. Nicoll, R.G. Harrison, and A. H. Reis, Air Quality, Atmosphere & Health 8 (2015); DOI:10.1007/s11869-015-0337-4.

Aerosol hygroscopic growth and the dependence of atmospheric electric field measurements with relative humidity, H.G. Silva**, R. Conceição**, M.D. Wright, J.C. Matthews, S.N. Pereira, and D.E. Shallcross, Journal of Aerosol Science 85, 42 (2015); DOI: 10.1016/j.jaerosci.2015.03.003.

Modulation of urban atmospheric electric field measurements with the wind direction in Lisbon (Portugal), H.G. Silva, J.C. Matthews, **R. Conceição**, M.D. Wright, A.H. Reis, D.E. Shallcross, (Journal of Physics: Conference Series, accepted).

Simulations of the Global Electrical Circuit coupled to local Potential Gradient measurements, **R. Conceição**, H.G. Silva, (Journal of Physics: Conference Series, accepted).

8.2 Papers in conference proceedings

Análise espectral do Campo Elétrico Atmosférico em Lisboa, **R. Conceição**, M. Melgão, H. G. Silva, M. Tlemçani, A. H. Reis, C. Serrano, Livro de Actas III CJIG, LEG 2013 & 6th *PG*UE, ISBN: 978-989-95398-1-5, p. 223.

Atmospheric Electric Field of Lisbon (Portugal) affected by the week urban pollution cycle, H.G. Silva, **R. Conceição**, M. Melgão, P. Mendes, M. Tlemçani, C. Serrano, and A.H. Reis, Geophysical Research Abstracts Vol. 16, EGU2013-12806, EGU General Assembly 2014.

8.3 Oral communications by invitation

Potential Gradient measurements in Portugal, H.G. Silva, **R. Conceição**, M. Melgão, A.H. Reis, M. Tlemçani, CTR Wilson meeting, Special group of Atmospheric Electricity, Royal Meteorological Society, 5th November, 2014 – University of Bath, UK. DOI:10.13140/2.1.1478.3680.

8.4 Other oral communications

Atmospheric Electric Field of Lisbon affected by the week urban pollution cycle, **R. Conceição**, M. Melgão, P.B. Mendes, H.G. Silva, M. Tlemçani, C. Serrano, A. H. Reis, and R.G. Harrison, 8th Portuguese and Spanish Assembly of Geodesy and Geophysics (8ALEGG) - 29 to 31 January 2014 – Évora, Portugal.

8.5 Poster communications

Atmospheric Electric Field of Lisbon (Portugal) affected by urban activity, H.G. Silva, **R. Conceição**, M. Melgão, M. Tlemçani, A. H. Reis, and C. Serrano, Fifteenth International Conference on Atmospheric Electricity (ICAE 2014) - 15 to 20 June 2014 - Norman (Oklahoma), USA.

Modulation of urban atmospheric electric field measurements with the wind direction in Lisbon (Portugal), H.G. Silva, J.C. Matthews, **R. Conceição**, M.D. Wright, A.H. Reis, D.E. Shallcross, Electrostatics 2015, 12-16 April 2015, Southampton Solent University, Southampton, UK.

Simulations of the Global Electrical Circuit coupled to local Potential Gradient measurements, **R. Conceição**, H.G. Silva, Electrostatics 2015, 12-16 April 2015, Southampton Solent University, Southampton, UK.

9 References

Alcoforado, M.J. (1987). Brisas estivais do Tejo e do Oceano na região de Lisboa. Finisterra – Revista Portuguesa de Geografia, Lisboa, XXII (43): 71-112. (in Portuguese)

Alcoforado, M.J., Andrade, H., Lopes, A., Vasconcelos, J., Vieira, R. (2006). Observational studies on summer winds in Lisbon (Portugal) and their influence on day time regional and urban thermal patterns. *MeRHavim,* 6: 90-112

Alcoforado, M.J., Andrade,H., Lopes, A., Vasconcelos, J. (2008). Application of climatic guidelines to urban planning. The example of Lisbon (Portugal). *Landscape And Urban Planning* 90, 56.

Andrade, H. (1996). A qualidade do ar em Lisboa. Valores médios e situações extremas, Finisterra 61, 43-66. (in Portuguese)

Aplin, K. (2012). Smoke emissions from industrial western Scotland in 1859 inferred from Lord Kelvin's atmospheric electricity measurements. Atmospheric Environment 50, 373.

Bell, T.L., Rosenfeld, D., Kim, K.-M., Yoo, J.-M., Lee, M.-I., and Hahnenberger, M. (2008). Midweek increase in summer rain and storm heights suggests air pollution invigorates rainstorms. J. Geophys. Res. 113 (D02209).

Bell, T.L., Rosenfeld, D., and Kim, K.-M. (2009). Weekly cycle of lightning: evidence of storm invigoration by pollution. Geophys. Res. Lett. 36 (L23805).

Bennett, A.J., and Harrison, R.G. (2009). Evidence for global circuit current flow through water droplet layer. Journal of Atmospheric and Solar-Terrestrial Physics 71, 1219–1221. Doi:10.1016/j.jastp.2009.04.011.

Bhartendu (1976). Relationship of the Ohm's Law Electrical Parameters with Meteorological Elements. Electrical Processes in Atmospheres. Spinger, Berlin. pp 100-108. ISBN: 978-3-642-85296-1 Doi:10.1007/978-3-642-85294-7_14.

Brett, 2001. http://www.mathworks.com/matlabcentral/fileexchange/993-lombscargle-m (retrieved on 2015-05-19).

Canton, J. (1753) Electrical experiments, with an Attempt to Account for Their Several Phenomena; Together with Some Observations on Thunder-Clouds, Philosophical Transactions 48.1, pp. 350-358.

Caprice, A., 2000, The Ultimate Quotable Einstein, Collected and edited by Alice Caprice With a foreword by Freeman Dyson, Princeton University Press.

Carrico C.M., Rood M.J., Ogren J.A., Neusüb C., Wiedensohler A. and Heintzenberg J. (2000). Aerosol optical properties at Sagres, Portugal during ACE-2. Tellus B 52, 694-715. Doi: 10.1034/j.1600-0889.2000.00049.x.

Chalmers, J. A. (1967). Atmospheric Electricity, Pergamon Press, London, 515 pp.

Charlson R.J., Anderson T.L. and Rodhe H. (1999). Direct climate forcing by anthropogenic aerosols: Quantifying the link between atmospheric sulphate and radiation. Contrib. Atmos. Phys. 72, 79-94.

Chauveau B., 1925 Electricitè Atmospherique (3 volumes) Libraire Octave Doin, Paris.

Chubb J.N., Two new designs of 'field mill' type fieldmeter not requiring earthing of rotating chopper, IEEE Trans Ind Appl 26 (6) Nov/Dec 1990 p 1178.

Conceição, R., Silva, H.G., Melgão, M., Nicoll, K., Harrison, R.G. and Reis, A.H. (2015). Transport of the smoke plume from Chiado's fire in Lisbon (Portugal) sensed by atmospheric electric field measurements. Air Quality, Atmosphere & Health 8 (2015); Doi:10.1007/s11869-015-0337-4.

Constant, K., Nourry, C., and Seegmuller, T. (2014), Population growth in polluting industrialization, Resource and Energy Economics 36, 229.

Costa, M.J., Salgado, R., Santos, D., Levizzani, V., Bortoli, D., Silva, A.M., and Pinto, P. (2010). Modelling of orographic precipitation over Iberia: a springtime case study. Adv. Geosci., 25, 103–110. Doi:10.5194/adgeo-25-103-2010.

Coulomb, C.A., 1745, Mémoires sur l'électricité et le magnétisme.

Deshpande, C.G., and Kamra, A.K. (2004). The atmospheric electric conductivity and aerosol measurements during fog over the Indian Ocean. Atmospheric Research 70(2) 77–87. Doi:10.1016/j.atmosres.2004.01.001

Duplissy, J., DeCarlo, P.F., Dommen, J., et al. (2011). Relating hygroscopicity and composition of organic aerosol particulate matter. Atmos. Chem. Phys., 11, 1155-1165. Doi:10.5194/acp-11-1155-2011

Dutta, P., and Horn, P.M. (1981). Low-frequency fluctuations in solids: 1/f noise. Reviews of Modern Physics 53(3), 497.

Everett J.D. (1868) Results of observations of atmospheric electricity at Kew Observatory, and at Kings College, Windsor, Nova Scotia Phil. Trans. Roy. Soc. Lond. A. 158, 347-361.

Fierz-Schmidhauser, R., Zieger, P., Wehrle, G., Jefferson, A., Ogren, J.A., Baltensperger, U. and Weingartner, E. (2010). Measurement of relative humidity dependent light scattering of aerosols. Atmos. Meas. Tech. 3, 39-50.

Figueira, M. (1965). Instruções para os apuramentos de electricidade atmosférica. Serviço Meteorológico Nacional, Lisboa. (in Portuguese).

Forster, P.M.F., and Solomon, S. (2003). Observations of a "weekend effect" in diurnal temperature range. PNAS 100(20), 11225.

Fleming J.A. (1939) Terrestrial Magnetism and Electricity (Physics of the Earth, volume VII) McGraw Hill.

Foster, P., Ramaswamy, V., Artaxo, P., Berntsen, T., Betts, R., Fahey, D.W., Haywood, J., Lean, J., Lowe, D.C., Myhre, G., Nganga, J., Prinn, R., Raga, G., Schulz, M., Van Dorland, R. (2007). Changes in atmospheric constituents and in radiative forcing. In: Solomon, S., Qin, D., Manning, M., Chen, Z., Marquis, M., Averyt, K.B., Tignor, M., Miller, H.L. (Eds.), Climate Change 2007. The Physical Science Basis, Contribution of Working Group I to the Fourth Assessment Report of the Intergovernmental Panel on Climate Change. Cambridge University Press, Cambridge, United Kingdom and New York, NY, USA.

Franklin, B. (1769). Experiments and Observations on Electricity, made at Philadelphia in America. London: for David Henry, sold by Francis Newbery.

Gendle, A. E.: Unpublished notebook, Eskdalemuir Observatory, 1912.

Gopalakrishnan V, Deshpande, CG, and Kamra, A.K. (1996) Measurements of atmospheric electric field and conductivity in the locality of a gas well flame. Geophysical Research Letters 23(24), 3615-3618.

Gunn, R. (1954). Diffusion charging of atmospheric droplets by ions and the resulting combination coefficients. Journal of Meteorology, 11, 339–347.

Harrison, R.G., Aplin, K.L. (2002). Mid-nineteenth century smoke concentrations near London, Atmospheric Environment 36, 4037.

Harrison, R.G., and Carslaw, K.S. (2003). Ion–aerosol–cloud processes in the lower atmosphere. Review of Geophysics, 41(3), 1012. Doi:10.1029/2002RG000114.

Harrison, R.G., and Aplin, K.L. (2003). Nineteenth century Parisian smoke variations inferred from Eiffel Tower atmospheric electrical observations. Atmos. Environ. 37, 5319-5324.

Harrison, R.G. (2006). Urban smoke concentrations at Kew, London, 1898-2004. Atmos. Environ. 40 (18), 3327-3332.

Harrison, R. G., and K. L. Aplin (2007). Water vapour changes and atmospheric cluster ions, Atmos. Res., 85, 199–208.

Harrison, R.G. (2009). Two daily smoke maxima in eighteenth century London air, Atmospheric Environment 43, 1364.

Harrison, R.G (2012). Aerosol-induced correlation between visibility and atmospheric electricity. Journal of Aerosol Science, 52, 121–126. Doi:10.1016/j.jaerosci.2012.04.011.

Harrison, R. G. (2013). The Carnegie Curve. Surveys in Geophysics, 34, 209-232. Doi:10.1007/s10712-012-9210-2.

Hocke, K., and Kampfer, N. (2009). Gap Filling and Noise Reduction of Unevenly Sampled Data By Means of the Lomb-Scargle Periodogram. Atmos. Chem. Phys. 9, 4197.

Holzworth, R.H., 1987. Electric fields in the middle atmosphere. Physica Scripta T18, 298, http://dx.doi.org/10.1088/0031-8949/1987/T18/030.

Hoppel, W.A. (1985). Ion-Aerosol Attachment Coefficients, Ion Depletion, and the Charge Distribution on Aerosols. J. Geophys. Res. 90(D4), 5917-5923.

INE (2011). Portuguese National Census, http://censos.ine.pt/ (retrieved on 2015-05-19).

Ippolitov II, Kabanov MV, Nagorskii PM, Pkhalagov YuA, and Smirnov SV (2013) Diurnal Variations in the Electrical Field Intensity under Smoke from Forest Fires. Doklady Earth Sciences 453(1):1137–1140.

Israelsson S, Lelwala R (1999). Space charge density measurements downwind from a traffic route. Atmos. Res. 51, 301–307.

Israelsson, S., and Tammet, H. (2001). Variation of fair weather atmospheric electricity at MarstaObservatory, Sweden, 1993–1998. J. of Atmospheric and Solar-Terrestrial Physics 63, 1693.

Jefimenko, O. D. (1973). Electrostatic motors, Their History, Types and Principles of Operation. Star City [W. Va.], Electret Scientific Co. LCCN 73180890.

Kamra, A.K., Deshpande, C.G., and Gopalakrishan, V. (1997). Effect of relative humidity on the electrical conductivity of marine air. Q. J. R. Meteorol. Soc., 123, pp. 1295-1305. Doi:10.1002/qj.49712354108

Kaufman, Y. J., Hobbs, P.V., Kirchhoff, V.W.J.H., et al., (1998). Smoke, Clouds, and Radiation-Brazil (SCAR-B) experiment. Journal of Geophysical Research 103(24), 31783–31808. Doi: 10.1029/98JD02281.

Klemens R., Von Naturbeobachtungen zuir Nanophysik, Graz, 2003, p. 194-196.

Kobylinski, Z., Michnowski, S., 2007. Atmospheric electric and electromagnetic field rapid changes as possible precursors of earthquakes and volcanic eruption: a brief review. Sun and Geosphere 2 (1), 43–47.

Koloutsou-Vakakis, S., Carrico, C.M., Kus, P., et al. (2001). Aerosol properties at a midlatitude Northern Hemisphere continental site, Jour. Geophys. Res. 106(D3), 3019-3032.

Krzyzanowski, M., and Cohen, A. (2008) Update of WHO air quality guidelines. Air Qual. Atmos. Health 1, 7–13.

Lang, T. J. and Rutledge, S. A. (2006) Cloud-to-ground lightning downwind of the 2002 Hayman forest fire in Colorado. Geophysical Research Letters 33, L03804.

Li, Z. (1998). Influence of absorbing aerosols on the inference of solar surface radiation budget and cloud absorption, Jour. Climate 11(1), 5–17.

Leblanc, F., Aplin, K. L., Yair, Y., Harrison, R. G., Lebreton, J. P., and Blanc, M. (eds.), (2008). Planetary Atmospheric Electricity. Space Sciences Series of ISSI, Vol. 30. Springer, New York. DOI: 10.1007/978-0-387-87664-1.

Lomb, N.R., 1976. Least-squares frequency analysis of unequally spaced data, Astrophysics and Space Science 39, 447-462.

Lopes, A., 2003. Modificações no clima urbano de Lisboa como consequência do crescimento urbano. Vento, ilha de calor de superfície e balanço energético, PhD Thesis. Faculty of Humanities. University of Lisbon. (in Portuguese).

Lyamani, H., Olmo, F.J., Alcántara, A., and Alados-Arboledas, L. (2006). Atmospheric aerosols during the 2003 heat wave in southeastern Spain I: Spectral optical depth. Atmospheric Environment 40(33), 6453–6464. Doi:10.1016/j.atmosenv.2006.04.048.

Manes, A., 1977. Particulate air pollution trends deduced from atmospheric electrical conductivity measurements at Bet-Dagan (Israel), Electrical Processes in Atmosphere, dited by H. Dolezalek and R. Reiter, 109-118, Darmstadt, Germany.

Mareev, E. A. and Volodin, E. M. (2014). Variation of the global electric circuit and Ionospheric potential in a general circulation model. Geophys. Res. Lett. 41, 9009–9016. Doi: 10.1002/2014GL062352.

Markowicz, K.M., Flatau, P.J., Ramana, M.V. Crutzen, P.J. and Ramanathan, V. (2002). Absorbing Mediterranean aerosols lead to a large reduction in the solar radiation at the surface, Geophys. Res. Lett. 29(20), 29-1–29-4. Doi: 10.1029/2002GL015767.

Markson, R., Ruhnke, L. H. and Williams, E. R. (1999). Global scale comparison of simultaneous ionospheric potential measurements. Atmos. Res. 51, 315–321.

Matthews, J.C., Ward, J.P., Keitch, P.A., and Henshaw, D.L. (2010). Corona ion induced atmospheric potential gradient perturbations near high voltage power lines. Atmospheric Environment, 44, 5093-5100. Doi:10.1016/j.atmosenv.2010.09.007.

Matthews, J.C. (2012a). The effect of weather on corona ion emission from AC high voltage power lines. Atmospheric Research, 113, 68–79. Doi:10.1016/j.atmosres.2012.03.016.

Matthews, J.C. (2012b). Diurnal variations of atmospheric potential gradient disruption near to high voltage power lines. Journal of Atmospheric and Solar-Terrestrial Physics, 77, 235–240. Doi:10.1016/j.jastp.2012.01.014.

Matthews, J.C., Buckley, A.J., Wright, M.D., and Henshaw, D L. (2012c). Comparisons of ground level measurements of ion concentration and potential gradient upwind and downwind of HV power lines in corona. Journal of Electrostatics, 70 (4), 407-417.

Moreira, M.J.G., Rodrigues, T.F., 2008. The Demographic Regionalities of Contemporary Portugal, CEPESE Working Paper (in Portuguese), http://www.cepese.pt (retrieved on 2014-01-11).

Nicoll, K.A., and Harrison, R.G. (2010). Experimental determination of layer cloud edge charging from cosmic ray ionisation. Geophys. Res. Let. 37, L13802. Doi:10.1029/2010GL043605, 2010.

Obregón, M.A., Pereira, S., Salgueiro, V., Costa, M.J., Silva, A.M., Serrano, A., and Bortoli, D. (2015). Aerosol radiative effects during two desert dust events in August 2012 over the Southwestern Iberian Peninsula. Atmospheric Research 153, 404–415. Doi:10.1016/j.atmosres.2014.10.007.

Odzimek, A., Lester, M., and Kubicki, M. (2010). EGATEC: A new high-resolution engineering model of the global atmospheric electric circuit – Currents in the lower atmosphere. J. Geophys. Res., 115, D18207. Doi:10.1029/2009JD013341.

Petters, M.D. and Kreidenweis, S.M. (2007). A single parameter representation of hygroscopic growth and cloud condensation nucleus activity. Atmos. Chem. Phys. 7, 1961-1971. Doi:10.5194/acp-7-1961-2007.

Phalagov, Yu. A, Ippolitov, I. I., Nagorskii, P. M., Odintsov, S. L., Panchenko, M. V., Smirnov, S. V. and Uzhegov, V. N. (2009). Relation of Anomalous Atmospheric Conditions to Electric Field Variation. Atmospheric and Oceanic Optics 22(1), 113–117.

Pierce, E.T. (1972). Radioactive fallout and secular effects in atmospheric electricity, J. Geophys. Res. 77(3), 482.

Pilat, M.J., and Charlson, R.J. (1966). Theoretical and optical studies of humidity effects on the size distribution of hygroscopic aerosol. Journal de Recherches Atmospheriques 1, 165-170.

Piper, I. M., and Bennett, A. J. (2012). Observations of the atmospheric electric field during two case studies of boundary layer processes. Environment Research Letters 7:014017.

Press, W.H., Teukolsky, S.A., Vetterling, W.T., Flannery, B.P. (1992). Numerical Recipes in C: The Art of Scientific Computing, Second Edition (Cambridge University Press).

Pruppacher, H.R., and Klett, J.D. (2010). Microphysics of Clouds and Precipitation. Springer, Berlin. ISBN:978-0-7923-4211-3. Doi:10.1007/978-0-306-48100-0.

Pulinets, S., 2007. Natural radioactivity, earthquakes, and the ionosphere, EOS. Transactions American Geophysical Union 88 (20), 217, http://dx.doi.org/ 10.1029/2007EO200001.

Reddell, B.D., Benbrook, J.R., Bering, E.A., Cleary, E.N., and Few, A.A., 2004. Seasonal variations of atmospheric electricity measured at Amundsen-Scott South Pole Station, J. Geophys. Res., 109, A09308.

Retalis, D.A. (1977). On the relationship between small atmospheric ions concentration and (1) smoke, (2) sulfur dioxide and (3) wind speed, Pure and Applied Geophysics 115(3), 575-581. Doi: 10.1007/BF00876122.

Retalis, D., Pitta, A., and Psallidas, P. (1991). The conductivity of the air and other electrical parameters in relation to meteorological elements and air pollution in Athens. Meteorology and Atmospheric Physics 46(3-4), 197-204.

Retalis, D., and Retalis, A. (1997). The atmospheric electric field in Athens – Greece. Meteorology and Atmospheric Physics 63(3-4), 235-241.

Rickards, A.M. J., Miles, R.E.H., Davies, J.F., Marshall, F.H., and Reid, J.P. (2013). Measurements of the Sensitivity of Aerosol Hygroscopicity and the κ Parameter to the O/C Ratio, J. Phys. Chem. A, 117, 14120−14131. Doi:10.1021/jp407991n.

Rosenfeld, D., and Bell, T.L. (2011). Why do tornados and hailstorms rest on weekends? J. Geophys. Res. 116 (D20211).

Rycroft, M. J., Israelsson, S. and Price, C. (2000). The global atmospheric electric circuit, solar activity and climate change Jour. Atmosph. Solar-Ter. Phys. 62 1563-1576.

Rycroft, M.J., Odzimek, A., Arnold, N.F., et al., 2007. New model simulations of the global atmospheric electric circuit driven by thunderstorms and electrified shower clouds: the roles of lightning and sprites. Journal of Atmospheric and Solar-Terrestrial Physics 69, 2485–2509.

Rycroft, M.J., Harrison, R.G., Nicoll, K.A., et al., 2008. An overview of Earth's global electric circuit and atmospheric conductivity. Space Science Reviews 137, 83–105, http://dx.doi.org/10:1007/978-0-387-87664-1_6.

Rycroft, M.J., Odzimek, A., 2010. Effects of lightning and sprites on the ionospheric potential, and threshold effects on sprite initiation, obtained using an analog model of the global atmospheric electric circuit. Journal of Geophysical Research 115, A00E37, http://dx.doi.org/10.1029/2009JA014758.

Scargle, J.D. (1982). Studies in astronomical time series analysis. II – Statistical aspects of spectral analysis of unevenly spaced data. Astrophysical Journal 263, 835.

Schulz, M., and, Stattegger, K. (1997). Spectrum: Spectral Analysis of Unevenly Spaced Paleoclimatic Time Series. Computers & Geosciences 23(9), 929.

Seinfeld, J.H., and Pandis, S.N. (1998). Atmospheric Chemistry and Physics: From Air Pollution to Climate Change. Wiley, New York, 1326pp.

Serrano, C., Reis, A.H., Rosa, R., Lucio, P.S. (2006[a]). Influences of cosmic radiation, artificial radioactivity and aerosol concentration upon the fair-weather atmospheric electric field in Lisbon (1955-1991), Atmospheric Research, 81, 236.

Serrano, C., Reis, A.H., Rosa, R., Lucio, P.S. (2006b). Wind induced anomalies on the fair weather atmospheric electric field in Lisbon, in Proceedings of 6th Annual Meeting of the EMS, Lubljana, Slovenia, EMS2006-A-00071.

Serrano, C. (2010). Contribution to the study of atmospheric electric field in the Lisbon region. PhD Thesis, University of Évora, Portugal (in Portuguese).

Sheftel, V.M., Chernyshev, A.K, Chernysheva, S.P. (1994). Air conductivity and atmospheric electric field as an indicator of anthropogenic atmospheric pollution. Journal of Geophysical Research 99, 10,793–10,795.

Shigeno, N., Takizawa, T., Itoh, N., Yokoyama M., and Owada, T. (2001). Preliminary Test for Atmospheric Electricity Measurement Using an Electrostatic Sensor. Translated to English from paper in Japanese, originally published in: Gijutsu Houkoku 41, No.1(No.112), 8-13.

Silva, H.G., Oliveira, M.M., Serrano, C., Bezzeghoud, M., Reis, A.H., Rosa, R.N., Biagi, P.F., 2012. Influence of seismic activity on the atmospheric electric field in Lisbon (Portugal) from 1955 to 1991, Annals of Geophysics 55 (1), 193.

Silva, H.G., Conceição, R., Melgão, M., Nicoll, K., Mendes, P.B., Tlemçani, M., Reis, A.H., and Harrison, R.G. (2014). Atmospheric electric field measurements in urban environment and the pollutant aerosol weekly dependence. Environment Research Letters 9, 114025. Doi:10.1088/1748-9326/9/11/114025.

Silva, H.G., Matthews, J.C., Conceição, R., Wright, M.D., Reis, A.H. and Shallcross, D.E. (2015). Modulation of urban atmospheric electric field measurements with the wind direction in Lisbon (Portugal). J. Phys.: Conf. Ser. Paper (accepted).

Sjogren, S., Gysel, M., Weingartner, E., Baltensperger, U., Cubison, M.J., Coe, H., Zardini, A.A., et al. (2007). Hygroscopic growth and water uptake kinetics of two-phase aerosol particles consisting of ammonium sulfate, adipic and humic acid mixtures. Jour. Aerosol Sci. 38, 157-171.

Singh, A.K., Siingh, D., Singh, R.P., et al., 2011. Electrodynamical coupling of Earth's atmosphere and ionosphere: an overview. International Journal of Geophysics, 2011, http://dx.doi.org/10.1155/2011/971302.

Stull, R.B. (1950). An Introduction to Boundary Layer Meteorology. Atmospheric Sciences Library.

Tacza, J., Raulin, J.-P., Macotela, E., Norabuena, E., Fernandez, G., Correia, E., Rycroft, M.J., and Harrison, R.G. (2014). A new South American network to study the atmospheric electric field and its variations related to geophysical phenomena. J. Atmos. Sol-Terr. Phys., 120, 70–79. Doi: 10.1016/j.jastp.2014.09.001.

Takeda, M., Yamauchi, M., Makino, M., and Owada, T. (2011). Initial effect of the Fukushima Accident on atmospheric electricity. Geophys. Res. Lett. 38, L15811.

Tammet, H., Hõrrak, U., Laakso, L. and Kulmala, M. (2006). Factors of air ion balance in a coniferous forest according to measurements in Hyytiälä, Finland. Atmos. Chem. Phys. 6, 3377−3390.

Tammet, H. (2009). A joint dataset of fair-weather atmospheric electricity. Atmospheric Research 91, 194.

Tammet, H. and Kulmala, M. (2014). Empiric equations of coagulation sink of fine nanoparticles on background aerosol optimized for boreal zone, Boreal Environ. Res. 19, 115-126.

Tchepel, O. and Borrego, C. (2010). Frequency analysis of air quality time series for traffic related pollutants, J. Environ. Monit. 12, 544–550. doi: 0.1039/b913797a.

Titos G., Lyamani, H., Cazorla, A., Sorribas, M., Foyo-Moreno, I., Wiedensohler A., and Alados-Arboledas, L. (2014a). Study of the relative humidity dependence of aerosol light-scattering in southern Spain, Tellus B 66, 24536. Doi:10.3402/tellusb.v66.24536.

Titos G., Jefferson A., Sheridan P.J., Andrews E., Lyamani H., Alados-Arboledas L. and Ogren J.A (2014b). Aerosol light-scattering enhancement due to water uptake during the TCAP campaign. Atmospheric Chemistry and Physics 14, 7031–7043.

Tuzlukov, V. (2002). Signal Processing Noise (Electrical Engineering & Applied Signal Processing Series). CRC Press; 1 edition (USA).

Vanderviere E, Huber M (2004) An Adjusted Boxplot for Skewed Distributions, COMPSTAT'2004 Symposium, Physuca-Verlag/Springer, 933–1940.

Voeikov, A.I. (1965). Instruction on Preparation of the Material and Publication of the results of Atmospheric Electric Observations, Ed. Main Geophysical Observatory, Leningrad.

Vonnegut, B., Latham, D. J., Moore, C. B., and Hunyady, S. J. (1995) An explanation for anomalous lightning from forest fire clouds. Jour. Geophysical Research 100, 5037–505

Weingartner E, Burtscher H., and Baltensperger U. (1997). Hygroscopic properties of carbon and diesel soot particles. Atmospheric Environment 31(15), 2311-2327.

Whipple, F. J. W. (1929), On the association of the diurnal variation of the electric potential gradient in fine weather with the distribution of thunderstorms over the globe, Q. J. R. Meteorol. Soc., 55, 351–362, doi:10.1002/ qj.49705523206

Whipple F.J.W and Scrase F.J.:1936 Point discharge in the electric field of the earth Geophysical Memoirs 68, Meteorological Office, HMSO, London.

Wilding, R.J., and Harrison, R.G. (2005). Aerosol modulation of small ion growth in coastal air, Atmospheric Environment, 39, 5876–5883. Doi:10.1016/j.atmosenv.2005.06.020.

Williams, E., and Mareev, E. (2014). Recent progress on the global electrical circuit, Atmospheric Research 135–136, 208–227.

Wilson C.T.R. (1906). On the measurement of the earth-air current and on the origin of atmospheric electricity. Proc. Camb. Philos. Soc. 13, 6, 363-382.

Wilson, C. T. R. (1908). On the measurement of the atmospheric potential gradient and Earth-air current, Proc. R. Soc. London, Ser. A, 80, 537– 547, doi:10.1098/rspa.1908.0048.

Wilson, C.T.R. (1920). Investigations on lightning discharges and on the electric field of thunderstorms. Phil. Trans. Roy. Soc. A 221, 73–115.

Wormell, T.W., 1930. Vertical electric currents below thunderstorms and showers. Proceedings of the Royal Society A 127, 567–590.

Wright, M.D., Holden, N.K., Shallcross, D.E., and Henshaw, D.L. (2014a). Indoor and outdoor atmospheric ion mobility spectra, diurnal variation, and relationship with meteorological parameters. J. Geophys. Res. Atmos., 119. Doi:10.1002/2013JD020956.

Wright, M.D., Buckley, A.J., Matthews, J.C., Shallcross, D.E., and Henshaw, D.L. (2014b). Air ion mobility spectra and concentrations upwind and downwind of overhead AC high

voltage power lines. Atmospheric Environment 95, 296-304. Doi:10.1016/j.atmosenv.2014.06.047.

Xu, B., Zou, D., Chen, B.Y., Zhang, J.Y., and Xu, G.W. (2013). Periodic variations of atmospheric electric field on fair weather conditions at YBJ, Tibet. Journal of Atmospheric and Solar-Terrestrial Physics 97, 85.